2017•2018

Faculteit Industriële ingenieurswetenschappen

master in de industriële wetenschappen: chemie

Masterthesis

Design and characterization of a cascade of continuous stirred-tank reactors for a Grignard reaction

PROMOTOR :

Prof. dr. ir. Leen THOMASSEN

PROMOTOR :

ing. Joris CLAES

Dries Cornelissen, Robin Debrie

Scriptie ingediend tot het behalen van de graad van master in de industriële wetenschappen: chemie

Gezamenlijke opleiding UHasselt en KU Leuven

UHASSELT KU LEUVEN

UHASSELT KU LEUVEN

2017 • 2018

Faculteit Industriële ingenieurswetenschappen

master in de industriële wetenschappen: chemie

Masterthesis

Design and characterization of a cascade of continuous stirred-tank reactors for a Grignard reaction

PROMOTOR :

Prof. dr. ir. Leen THOMASSEN

PROMOTOR :

ing. Joris CLAES

Dries Cornelissen, Robin Debrie

Scriptie ingediend tot het behalen van de graad van master in de industriële wetenschappen: chemie

UHASSELT KU LEUVEN

ACKNOWLEDGEMENTS

Dries Cornelissen

Met deze thesis wordt de laatste halte van mijn vierjarige opleiding tot industrieel ingenieur in de chemie bereikt. Deze vier jaar zijn ongelofelijk snel voorbij gevlogen, wat natuurlijk betekent dat ik het hier helemaal naar mijn zin heb gehad. Vooral het laatste semester, dat volledig besteed werd aan het uitwerken van deze thesis met Robin Debrie, heeft me enorm geïnteresseerd. Hier heb ik me dan ook met alle motivatie die ik had in vastgebeten, om er samen met Robin een zo mooi mogelijk resultaat van te maken.

Deze thesis was nooit gelukt zonder een aantal personen, die ik persoonlijk wil bedanken. Allereerst zou ik prof. Leen Thomassen willen bedanken voor de begeleiding, de overvloedige kennis en het vertrouwen in onze ideeën om deze thesis tot een goed einde te brengen. Ik ben zeer blij dat ze me het vertrouwen gaf om dit onderwerp te kiezen. Daarna wil ik ook ing. Joris Claes bedanken, die gigantisch veel energie heeft gestoken in het nauwgezet begeleiden van onze thesis, en dit altijd met een lach op het gezicht deed. Voor elk probleem wist hij wel een oplossing, en elke tegenslag verzachtte hij dan weer met een grap. Daarnaast hebben we ook veel te danken aan Marleen Segers, die altijd met haar brede kennis een gepast antwoord wist te geven en ons hiermee veel tijd bespaarde, en dit ook nog eens met een brede glimlach op het gezicht deed. Sven Gobert verdient ook zeker een dankwoordje, aangezien hij ons geholpen heeft met de installatie van de complexe pompen die in deze thesis gebruikt werden. Verder wil ik graag iedereen van de opleiding bedanken, van de docenten en medewerkers van Lab_4U tot mijn vrienden, die er allemaal voor gezorgd hebben dat ik deze opleiding met plezier gevolgd heb. Hiernaast wil ik zeker ook nog mijn thesispartner en vriend Robin Debrie bedanken, voor alles wat we samen bereikt hebben en de fijne werksfeer die we wisten te creëren, waardoor geen enkele dag saai was.

Ook buiten de opleiding heb ik een aantal mensen te bedanken. Allereerst wil ik mijn familie en vrienden bedanken, waarvan ik mijn ouders en mijn zus het meest dankbaar ben. Ze hielpen me ontspannen, lachen en zorgden dat ik zo weinig mogelijk weerstand had om deze opleiding te voltooien. Daarnaast wil ik ook mijn vriendin Lauren bedanken, die me altijd door dik en dun gesteund heeft.

Van mijn kant wil ik deze thesis graag opdragen aan mijn opa, die jammer genoeg tijdens mijn opleiding overleed. Niemand was zo geïnteresseerd in mijn opleiding als hij. Ik ben er zeker van dat hij de meest trotse persoon is als hij mij ziet afstuderen.

Robin Debrie

Deze thesis, samen met Dries Cornelissen, is het laatste hoofdstuk van het verhaal dat hier gedurende mijn opleiding tot chemisch ingenieur geschreven is. Het onderwerp heeft me enorm geboeid, de vele gespendeerde uren zijn er dan ook met volle zin ingestoken.

Ik wil dan ook prof. Leen Thomassen bedanken voor de kennis, kritische vragen, ondersteuning, en het vertrouwen. Vervolgens wil ik onze persoonlijke begeleider ing. Joris Claes bedanken. Naast de opbouwende kritiek en de openheid om altijd paraat te staan bij problemen en vragen, was er altijd ruimte om even minder serieus te zijn. Daarnaast wil ik zeker Marleen Segers niet vergeten, ze was veel te goed voor de masterstudenten aanwezig in Lab4U in de positieve zin. Geen moeite was te veel om ons even verder te helpen, of even mee te denken bij een probleem, en altijd met een lach. Vooral met de analyse hebben we gretig gebruik gemaakt van haar kennis. Het eindresultaat van deze thesis

was niet behaald zonder hen. Verder wil ik nog alle docenten en medewerkers bedanken die allen bijgedragen hebben tot het slagen voor de opleiding.

Tot slot wil ik mijn familie en vrienden bedanken. Mijn ouders en zus hebben me doorheen de opleiding altijd gesteund en in me geloofd. Dries Cornelissen mag ik zeker niet vergeten, zonder de uitermate goede, vlotte en losse samenwerking was de thesis niet gelukt. Op gepaste tijden kon er zeker gelachen worden. Verder wil ik ook mijn kotgenoten van Hubertus bedanken, bij hen kon ik altijd terecht voor een gepaste pauze tijdens het vele werk.

TABLE OF CONTENTS

LIST OF TABLES

LIST OF FIGURES

LIST OF SYMBOLS AND ABBREVIATIONS

2-MBP	2-(N-methylbenzyl)pyridine
ACN	Acetonitrile
API	Active pharmaceutical ingredient
C	Concentration (mole/l)
CH_3MgBr	Methylmagnesium bromide
CSTR	Continuously stirred-tank reactor
D	Dispersion coefficient (m^2/s)
DIBAH	Diisobutylaluminum hydride
E(t)	Residence time distribution function
Ea	Activation energy (J/mole)
Et_2O	Diethyl ether
F(t)	Cumulative distribution function
H_2SO_4	Sulfuric acid
HCl	Chloric acid
HPLC	High-performance liquid chromatography
ID	Internal diameter
k	Rate constant ($min^{-1}*(mole/l)^{-1}$)
k_0 or A	Pre-exponential factor ($min^{-1}*(mole/l)^{-1}$)
KCl	Potassium chloride
K_s	Equilibrium constant
L	Length (m)
$MgCl_2$	Magnesium chloride
NaCl	Natrium chloride
NH_4Cl	Ammonium chloride
OD	Outer diameter
PFA	PerFluorAlkoxy
PFR	Plug flow reactor
pKa	Acid dissociation constant
R	Gas constant ($J*mole^{-1}*K^{-1}$)
$-r_a$	Reaction rate ($mole*min^{-1}*(m^2)^{-1}$)
R-group	An abbreviation for any group in which a carbon or hydrogen atom is attached to the rest of the molecule
RTD	Residence time distribution
SET	Single electron transfer
S_{Mg}	Surface area of magnesium (m^2)
T	Temperature (K, or °C if mentioned)
t	Time (min)
THF	Tetrahydrofuran
$\bar{t}$ or τ	Residence time (min)
UV	Ultraviolet
μ	Flowrate (m^3/s)
v	Flow rate (m^3/min)
V	Volume (m^3)
wt%	Weight percent

X	Halide, iodine, chlorine or bromine
θ	Theta, dimensionless time ($t/\bar{t}$)
σ^*	Antibonding molecular orbital
σ_t	Measurement for the spread around the average
σ_θ	Measurement for the spread around the average in dimensionless time

ABSTRACT

Currently, the pharmaceutical and fine chemical industry performs Grignard reactions in large semi-batch reactors. Due to the exothermic nature of this reaction, heat dissipation problems occur. This requires dosing of reagents and therefore a long reaction time. Also, each batch needs an initiation, causing varying product quality. A continuous-flow process improves heat dissipation, has only one transient start-up initiation and decreases production area, which increases production capacity and stability. This Master's thesis describes the design and characterisation of a continuous-flow Grignard process of which the research was executed in Lab_4U and in collaboration with Janssen Pharmaceutica.

Based on literature research a reactor setup was designed, consisting of two Continuous Stirred Tank Reactors (CSTRs) in series with a solids settler in between to keep magnesium in the first reactor. Next, the reactor setup and the reactions were characterised. The residence time distribution was measured for the CSTR cascade and separate CSTRs, showing that the solids settler had a clear influence on the residence time. Reaction characterisation was performed in an Easymax 102. The formation of phenylmagnesium bromide out of bromobenzene and magnesium powder was second-order with an activation energy of 44.8 kJ/mol.

A total yield of 70% 1,1-diphenylethanol was achieved when the reaction was carried out with acetophenone in the CSTR cascade at 1.2 l/h. No particles above 25 µm were found in the final product flow.

ABSTRACT IN HET NEDERLANDS

De farmaceutische en fijnchemie industrie voert Grignard reacties uit in grote semi-batch reactoren. Door de exotherme aard van de reactie treden warmteafvoerproblemen op. Hierdoor zijn dosering van reagentia en bijgevolg lange reactietijden nodig. Ook vereist elke batch reactie-initiatie, wat leidt tot een variërende productkwaliteit. Een continu-stroomproces verhoogt de productiecapaciteit en stabiliteit door betere warmteafvoer, slechts 1 transiënte startup initiatie en beperkt het productiegebied. Deze masterthesis beschrijft het ontwerp en de karakterisering van een continu-stroomproces voor Grignard reacties, onderzocht in Lab$_4$U en in samenwerking met Janssen Pharmaceutica.

Eerst werd een reactoropstelling ontworpen op basis van literatuuronderzoek, resulterend in 2 continu geroerde tankreactoren (CSTR's) in serie met een deeltjesbezinker ertussen om magnesium in de eerste reactor te houden. Daarna werden de reactoropstelling en de reacties gekarakteriseerd. De verblijftijdspreiding werd gemeten voor de cascadeopstelling en de aparte CSTR’s, waaruit bleek dat de deeltjesbezinker een duidelijke invloed op de verblijftijd had. De reactiekarakterisering werd uitgevoerd in een Easymax 102. De vorming van fenylmagnesiumbromide uit broombenzeen en magnesiumpoeder was tweede orde met een activeringsenergie van 44,8 kJ/mol.

Wanneer de reactie uitgevoerd werd met acetofenon in de CSTR-cascade op 1,2 l/uur werd een totale opbrengst van 70% 1,1-difenylethanol bekomen. Deeltjes boven 25 µm werden niet teruggevonden in de eindstroom.

1 INTRODUCTION

In today's world, there is a continuously growing global industrial production. Hence the introduction of environmental protection measures to reduce the impact of human actions on nature [1] [2] [3]. The chemical industry is often considered as highly polluting, but despite these ecological measures that could reduce the production capacity, it still follows this global production growing trend. It thus appears that the chemical industry has found a balance between the economic and ecological aspect by investing in innovative and less polluting techniques [1] [3] [4] [5]. As the environmental protection measures are becoming more stringent, continuous innovation is needed to maintain this balance.
The chemical industry tries to meet this requirement by, among other things, focusing on process intensification [4] [6] [7] [8]. While the primary purpose of process intensification is to improve profit by increasing their production efficiency, capacity and quality, often a parallel reduction of the ecological footprint is realized [7].

A technique that often is used in process intensification and that is gaining more importance in the chemical industry, is the transition from batch to continuous processing [9]. In bulk chemical and petrochemical industries, this type of process intensification is regularly applied. However, in the fine and pharmaceutical industry, this changeover from batch to continuous processing is only in its infancy due to the diversity and complexity of the syntheses to make the products, which often includes many reactions steps. Moreover, the active pharmaceutical ingredients (API's) usually have to be made in relatively small quantities [10].

Janssen Pharmaceutica, part of the pharmaceutical group Johnson & Johnson, is a company that is engaged in drugs to treat, cure, stop and prevent complex, calamitous diseases like Alzheimer's, cancer and heart diseases [11]. In addition to producing their API's on an industrial scale, Janssen Pharmaceutica also conducts research into new API's and optimisation of their production processes. One of their current research topics is the implementation of continuous-flow processing in development and production scale.

Lab4U is a research group from KU Leuven, located at Diepenbeek, that integrates chemistry and industrial (bio)technology. Commissioned by various companies, it focuses on research topics such as process intensification, environmental cleantech and bio(med)tech [11] [12].
Janssen Pharmaceutica is one of those companies that is frequently involved in projects together with Lab4U. This current project is situated in the field of process intensification. The task consists of the switch from batch production to continuous flow production for a highly exothermic organometallic Grignard reaction, which will be discussed briefly below.
Two Grignard reactions were chosen to be tested, of which the first is shown in Figure 1.

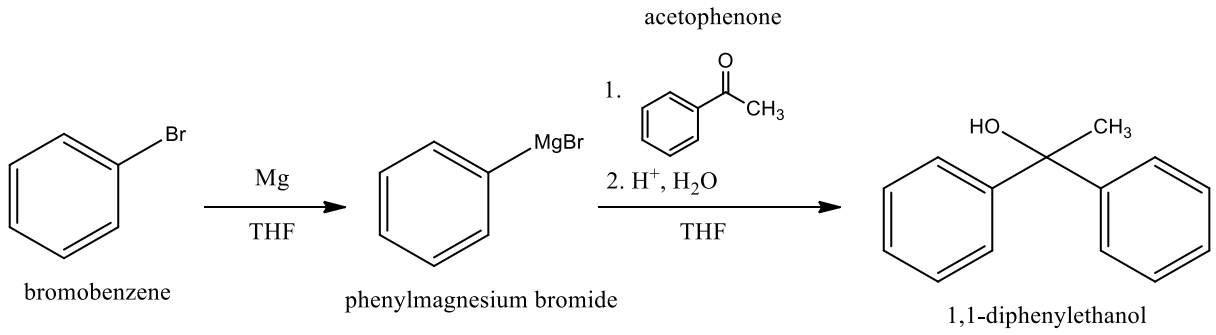

Figure 1: Reaction scheme of the first reaction

In the first part of this reaction scheme, bromobenzene and magnesium react exothermically to phenylmagnesium bromide, the Grignard reagent. The reaction takes place in an organic solvent, preferably tetrahydrofuran (THF), in which magnesium is held in suspension. In the next step, this Grignard reagent reacts with acetophenone, a ketone, in THF. Finally, 1,1-diphenylethanol is formed by adding acidified water. Simultaneously, the remaining phenylmagnesium bromide is destroyed or quenched, and the Grignard reaction is completed.

The second reaction is shown in Figure 2.

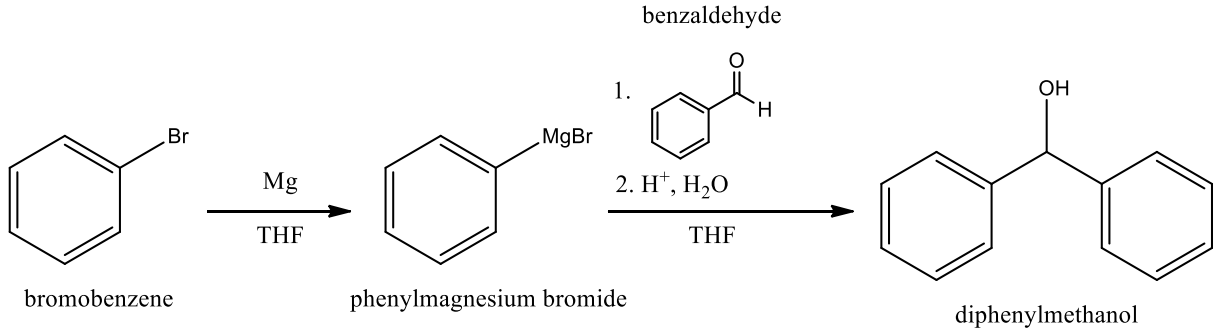

Figure 2: Reaction scheme of the second reaction

This reaction is analogous to reaction 1, only benzaldehyde, an aldehyde, is used in the second reaction instead of acetophenone. As a result, diphenylmethanol is formed. This alcohol, also known as benzhydrol, is used in the perfume, pharmaceutical, polymer and agrochemical industry. In the perfume industry, it is used as a fixative, which equalizes vapor pressures of volatile components. In the pharmaceutical sector, benzhydrol is frequently used in the synthesis of antihypertensive, antihistamines and anti-allergenic agents, as well as histamine H1 antagonists. It is also used as a precursor when making Modafinil, benztropine and diphenhydramine. At last, it is also used in the polymer industry as a terminating group [14].

1.1 PROBLEM STATEMENT

Nowadays, Grignard reactions are usually carried out in large batch and semi-batch reactors [9] [15] [16]. However, carrying out this reaction in this type of reactor involves cooling problems which still cause difficulties to this day. It is well known that the Grignard reaction is a highly exothermic reaction, which causes problems with heat dissipation in large batch reactors. This can make fast and precise temperature control difficult. The problem of the heat dissipation is due to a small contact surface to volume ratio of the large batch reactor [17] [18]. The reagent is dosed into the reactor to reduce this problem. Nevertheless, care must be taken with hotspot formation at the dosing point. As a result, the reagents must be diluted and carefully dosed when added. Because all the products are already in the reactor, all products can react theoretically at the same time. The reaction temperature increases much more than in a CSTR, which is continually dosed. Therefore, the cooling capacity must be greater, leading to a greater cost. Another benefit of developing a continuous-flow process, in this case carried out in a cascade of two CSTRs, is the possibility to produce for days or weeks without having a shutdown of the process. This is completely in contrast with the more frequently used batch setup, where each completed batch needs to be emptied, followed by a thorough cleaning procedure. The time span that covers these steps is dead time in which only costs are incurred, and no product is made. Thereby, the product used to clean each batch is not necessary in those quantities in a continuous-flow process as the CSTR only needs to be cleaned after a process time of weeks. This is ecologically of great value. Furthermore, it is possible that a batch is of lesser quality due to impurities or a human error, and one or multiple additional purification processes must be performed on the whole batch. In the worst case, the batch must be discarded which means lost profit.

With continuous-manufacturing, alterations can be made during the process, preventing high volumes of lost product. In that case, only the product produced during the start-up must be purified if it does not meet the specification. Furthermore, a continuous system takes less equipment, and therefore space, than a batch system. At last, a continuous system can provide more product in less time when working with fast reactions, like the Grignard reaction [19] [20].

In the innovative cascade setup of two CSTRs, the first reactor will ensure the formation of the actual Grignard reagent by adding a continuous flow of an aryl halide, while magnesium is pre-loaded or periodically added into the reactor. At the same time, the formed Grignard reagent is continuously withdrawn from the reactor and transferred to a second CSTR. A solids settling mechanism keeps the magnesium in the first reactor. In the second reactor, the Grignard reagent reacts with a carbonyl compound to form the final product.
A big advantage when using this continuous Grignard reaction, is that only one initiation is required during a run because the reacting and shrinking magnesium can be replenished periodically or continuously with fresh magnesium. The challenge here is to maintain steady-state.

1.2 OBJECTIVES

The goal is to obtain a continuous flow process in a cascade CSTR reactor system. The continuous reactor system is considered successful if the following conditions are met.

- The solids settling system is properly working, thus no magnesium from the first reactor is transported to the second reactor. The ultimate objective is a settling system that is incorporated internally in the first reactor;
- the total yield of the whole Grignard reaction in the reactor system is at least 90%;
- no positive or negative accumulation is observed during the experiments, meaning that the volume of the reactive mixture is constant and the reaction can proceed under steady-state conditions (not taking the decrease of magnesium into account).

1.3 PLAN OF ACTION

To acquire knowledge of the most advanced techniques available, first a literature study is performed, followed by the development of a two CSTR cascade lab scale setup. The reactors are then characterised by defining the residence time distribution. In addition, the initiation of the reactions is also thoroughly studied to obtain a quick and controlled initiation in the experiments.

After these preliminary tests, the cascade of CSTRs is tested. The first reactor, which is responsible for the formation of Grignard reagent from magnesium and the aryl halide, is driven to an optimum conversion by varying residence time, concentration of reagents, feed rate and the ratio magnesium to bromobenzene. Next, the solids settling system is tested and optimized. The most efficient settling system is implemented in the CSTR cascade. Thereafter, the entire CSTR cascade setup is tested with the two different reactions, to get an idea of the performance of the system. This performance consists of two parts: looking if magnesium particles are present in the final product stream, and finding out the total yield of the desired product. In addition, the reactivity of acetophenone (a ketone) and benzaldehyde (an aldehyde) in the Grignard reaction is also studied.

A reaction characterisation was also performed on the formation of phenylmagnesium bromide out of bromobenzene and magnesium. The activation energy, rate constant and order of the reaction could be deduced by testing at different temperatures and concentrations of the starting products.

All samples that are taken while testing, are analysed with High-Performance Liquid Chromatography (HPLC). Firstly, a selection is made of the compounds that should be analysed. Then, a suitable method is set up by searching in literature for standard operating procedures for the used components, followed by further optimization and validation to be able to measure both quantitatively and qualitatively.

2 LITERATURE STUDY

2.1 THE GRIGNARD REACTION

Named after François Auguste Victor Grignard (1871-1935), Grignard reactions are the most widely used organometallic reagents, which are compounds containing a carbon-metal bond. The mechanism was discovered in 1900 and was awarded with a Nobel Prize in Chemistry in 1912.
During the past 100 years, they are used in flavour, food, fragrance, petrochemical and pharmaceutical industries because of their feasibility as a building block for an extensive range of organic compounds [21]. This organometallic reaction can be applied to groups containing polar multiple bonds or some highly polar single bonds, but it is most known as a versatile reaction in the formation of carbon-carbon bonds on ketones and aldehydes [21] [22] [23].

The Grignard reaction consists of 2 steps which will be discussed comprehensively in the following paragraphs. The first step is the formation of the Grignard reagent, as seen in Figure 3.

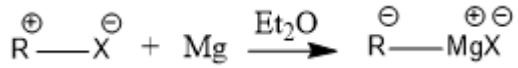

Figure 3: Partial charges during the formation of a Grignard reagent in diethyl ether [21]

In this step, an alkyl, aryl or alkenyl halide is slowly added to an excess of solid magnesium in an organic solvent. Usually, this solvent is diethyl ether or THF, as will be discussed in section 2.1.6 Choice of solvents. Magnesium can be used in different physical forms (powder, turnings...), with each their advantage and drawback. This will be discussed in section 2.1.7 Activation of magnesium.

Afterwards, there is an addition of the organomagnesium compound (Grignard reagent) to the substrate, shown in Figure 4.

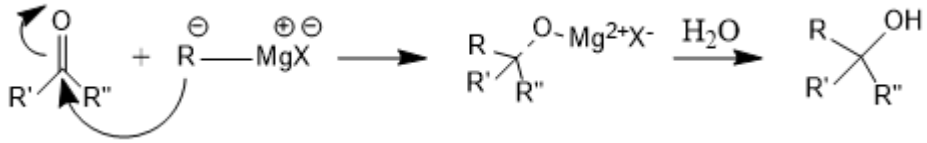

Figure 4: Grignard Coupling [21]

This substrate mostly contains a carbonyl (C=O) bond, but could also be another electrophile like nitriles and epoxides. However, in this Master's thesis, only the addition on ketones and aldehydes will be discussed comprehensively, as this is the type of reaction in the experiments that were carried out.

After a quench with acidified H_2O, it results in alcohols, aldehydes, ketones, carboxylic acids, esters, or amines depending on the substrate used. It is often referred to as the coupling reaction [24].

2.1.1 Formation Grignard reagent

In an organic halide, the carbon atom is attached to a halide, commonly bromide or chloride when using Grignard reactions. The electronegativities of those halides are respectively 2.74 and 2.83, compared to the lower electronegativity of 2.50 for a carbon atom. The greater electronegativity of the halides translates to a higher attraction of the shared electrons. This makes the halide atoms partially negatively charged, or nucleophilic. The carbon atom itself is partially positively charged, or electrophilic [25].
The first step in the formation of the Grignard is initiated by a single electron transfer (SET). The electron originates from the metallic magnesium and transfers to the σ*-orbital of the C-X bond of the

organohalide. Because of this transfer, radical-anion and radical-cation pairs are formed at the magnesium surface, pathway 1 seen in Figure 5.

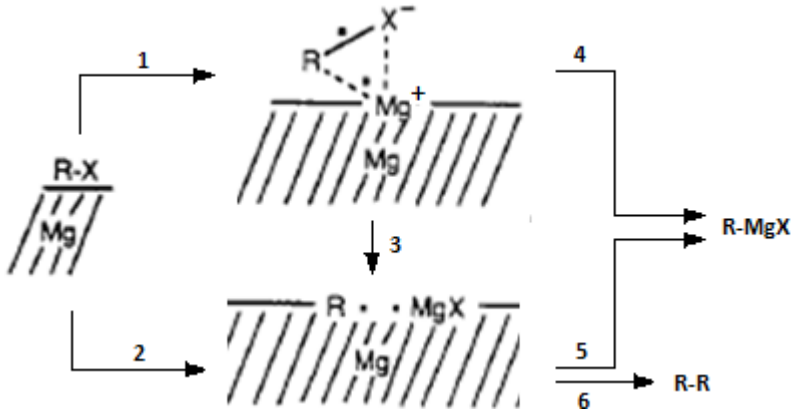

Figure 5: Formation of the Grignard reagent [26]

A second pathway involves free radicals, which could be formed if the radical anion-cation pairs collapse (3) or an inner-sphere electron is directly transferred from the magnesium surface (2). Until this point, there is a general agreement [26] [27] [28] [29]. It was Walborsky and Topolski who discovered that the formation of Grignard reagent didn't occur in the solution after diffusion of Mg^{+}-ions. Instead, the radicals remained largely at the magnesium surface. The formation could be by collapse of the radical anion-cation pair (4) or through combination of the magnesium halide and the radical (5). Further, it is important to know that a R-radical can diffuse and lead to dimer formation (R-R), which is often generalized as Wurtz coupling (6) [26] [30].

2.1.2 Schlenk equilibrium

Although it is widely used, the notation RMgX in Figure 5 is not accurate in describing the solvated aggregate structure, but it is useful for calculations relating to stoichiometry and to illustrate simple mechanisms [21]. However, the formed Grignard reagent experiences an equilibrium which is called the Schlenk equilibrium, as shown in Figure 6.

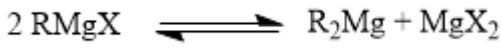

Figure 6: Schlenk equilibrium

As will be discussed in 2.1.6 Choice of solvents, RMgX is favoured when using diethyl ether while in THF all components of the equilibrium are present.

2 RMgX, a dimer in diethyl ether, has an equilibrium as well. As seen in Figure 7, both the R-group and the halogen can bond with the other magnesium atom.

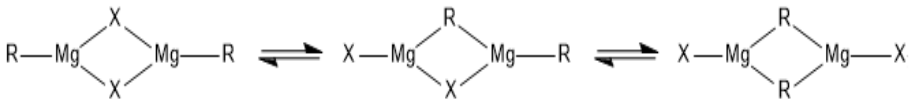

Figure 7: Schlenk equilibrium for RMgX in diethyl ether

Computer calculations verified other reports [31] that the halogen-bridged dimers are the most stable, taking the solvent, diethyl ether, into account. These calculations also predicted that the favoured number of solvent molecules solvated on the Mg atoms is one Et_2O molecule per magnesium [32]. Although Grignard reagents are monomeric in THF [33], two RMgX molecules do form these halogen-bridged dimers as well during the coupling reaction [34].

2.1.3 Coupling reaction: addition of Grignard reagent

The most relevant mechanisms to describe the addition reaction are the polar and SET mechanism. Prior to these mechanisms described by Ashby et al., an aggregated halogen-bridged dimer is formed by combining RMgX and the ketone or aldehyde twice, seen in Figure 8 [35].

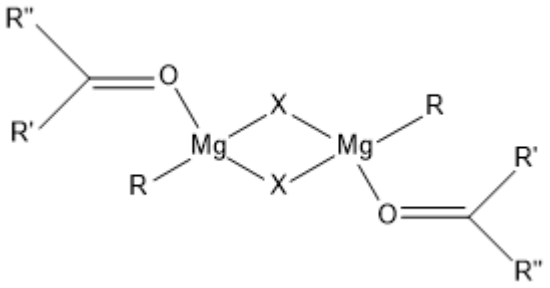

Figure 8: Aggregated halogen-bridged dimer

The present molecule R_2Mg combines with a ketone or aldehyde too, and reacts further with the auxiliary MgX_2, seen in Figure 9.

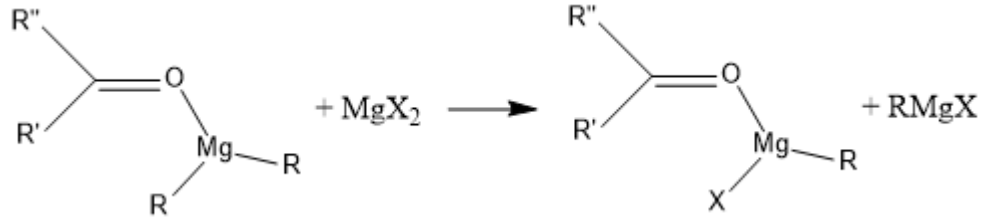

Figure 9: Reaction of R_2Mg and MgX_2

This results in an exchange of a Mg atom and R-group to form a new RMgX reagent and half of the dimer that is shown in Figure 8 [34].

It is also possible that the R_2Mg complex with the ketone doesn't react with MgX_2 and follows the pathways described in 2.1.3.1 Polar mechanism or 2.1.3.2 Single Electron Transfer, but it is proven that the rate constant is negligible compared to the reaction with MgX_2 [34].

2.1.3.1 Polar mechanism

The polar mechanism, a complex first-order reaction suggested by Yamazaki and Yamabe, is mostly favoured by aldehydes and aliphatic ketones [32]. Consequently, this mechanism is applicable for the reaction of benzaldehyde with phenylmagnesium bromide.

In the first step of the process, the dimer of the Grignard reagent reacts with the ketone or aldehyde. Because a 1:1 complex for ketones and Grignard reagent was reported by T. Holm [36], and stoichiometric amount of both reagents are usually enough, Yamazaki and Yamabe assume that the Schlenk dimer reacts with two molecules of the desired ketone or aldehyde, as seen in Figure 10 [32].

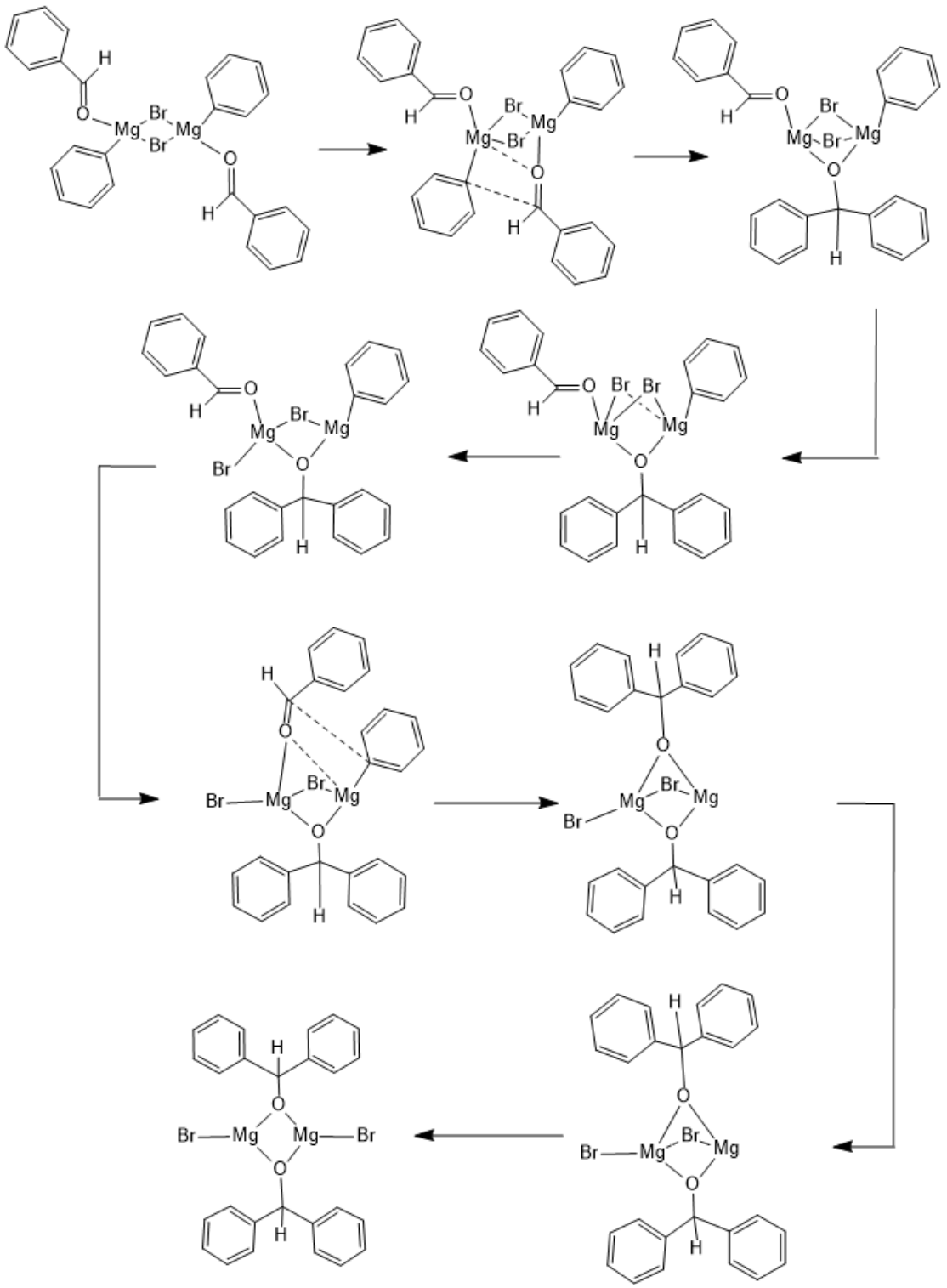

Figure 10: Polar mechanism by Yamazaki and Yamabe, illustrated with benzaldehyde

The oxygen atom, partially negatively charged and with two lone pairs, of each aldehyde (or ketone) is bound to a different partially positively charged magnesium atom. One aldehyde molecule shifts inward and links with the R-group of the second Grignard molecule, in this case the left one. Simultaneously, a link between the left magnesium atom and the oxygen atom of the concerned aldehyde is made. The R-group bonds with the aldehyde, and its oxygen atom is now bonded to two magnesium atoms.
At this point, a Mg-C and C=O bond is replaced by a newly formed O-Mg bond and C-C covalent

bond. It is remarkable that the C-C bond between the aldehyde and the R-group doesn't reside on the same magnesium atom, instead, the R-group of the vicinal magnesium is transferred.

Subsequently, the second addition starts. The triple-bridged trimer opens and one Br-Mg bond breaks. Analogue to the first addition, the remaining R-group is added to the second aldehyde, forming a molecule with four highly stable Mg-O bonds.

The driving force of this reaction is the formation of more stable C-C and Mg-O bonds in comparison to the broken C=O and Mg-C bonds. As examined by Yamazaki and Yamabe, the theoretical bond formation of formaldehyde and MeMgCl has an exothermal energy of 46.9 kcal/mole for the first addition, 44.9 kcal/mole for the second addition. These values are calculated without taking the solvation into account, the actual values would be somewhat lower as a tetravalent magnesium atom has tighter bonds than the solvated pentavalent magnesium atom [32].
Although these values are not valid for the used reaction in this Master's thesis, it does clearly show that the C-C and Mg-O bonds are more stable as the exothermal energy of formation is positive; and thus, the driving force for the reaction.

Surprisingly, when this mechanism applies, the choice of the halogen atom (Br or Cl) has a negligible effect on the reactivity. This contradicts our first instinct to assume that the halogen atom always influences the Grignard reaction [29] [30].

2.1.3.2 Single Electron Transfer

The SET mechanism is favoured by Grignard reactions concerning bulky ketones, like aromatic ketones [32]. Thus, it is applicable for the reaction of phenylmagnesium bromide with acetophenone.

Although different hypothesis exist for this mechanism, in this Master's thesis, the most recent ideas will be explained [32] [37]. The main difference is the monomeric or dimeric character. Yamazaki and Yamabe suggests a dimeric mechanism, similar to the polar mechanism. Only now, the R-group is pushed away as the magnesium atom keeps its tetravalency when the carbonyl oxygen approximates the second magnesium atom [32].

More recently, Bartolo et al. suggested a monomeric pathway for the SET mechanism with a ketyl intermediate, based on older research ([38]). This mechanism is more straightforward, as can be observed in Figure 11.

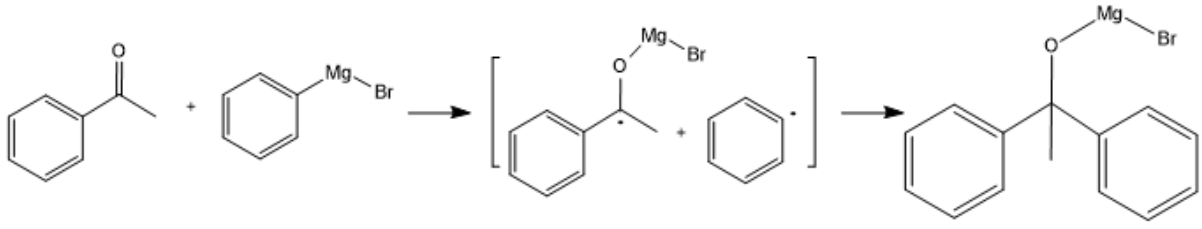

Figure 11: SET- mechanism, as described by Bartolo

First, an electron is transferred to the ketone, and MgBr binds with a lone pair of the oxygen which creates the stable O-Mg bond. The perennial nucleophilic benzene subsequently attacks the formed complex, leading to the end product before acidic quench. For aromatic carbonyl compounds, like acetophenone, the R-group stabilizes the intermediate, making this mechanism acceptable [37] [38].

2.1.4 Hydrolysis

Until this point, the molecule is a complex and the desired alcohol is not yet produced. Therefore, it must be quenched by adding an aqueous acidic solution after the coupling reaction, shown in Figure 12.

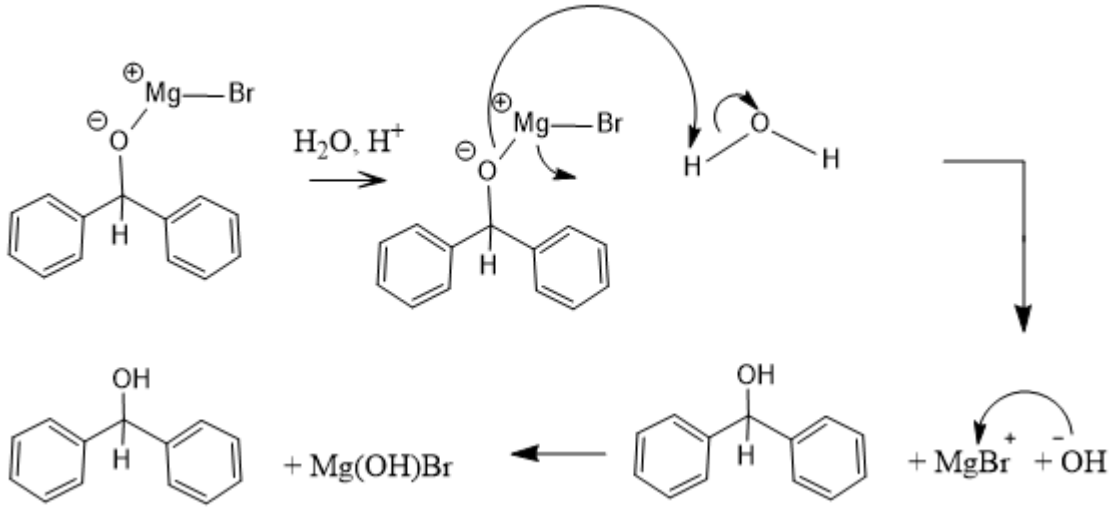

Figure 12: Quench reaction illustrated for the formation of diphenylmethanol

The acidity of water is sufficient, but a stronger acid like sulfuric or hydrochloric acid is added to hydrolyse the complex. The magnesium salts, as a result of quenching, produce a gel which is difficult to manipulate. With (diluted) acids, these basic salts are neutralized and become water-soluble, as illustrated in Figure 13.

$$Mg(OH)X + H^+ \rightarrow Mg^{2+}(aq) + X^-(aq) + H_2O$$

Figure 13: The reaction of the magnesium salt in an acidic environment

With tertiary alcohols, there is a potential risk of dehydration by protonating the alcohol group as the carbocations are relatively stable. The protonated alcohol group leaves the molecule, creating a double bond. To prevent this, a weaker acid should be used. This could be ammonium chloride [21].

The solvent THF could also be protonated by Brønsted acids like HCl and H_2SO_4, which leads to a cationic ring-opening polymerization. This could form a problem for the analysis as the formed alcohols dissolve in water, while the solvated apolar molecules form a different layer. The volume of the apolar layer would be dependent on the concentration of the reagents and products, resulting in a difficult sample preparation on the HPLC [39].

2.1.5 Influence of water and oxygen during the formation of Grignard reagents

Water and oxygen are the most common causes of problems during the formation of Grignard reagent. Therefore, it is important to create the Grignard reagent in an inert, anhydrous setting.
If there is more than 0.02 – 0.05 wt% H_2O, the reaction between Mg and RX will not initiate correctly [40] [41]. Especially the less reactive R-Halides are sensitive to the presence of water.
The induction period caused by H_2O is a danger as it could lead to accidents in the industry. It has happened before that operators were misled and added more RX to initiate the reaction. This results in a sudden, but highly exothermic runaway reaction which should be avoided at all time [21] [40].

The Grignard reagent reacts with H_2O because of the nucleophilic character of the partially negatively charged R-group, seen in Figure 14. The destruction of Grignard reagent can also be caused by alcohols.

$$H_2O + RMgX \rightarrow RH + Mg(OH)X$$

Figure 14: Reaction of Grignard reagent with water

To form the Grignard reagent, the alkyl or aryl halide must dissolve and the magnesium must be activated. When H_2O is present, it is observed that H_2O not only reacts with the formed Grignard reagent, but also inhibits the reaction itself.

In a recent study, Kumasaki et al. concluded that an interference of the removal of the oxide film on magnesium caused the inhibition, caused by quenching or retarding the generated radicals with the present water. This conclusion was made as the generated heat by dissolving was not delayed and the exothermic reaction of H_2O with the Grignard reagent itself would not cause a retarded rise of temperature. They assumed that the speed of removal of the oxide film exceeds the inhibition caused by H_2O when the reaction finally starts, or that the rise of temperature caused by dissolving would vaporize the existing H_2O [40].

Oxygen meanwhile does not delay the reaction, but induces a loss in efficiency by reacting with the Grignard reagent. This rapid reaction with O_2 was already investigated in 1903 by Bodroux and Bouveault.

In the first step, a hydroperoxide salt is formed as intermediate. In the following step, this peroxide reacts with another Grignard reagent to form an oxidized Grignard reagent, as shown in Figure 15 [30] [42].

$$RMgX + O_2 \rightarrow ROOMgX$$

$$ROOMgX + RMgX \rightarrow 2\,ROMgX$$

$$2\,ROMgX + H_2O \rightarrow ROH + Mg(OH)X$$

Figure 15: Reaction of Grignard reagent with oxygen

Perceived side products of phenylmagnesium bromide are phenol, diphenyl ether, and diphenyl-benzene as oxidation products [43].

2.1.6 Choice of solvents

The choice of the solvent is an important decision. Solvents can improve or undermine the chemistry of the Grignard reagent. The solvent itself cannot react with the reagent, it must be apolar protic or non-polar, because polar protic solvents could protonate the Grignard reagent. The most important consideration of all is the safety or hazard that comes with the solvent.

The Schlenk equilibrium, seen in Figure 6, is one of the possible compositions of the Grignard reagent and is accepted for concentrations up to 3.5 M in THF when X = I, Br or Cl [32]. However, when using diethyl ether and X = Cl at all concentrations, the dimer composition is more accurate [34]. In THF, all three components RMgX, R_2Mg and MgX_2 are present With a K_s value of 0.27, defined as $K_s = \frac{[RMgX]^2}{[MgX_2][R_2Mg]}$ [44].

As discussed before, RMgX is a polar molecule. To keep these molecules in solution, a coordinating solvent is needed. Ethereal solvents have a hetero-atom with lone-pare electrons to coordinate the magnesium which makes solubilization in organic media possible [30].

In the industrial processes that involve Grignard, diethyl ether was mostly used after considering these necessities. Nowadays, it is partly traded in for THF. The main reasons are the greater boiling point of THF, a higher flash point and a greater solvating power. Therefore, reactions can take place at more elevated temperatures, and a lower fire-hazard is obtained [33] [34] [45]. On top, the formation of Grignard reagent is more stable as it stabilized by four molecules THF per magnesium atom in comparison to only one molecule of diethyl ether [30] [46].

2.1.7 Activation of magnesium

The chemical or physical activation of magnesium is a crucial step during the Grignard formation. If the addition of halide is started before the magnesium is activated, an accumulation of halide can lead to a runaway reaction when the Grignard formation does start to form. The initiation is after all these years of large-scale use still a part of the process that can be improved. An important factor in the activation is the form of magnesium itself. Each physical form has its own advantages.

Magnesium powder is more reactive, as the surface area to volume ratio is higher. The drawback is the quick oxidation and the pyrophoric surface. Turnings have a decent surface area to volume ratio and are easy to handle, but they can damage glass-lined reactors. Magnesium chips have the lowest reactivity on the downside, but their benefit is their greater purity. At last, highly reactive Rieke magnesium, acquired by the reduction of $MgCl_2$ with potassium in anhydrous THF, is very pyrophoric and the potassium metal is difficult to handle on large scale [47].

The most frequently used techniques to activate magnesium will be discussed in the following paragraphs.

2.1.7.1 Iodine

To activate magnesium and improve its reactivity, iodine can be added in the mixture under reflux conditions. This chemical activation was introduced by Grignard. It may not be the most effective method, with initiation periods of 1 to 1000 sec, but it is a quick and simple method [45]. A big advantage is the change of colour when iodine reacts with magnesium as a catalyst, turning the yellow colour into a transparent colour [29] [47].

2.1.7.2 Iodine vapour

The added iodine can be heated as well. Eckert explored the influence of iodine vapour. This method is a simple variant of the normal iodine addition. The difference is that iodine and magnesium is added prior to flame drying. The iodine will sublime, purple vapor will spread in the reactor and activate the magnesium surface. It was found that the initiation time was decreased, and less random upon application of this additional procedure [48].

2.1.7.3 1,2-dibromoethane

Later, 1,2-dibromoethane replaced iodine as an activator as it was deemed more reliable. In THF, a temperature of 50-55 °C was recommended. This means that reflux was no longer necessary. Although this method was more reliable, it still had issues with initiation on pilot scale and therefore this is this method not the ideal solution as well [21] [47].

2.1.7.4 Mineral acid

The available surface area can be increased by removing the oxide layer. To achieve this, the surface is washed with a mineral acid. The downside is the removal of acid and water. Especially the water poses a problem with the formation of Grignard reagent, as discussed in 2.1.5 [21] [47].

2.1.7.5 Dry stirring

It is reported that dry stirring was a promising technique. The magnesium is stirred during at least one day in an inert nitrogen atmosphere in advance. Although this activation technique resulted in a near complete reaction, it is not realistic to use in an industrially-scaled reactor. However, it is not time efficient and in order to adequately stir the magnesium, the stirrer needs to be very low in the reactor, the glass inside the reactor could be damaged [21] [47] [49] [50].

2.1.7.6 Equipment drying

It is self-evident that dry equipment is necessary. On laboratory scale, this is easily achieved. On commercial scale it is difficult due to the complex piping and large equipment. Multiple solvent rinsings, and dry-blowing with an inert gas is advised [47].

2.1.7.7 Grignard reagent

To initiate the reaction very effectively, a small dose of previously formed Grignard reagent can be added. The Grignard reagent dries the system by reacting with water. In addition, there are no new molecules introduced with this method, which means that only previously-existing impurities are a concern. The added Grignard reagent must be checked if it meets the specifications [47].

2.1.7.8 DIBAH

At last, 1 mole% diisobutylaluminum hydride, DIBAH, can be added to react with the moisture, alcohols and peroxides as a reducing agent. In a research of Tilstam and Weinmann appeared that the initiation and formation of the Grignard reagent could be implemented at room temperature, and even below, making it a safe and energy-efficient method [47].

2.1.8 Parameters

A reaction is influenced by numerous parameters. Some may cause more side products, others may accelerate the reaction in general. In this Master's thesis, four parameters were altered to optimize the reaction.
These parameters include the concentration, temperature, the ratio of magnesium to bromobenzene, the ratio Grignard reagent to ketone or aldehyde and the residence time.

2.1.8.1 Concentration and temperature

The reaction kinetics will be discussed in the section 2.2 Reaction kinetics. After reading that section, it will be clear that with an increasing concentration, resulting in an increased temperature for exothermic reactions like the Grignard reactions, the reaction rate will increase as well. Because more molecules are present, more collisions occur, making a collision that leads to a reaction more frequent. When the temperature increases, the molecules gain more kinetic energy. Like the increasing concentration, this too leads to more collisions. These two reasons ensure that more product will be formed in less time [51] [52].

A consequence is that the selectivity of the reaction descends with a greater reaction rate. This benefits Wurtz coupling, an unwanted side reaction. Although the reaction rate increases, this doesn't translate in a higher yield of the desired product. Furthermore, a Grignard reaction is exothermic, causing a shift of the dynamic equilibrium to the side of the reagents to counteract an increment of temperature [53].

2.1.8.2 Ratio magnesium to bromobenzene

It has already been established that both the concentration of bromobenzene and the surface area of magnesium influence the reaction rate. However, a kinetic study concluded that the influence of magnesium was constant if a sufficient amount of magnesium (two times the concentration of bromobenzene) is present, higher ratios of magnesium to bromobenzene resulted in minimal change to the reaction rate [54].

2.1.8.3 Ratio Grignard reagent to ketone or aldehyde

In the subsequent reaction, it is favoured that the ratio Grignard reagent to ketone or aldehyde is preferably 1:1. Research showed that a ratio beneath 1:1 resulted in no side products for the reaction of CH_3MgBr with 2-(N-methylbenzyl)pyridine (2-MBP) in ether at room temperature. When ratio's greater than 1:1 were implemented, more side products were formed with the increase of Grignard reagent and/or decline of ketone/aldehyde [34].

2.1.8.4 Residence time

The residence time is straightforward, the yield increases as the residence time increases. However, the rate of increment in yield lowers as the reaction progresses. It is important to know at what point it is not beneficial to continue the reaction as a full conversion is reached. That point should be the set as the residence time [55]. More information about the residence time can be found in 2.3 Ideal chemical reactors and solids settling system and 2.4 Non-ideal flow in CSTRs.

2.1.9 Reactivity Halide and R - group

Starting with the halides, I, Br and Cl are possible for Grignard reagents. With a respectively augmenting electronegativity, the polarity of the carbon-magnesium bond increases. This results in a greater reactivity. Cl has the highest electronegativity, I the lowest. Therefore, RMgCl will be the most reactive, yet less selective than RMgBr or RMgI. The importance of the selectivity or reactivity should be evaluated to choose a suiting halide [30].

Grignard reagents are strong bases. In general, a carbanionic reagent is more reactive when the pKa of the conjugated acid increases. An increasing p-character, (sp<sp2<sp3), will affect its reactivity positively as well. Another property that affects the reactivity are steric requirements. A larger, bulkier reagent will decrease the reaction rate considerably [30] [34].

2.2 REACTION KINETICS

Reaction kinetics are useful to determine the reaction rate, and therefore the desired residence time (see section 2.4 Non-ideal flow in CSTRs), the rate constant k and the activation energy for a reaction.

In general, the reaction rate ($mole*l^{-1}*min^{-1}$) is in function of the concentration of the reagents, seen in the equation below. [A] and [B] are respectively the concentrations of a reagent A and B in mole/l, with a and b are coefficients that determine the influence of the reagents. The sum of a and b is called the reaction order and k is the rate constant in $min^{-1}* (mole/l)^{-(a+b-1)}$.

$$-r_a = k[A]^a[B]^b$$

The rate constant itself is defined by the Arrhenius equation below, where A is a pre-exponential factor, also referred to as k_0. E_a is the activation energy in J/mole, R the gas constant in $\frac{J}{mole*K}$, and T the temperature in K [55].

$$k = Ae^{-E_a/RT}$$

With these two equations, it is evident that the reaction rate is dependent of both concentration and temperature.
When forming the Grignard reagent phenylmagnesium bromide, the reaction rate is dependent on the halide concentration and the surface area of the magnesium particles, as can be seen in following equation:

$$-r_a = k[RX]S_{Mg}$$

With S_{Mg} the surface area of magnesium in m².
However, with a sufficient molar excess of magnesium turnings (1 or more), the surface area of the magnesium turnings is of pseudo zeroth-order as the active surface area can be considered constant, resulting in following equation [54]:

$$-r_a = k[RX]$$

The coupling reaction of Grignard reagent to the ketone or aldehyde is a second-order reaction, present with the accompanying equation [33] [56]:

$$-r_a = k[RMgX][\text{R}\overset{\text{O}}{\overset{\|}{\text{C}}}\text{R}']$$

2.3 IDEAL CHEMICAL REACTORS AND SOLIDS SETTLING SYSTEM

Since a reaction is carried out in this Master's thesis, the necessary knowledge must also be acquired about chemical reactors in which this reaction takes place. In this way, the right reactor type can be chosen to design a continuous-flow reactor system for a complete Grignard reaction.

First, the most common reactors currently used in the industry are discussed. These are followed by the advantages and disadvantages of the reactors, together with their most common areas of application. Finally, the known literature about a solids settling system is discussed.

2.3.1 Types of reactors

The most common option to classify reactors is by looking at the mode of operation [57] [58] [59] [60]. In Figure 16, the different types of reactors are shown, which will also be discussed further in the paragraphs below.

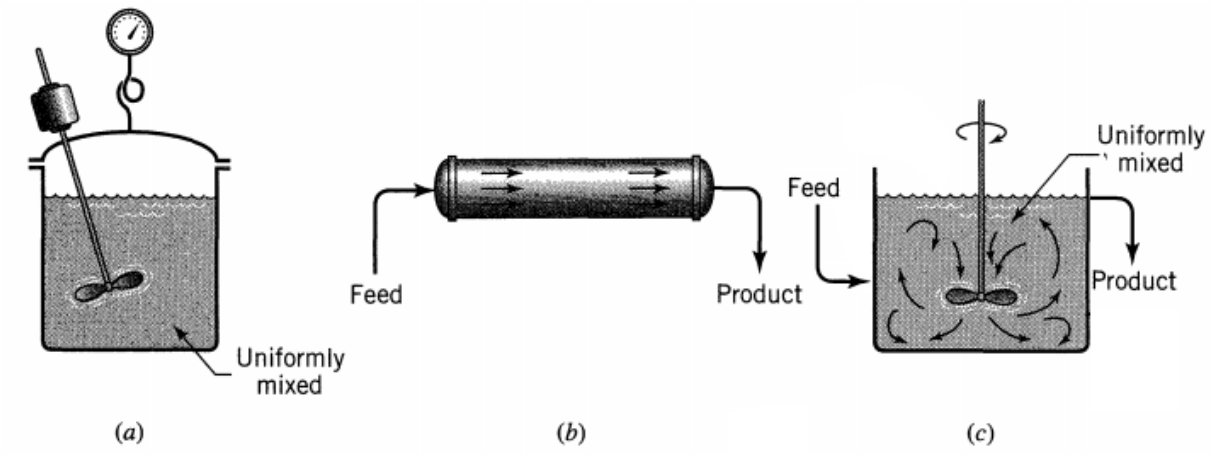

Figure 16: Chemical reactor types (a) Batch reactor; (b) Plug flow reactor (PFR); (c) CSTR [61]

With this way of classification, three types of chemical reactors are subsumed: the batch reactor (no flow), PFR and CSTR. These last two are continuous-flow (steady-state flow) reactors, where as much material enters the reactor as goes out. In these three types of reactors, a homogeneous or heterogeneous reaction can be carried out.

2.3.1.1 Batch reactor

The reaction vessel (a) in Figure 16, also called the agitated batch reactor, is the simplest reactor in the chemical industry. Nowadays, it is mainly used for small scale laboratory experiments and to produce

small volumes (in comparison with the bulk chemical industry) or fine chemicals, such as API's, dyes and pigments, agrochemicals and flavours [61] [62] [63] [64]. Fine chemicals all have their own (often complex) synthesis method, so the production time can be very diverse for the different substances. A batch reactor can provide this much needed flexibility, with a large product variety as a result. Further, this reactor does not need complicated equipment [59]. In Figure 17, a batch reactor system is shown.

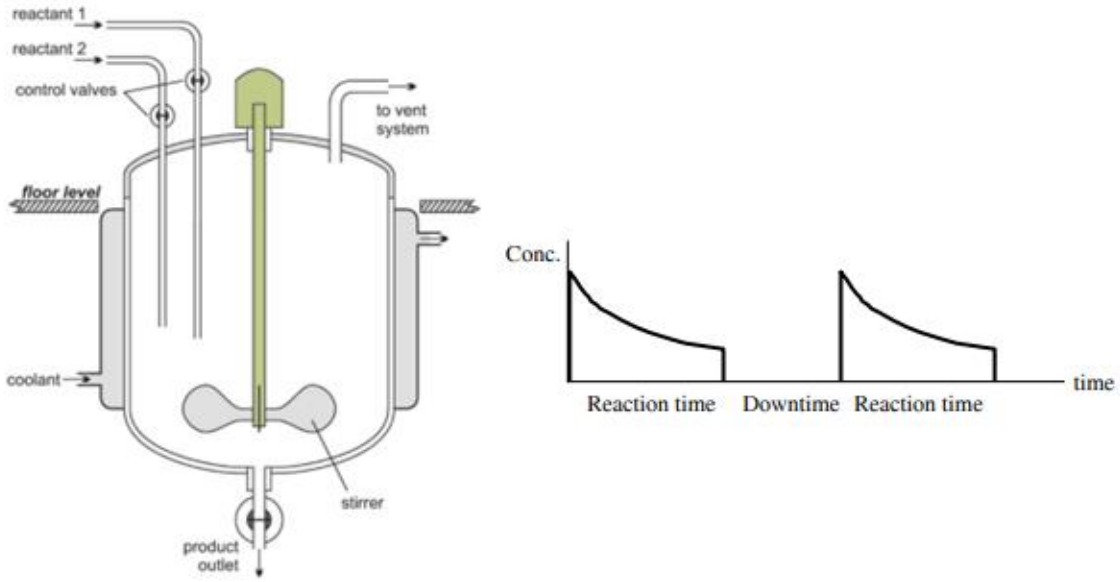

Figure 17: A typical batch reactor (Left) and a timeline of batch operation (concentration of reagent versus time) (Right) [65]

The batch reactor consists of a reaction vessel equipped with a stirrer that ensures uniform mixing. They are filled with feed lines which fill up the reactor before the reaction takes place. After filling, the mixture is parametrized to reaction conditions and reacts for a certain amount of time, called the reaction time *t*. In this type of reactor, the composition changes over time. Often, cooling or heating of the reactor is needed due to exothermic or endothermic reactions to maintain the desired reaction temperature. Hereafter, the reaction mixture is drained through the product outlet, followed by purification steps that lead to a pure product. Before performing the next batch, the reactor is thoroughly cleaned. This last step, along with filling and emptying, is called the downtime, seen on the right figure. This discontinuous production is also the biggest disadvantage of the batch reactor, and is also one of the reasons why companies consider and implement the switch to a continuous process [59] [65].

Semi-batch or unsteady-state reactor

A variant of the batch reactor is the semi-batch reactors (unsteady-state flow). In this type, the volume and/or composition of the reaction mixture can be changing. An example of a semi-batch reactor is shown in Figure 18.

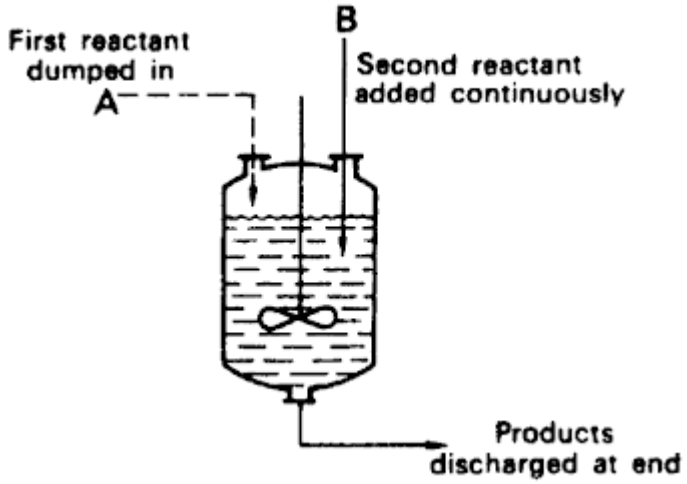

Figure 18: Semi-batch reactor [57]

A general production cycle when operating a semi-batch reactor consist of filling the reactor with the first reactant A, after which reactant B is added continuously with a feeding program that fits best with the reaction that is carried out. After the conversion of desired product is reached, the reactor is discharged, followed by cleaning and filling of the reactor. Then, the following reaction can proceed [57] [60] [66].
However, semi-batch reactors can also operate when product is continuously withdrawn, while one reagent is constantly added and the second reagent is preloaded. In this case, the composition in the reactor is constantly changing [61]. This is in difference with the continuous reactors, where the composition is always the same in a certain point of the reactor.

This type of reactor is frequently used in fine chemical industry (such as pharmaceutical processing), biotechnical processes, gas-liquid reactions and by-product sensitive reactions. Highly exothermic reactions, such as the Grignard or nitration reaction, are also carried out in semi-batch reactors. By controlling the feed rate of one reagent, not all heat is released at once, and thus the reaction does not run out of control [57] [63].

In addition to the advantages that this system gives to the above reaction types, this type of reactor is also a flexible system, analogue to the batch type reactor. However, it has the same disadvantage, which is the downtime for emptying, cleaning and filling after each completed reaction [61] [63]. It is especially good when producing on a small scale, but a high output often is difficult to achieve [63] [66]. The unsteady-state operation makes it more difficult to analyse the progress of the reaction, and often a more complex control and feed strategy is necessary [61]. Due to those complexities, the operation cost of semi-batch reactors is mostly higher than batch operation [63].

2.3.1.2 Continuous-flow or steady-state reactor

The second type of reactors are those where a continuously reagent flow is introduced into the reactor while a product flow is withdrawn [59]. In those reactors, no accumulation occurs during their operating time. It is mainly used for industrial activities, when rate of reaction is high and large-scale production is needed. Examples are the oil, food, bulk chemical and polymerisation industries [57] [59] [61] [63]. The two ideal types of continuous-flow reactors are the CSTR and PFR [58] [67]. However, combinations can be made from these two types of reactors, such as a CSTR in series or a CSTR followed by a PFR [57] [63].

When characterizing continuous flow reactors, the term residence time τ is often used. It is the time needed to treat one reaction volume of incoming feed [59] [68]:

$$\tau = \frac{V_{reaction}}{v_0} \xrightarrow{Constant\ density} \tau = \bar{t}$$

With $V_{reaction}$ the volume of reaction material in the reactor, and v_0 the volumetric flow rate of the feed in m³/min. Often, the mean residence time $\bar{t}$ is also used which defines how long a particle stays on average in the reactor. If density of the reaction mixture can be assumed constant (as in this Master's thesis), τ and $\bar{t}$ are identical to each other [68].

When operating those continuous flow models, they all follow the same timeline of operation, as given in Figure 19.

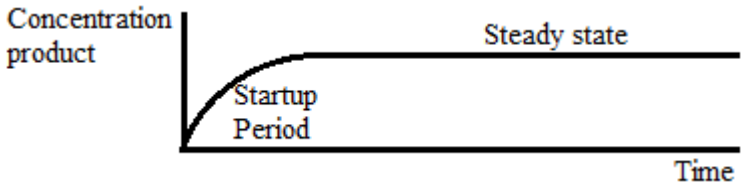

Figure 19: Timeline of continuous-flow operation (concentration of desired product versus time) [63]

Continuous-flow manufacturing is a process which converges to steady-state after a start-up period. After this start-up period, which usually lasts 4 residence times, a constant concentration of outgoing product is accomplished if the system's parameters and feed remain constant. At a certain point in the reactor, the same reaction rate is always maintained.

Throughout this Master's thesis, advantages of the continuous versus the batch process already have been cited in the section 1 Introduction. These will not be discussed again in this paragraph. However, a brief overview of the general advantages and disadvantages of these two operating modes is given in Table 1 [57] [63] [64] [69].

Table 1: (Dis)advantages of batch and continuous operating mode

Batch operating mode	**Continuous operating mode**
Disadvantages	*Advantages*
Downtime (emptying, cleaning and filling) between batches	No downtime, only start-up procedure (Reduced waste and gain of time)
High operating cost	Low operating cost (automatic process control and no filling, cleaning, emptying…)
Buffering required when downstream processes are continuous	Easy coupling with continuous downstream processes
Variating product quality with each batch	Better and more consistent product quality
	Suitable for long production runs

Advantages	*Disadvantages*
Very flexible when more products should be made	Low flexibility, process often optimised for one product
Low capital cost	Higher capital cost
More suitable for small production volumes	

In the next three paragraphs, the two ideal reactor models (Continuous Stirred Tank Reactor and Plug Flow Reactor (PFR)), as well as the Cascade of CSTRs will be explained in more detail.

Continuous Stirred Tank Reactor

The first ideal continuous model, the CSTR, is an agitated reaction vessel where reactants are continuously entering the reactor, and reacted material (sometimes with a fraction of unreacted reactants) is being withdrawn, as can be seen in Figure 20 [57] [67].

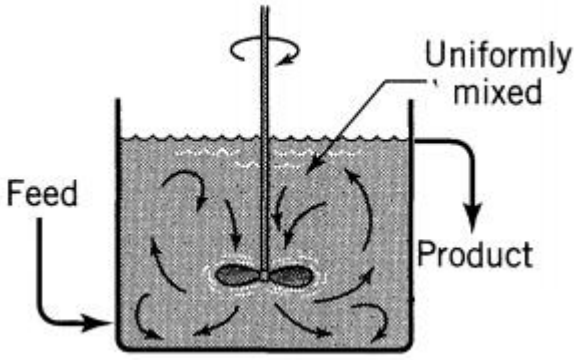

Figure 20: CSTR [67]

What characterises this type of reactors is that all incoming reactants are instantly mixed throughout the whole reactor volume, resulting in a uniform composition where concentrations are the same at every point [59]. It is therefore assumed that the outgoing flow has the same composition as in the reactor itself. This flow model is called *mixed flow* [67]. This model and its non-idealities are discussed further in 2.4 Non-ideal flow in CSTRs.

The CSTR is mainly used for homogeneous liquid-phase and heterogeneous reactions, when thorough mixing is needed [57] [59] [64]. They are used in biological processes (e.g. fermentation), the pharmaceutical industry, continuous polymerization, sulphonation and nitration processes, as well as explosives and rubber processing [64] [70].

There are several advantages that make the use of a CSTR very attractive [64]. It is known for its simplicity of construction, together with openness of construction, making the inside of the reactor easy to clean. This can be a decisive factor in a continuous process where deposition of material can occur, such as polymerization processes that form tarry material. Furthermore, the temperature in a CSTR can also be easily controlled during processing due to the reagents feeding directly into the large agitated reactor volume which consists of partially reacted material. This way, hotspots can also be avoided, which can reduce the formation of side products.

However, a large disadvantage is observed when operating a CSTR. Nearly always, a bypassing loss is present [57] [64]. Here, a part of the unreacted product entering the reactor immediately finds its way back out, causing a loss of conversion. This is especially undesirable when high conversions are needed, for example when working with harmful intermediates.

Cascade of CSTRs

A solution to the bypassing loss can be found in the application of multiple (2 or more) CSTRs in series, as showed in Figure 21 [57] [59] [63] [64].

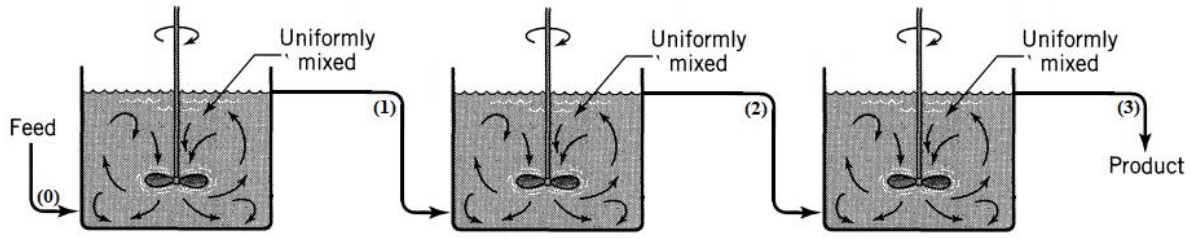

Figure 21: Setup of 3 CSTRs in series [59]

In this setup, the outlet of the first reactor is connected to the inlet of the next reactor (1), so that the remaining initial product can react in the next CSTR, which limits the bypassing losses when using one CSTR. This principle is repeated once again, and the last output flow (3) contains the desired reaction mixture with the desired conversion, while keeping each reactor at a steady-state. This sequential reaction of residual initial product from the previous reactor results in a stepwise conversion, which increases between the successive reactors [64]. In this way, high conversions can be achieved.
CSTRs in series are mostly used in biochemical processes which need a longer reaction time, such as nitrification, denitrification, wastewater treatment and biogas production [71] [72]. It is also used to prepare desired compounds that are made in several reaction steps in a continuous system. This way, each reaction can take place in a different CSTR, without obstructing the continuity.

Often, this type of reactor setup is chosen for its ease and cheapness of construction [64]. As long as the CSTRs do not have extreme requirements, such as high pressures or special materials, this system is milder in terms of price on an industrial scale compared to the PFR, which will be discussed in the next paragraph. The disadvantage of a cascade CSTR implies that the average reaction rate is not as fast as in a PFR in most cases [64]. As a result, the reactor volume is often quite large compared to a PFR with the same output. Mostly, this is compensated by the low cost of a cascade CSTR, as quoted above.

Plug Flow Reactor (PFR)

The second ideal continuous reactor, is called the PFR or unmixed reactor, which can be seen in Figure 22 [67].

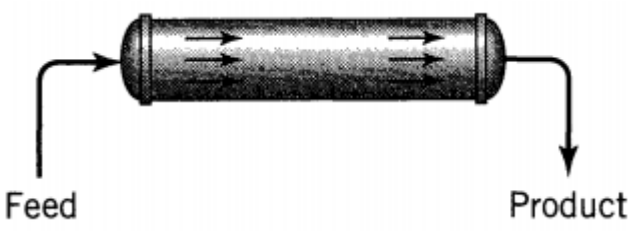

Figure 22: PFR [67]

The reactor can be compared with a tube in which reagents are initially added, then react until the correct conversion is achieved, and then are withdrawn from the tube outlet. It operates with a flow pattern, which is often referred to as *plug flow* [57] [58] [67]. In this model, the flow through the reactor is divided longitudinally in fluid elements. These elements may not show mixing along the longitudinal direction, while lateral mixing may occur. In principle, each fluid element can be represented as a separate batch reactor, whose composition changes as this element moves through the reactor. The requirement in this reactor is that each element has the same residence time: otherwise different compositions are obtained at the reactor's outlet. However, PFRs will not be explained in detail, since they will not be used in this Master's thesis.

2.3.2 Solids settling system

One of the main objectives in conducting this Master's thesis is to design an effective solids settling system which ensures that no magnesium is carried over to the consecutive segments of the reactor design. Specifically with the Grignard reaction, the transfer of magnesium would cause problems because magnesium creates hydrogen with the aqueous quenching. This system could also be used in other projects where particles (not specifically magnesium) should be kept in a reactor.

When searching in literature, a promising design was found. This system consisted of a settling pipe and a solids (magnesium) trap in series, of which the last one is shown in Figure 23.

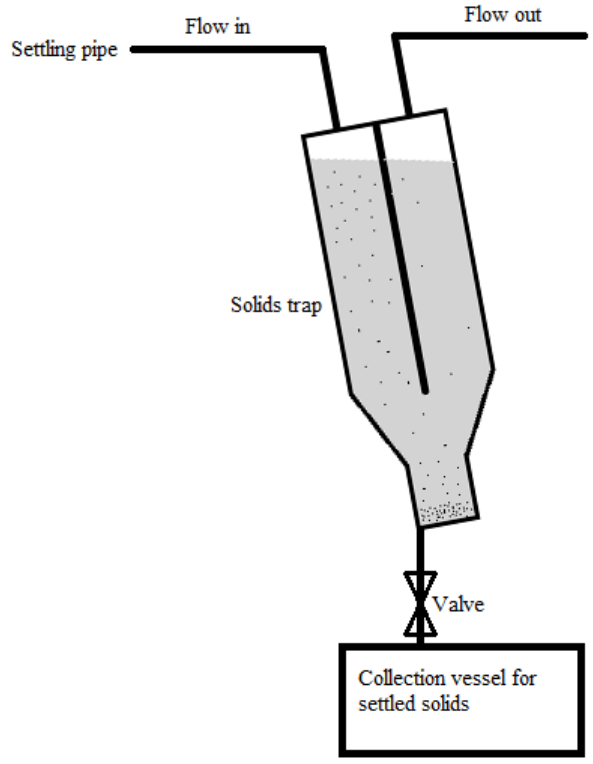

Figure 23: Solids trap

This solids trap is in fact a sedimentation basin for magnesium that was not settled by the settling pipe. At the bottom, the heaviest particles collect in the funnel shape. At the top right, a stream is then extracted that contains fewer and less heavy particles. When the solids trap starts to fill up, a valve can be opened at the bottom to drain the solids into a collection vessel [73].

The settling pipe (which is positioned before the solids trap) works through the power of gravity to hold the magnesium in its reactor [73]. This design is shown in Figure 24.

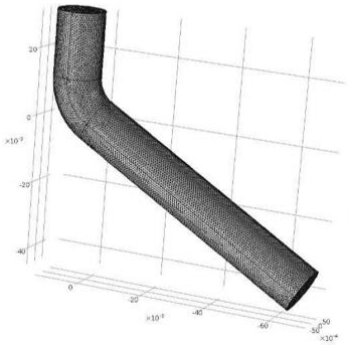

Figure 24: Settling pipe design [73]

A large amount of research and simulations were done to achieve this design, and it could therefore be a starting point for the settling pipe used in this Master's thesis. The angle of the settling pipe was determined by carrying out simulations at different angles with a fixed tube diameter, 60° was found to be the most satisfying [73]. Angles bigger than 60° were found unsatisfactory due to difficulties removing the settled magnesium particles back into the CSTR with gravity.

Furthermore, three different scales of reactors were tested, which are shown in Table 2.

Table 2: Testing parameters on three different scales [73]

	2 l reactor	30 l reactor	Commercial reactor (100 l)
Reactor diameter (mm)	140	400	508
Reaction volume (l)	1.01	23.4	48
Settling pipe inner diameter (mm)	14	38	50.8
Bend angle (°)	60	60	60
Vertical tube height to bend (mm)	42	111	141
Angled tube length (mm)	73	192	244
Flow rate (ml/min)	17	390	800
Average particle size found in Mg trap (µm)	6	/	/

These testing parameters can be useful when scaling is needed in this Master's thesis, to get a first impression on how the settling tube or other variations should be dimensioned.

The position of the settling pipe in the reactor was examined as well. This to ensure that the magnesium particles are not pushed into the settling pipe, which could disrupt the operation of the settling pipe. Through simulation, the velocity vectors in a tank reactor were calculated when mixed with a retreated curve impeller, as shown in Figure 25.

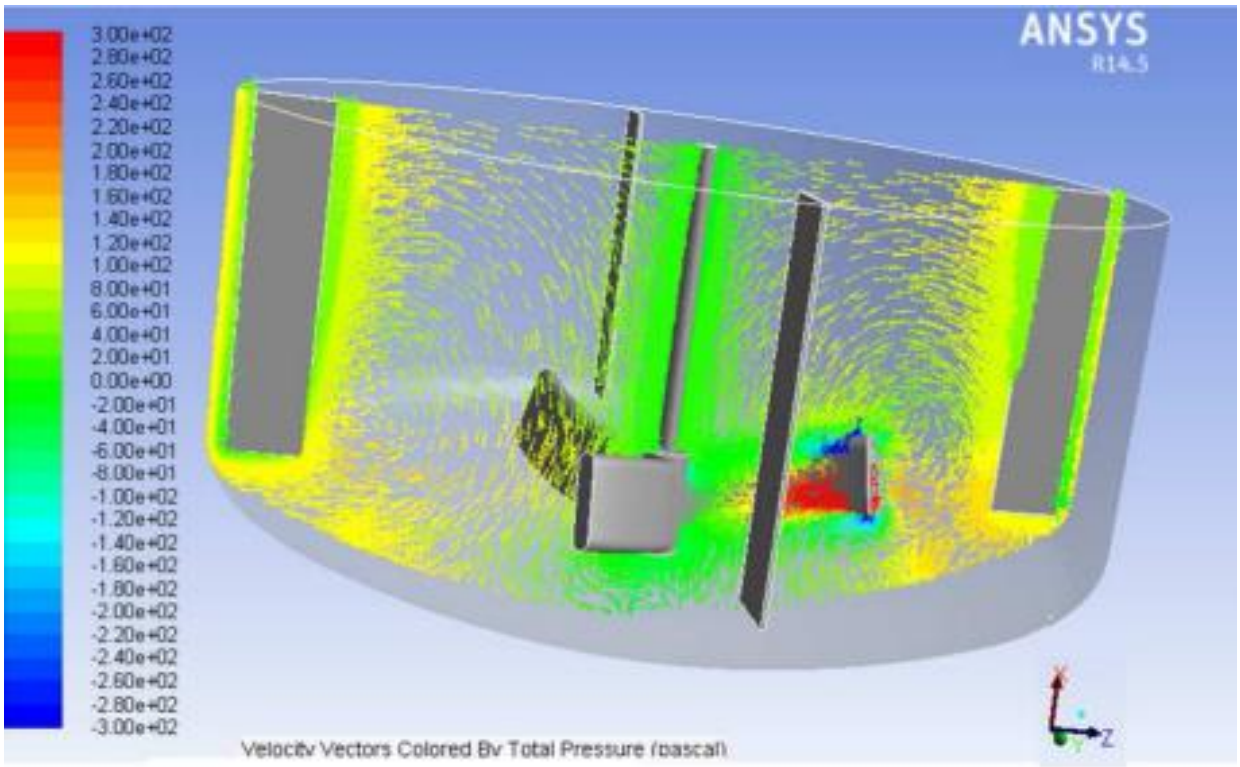

Figure 25: Velocity vector simulation in a tank reactor with retreated curve impeller (coloured by pressure in pascal)

It became clear that there were 2 positions that least hindered the operation of the settling pipe depending on the type of mixing. When no vortex was present, the best position for the settling pipe was above the agitator, away from the flow direction, to avoid that particles were pushed in. When a vortex was present, it is best positioned towards the reactor wall [73].

2.4 NON-IDEAL FLOW IN CSTRS

Since in this Master's thesis research is being performed on a setup with two CSTRs in series, it is important to know the residence time and the residence time distribution of those reactors. For the complete description of the reactor setup, reference is made to the section 3.2.5 Cascade CSTR setup. If the flow pattern and reaction kinetics are known, an estimate of the reaction conversion and reaction efficiency can be made. If necessary, reactor parameters can be adjusted to increase it. It should be clear that understanding the non-ideal flow in this reactor setup is critical to create as perfect as possible reaction conditions [74].

When speaking of non-ideal flow in an CSTR, a mixed flow pattern is assumed [75] [76]. However, the ideal model of mixed flow cannot be used for the characterisation of most practical setups, since practical equipment deviates from this ideal (theoretical) flow pattern, as explained in 2.4.1 RTD in one CSTR. When looking at mixed flow, the RTD and the state of aggregation are reviewed to indicate the deviation [77] [78].

The RTD provides insight into how long the individual molecules are remaining in the CSTR. It is in fact the distribution of the different residence times. In practice, these data are obtained by performing a simple step or pulse experiment. The RTD will be discussed further in the next paragraphs: 2.4.1 RTD in one CSTR and 2.4.2 RTD in cascade .

The second term, state of aggregation, questions if a macro- or microfluid is used. Liquids in motion are in a certain physical state, such as dimers or trimers depending on its natural properties. In the setup that is used in this inquiry, the first CSTR operates as a two-phase system (solids and fluid) and is therefore considered as macrofluid. Due to the solids present, there will be deviations from the ideal CSTR behaviour, which will be discussed later in section 4.4. As the second CSTR contains only fluids with low viscosity, it is taken as microfluid reactor.

When conducting a step or pulse experiment to determine the RTD, a nonreactive tracer is used in most cases [79]. In addition to being nonreactive, the tracer should be easily detectable, soluble and have similar physical properties as the reaction mixture that will be used [80]. There are three kinds of tracers, depending on their state of aggregation. Gas tracing can be conducted in gas-only, gas-liquid and gas-solid systems. These tracers usually are measured with photo-ionization, infra-red or thermal conductivity detectors. Commonly used gas molecules that could meet the conditions of a suitable tracer are: Propylene, propane, ethane, helium, hydrogen and carbon dioxide. Liquid tracing is fit for both liquid-only and liquid-solid flows. Frequently, a conductivity probe is used with a conducting tracer like KCl or NaCl, where the relationship between conductivity and concentration is considered linear at low concentrations [81]. Alternatively, a fluorescent dye solution can be introduced and traced with laser illumination [82]. It is also possible to measure radioactive tracer particles, as was applied to a study, by Lin et al., of the hydrodynamics of a commercially scaled circulated fluidized-bed boiler [83]. Lastly, solid tracers can be used in gas-solid reactors, mostly fluidized bed reactors. The solid particle tracers are UV phosphorescent-dyed and get charged by ultraviolet illumination or are dyed by a visible colour to trace visually [78] [84]. This paper only focusses on liquid tracers, as they are the most suitable in the used setup.

In both a step or pulse experiment with a conductivity detector and conducting tracers, a certain amount of a tracer, with a known conductivity, consequently a known concentration C_{max}, is injected [79]. A summary of the pulse experiment is given in Figure 26.

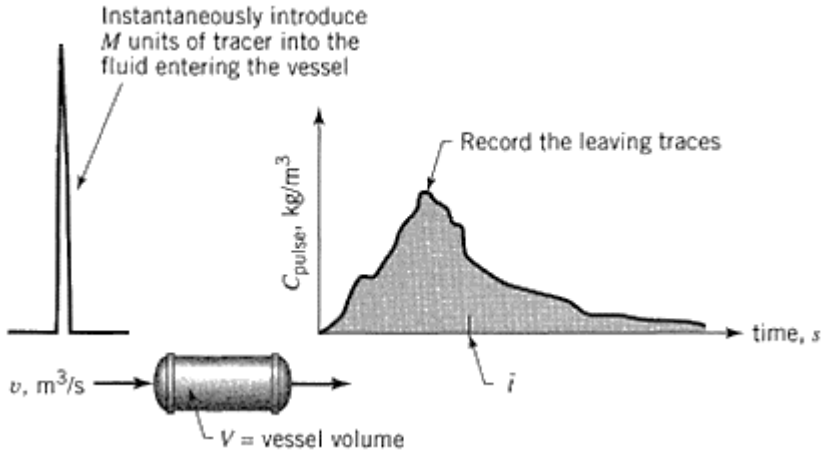

Figure 26: Implementation and results of a pulse experiment [79]

In this pulse experiment, all tracer is injected in a short period of time, as seen on the left side of Figure 26. The particles each have a different residence time inside the reactor, which has a volume V in m^3 and flow rate v in m^3/s. After the injection, the outlet tracer's conductivity or concentration is measured versus time, which results theoretically in a Gauss curve after dispersion [85]. In reality, the curve can be more irregular, seen on the right side in Figure 26.
In Figure 27, the implementation of a step experiment is shown.

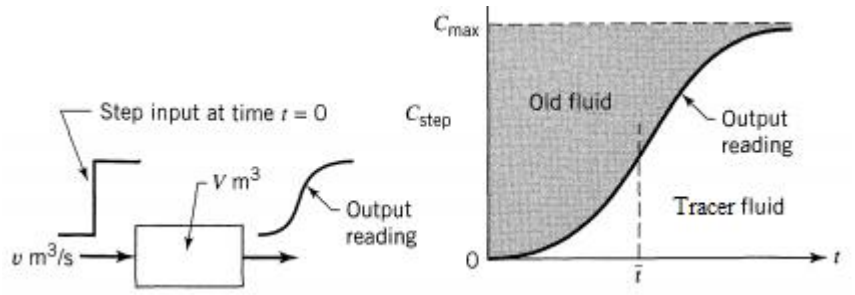

Figure 27: Implementation and results of a step experiment [79]

In this experiment the reactor inlet is switched from ordinary fluid to tracer fluid, as shown left in Figure 27. Again, the outlet tracer's conductivity or concentration is measured versus time. The distribution causes a fast increment of concentration until the residence time. Afterwards, the concentration increases more slowly until the fluid is 100% tracer fluid. Yet, this maximum would take infinitely long. In Figure 27, a positive step experiment is shown because the concentration of tracer is switched from 0 to C_{max}. However, it is also possible to opt for a negative step experiment, for example to save tracer material. The concentration of tracer at the input is then changed from C_{max} to 0.
From the obtained graphs in Figure 26 and Figure 27, the E(t)-curve (see 2.4.1 RTD in one CSTR) can be found, from which reactor behaviour can be derived. This curve represents the residence time distribution function that illustrates the time a fluid element could spend in the reactor.

2.4.1 RTD in one CSTR

In an ideal CSTR, the residence time distribution function E(t) can be obtained by deducing the material balance and incorporating it in the universal formula E(t) [80]. This results in following equation:

$$E(t) = \frac{C(t)}{\int_0^\infty C(t)dt} = \frac{C_{max}e^{-t/\bar{t}}}{\int_0^\infty C_{max}e^{-t/\bar{t}}dt} = \frac{e^{-t/\bar{t}}}{\bar{t}}$$

With $\bar{t}$ the residence time, t the time at a certain point of the experiment, and C_{max} the tracer concentration at t = 0. The cumulative distribution function F(t) is defined by $\int_0^t E\ dt$, which gives the following expression after integrating the E(t)-curve [86]:

$$F(t) = \int_0^t E(t)\ dt = 1 - e^{-t/\bar{t}}$$

Furthermore, the average residence time can then be calculated by the following formula [87]:

$$\bar{t} = \int_0^\infty t\ E(t)\ dt$$

The F(t)- and E(t)-curves are shown in Figure 28, in which the left and right graph represent respectively the ideal F(t)- and E(t)-curve when conducting a positive step experiment [86].

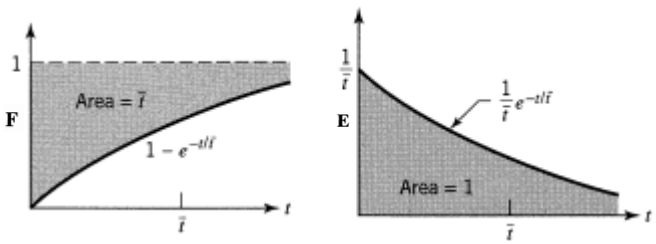

Figure 28: F(t)- (left) and E(t)- (right) curves for mixed flow when using the positive step method in a CSTR [86]

The F(t)-curve on the left represents the dimensionless form of the concentration versus time curve, previously measured by a step or pulse experiment. The vertical axis varies from zero to unity, because it is dimensionless, as can be seen in the next formula:

$$F(t) = \frac{C(t)}{C_{max}} \; with \; F(t) = 1 \; if \; C(t) = C_{max}$$

When integrating from 0 to ∞, the area below the E(t)-curve is always 1, as illustrated with the grey area at the bottom of Figure 28.

However, these theoretical E(t)- and F(t)-curves are merely an approach as a real CSTR has several practical problems, such as stagnant regions and short-circuiting flow [75]. These two imperfections are shown in Figure 29.

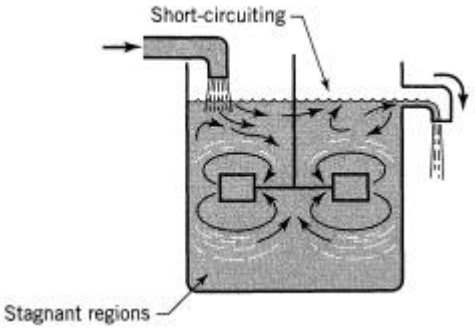

Figure 29: Short-circuiting and stagnant regions in a CSTR [75]

As can be seen in this figure, short-circuiting is the flow of material that is transported directly from the inlet to the outlet of the reactor, without being mixed in the reactor's volume. Therefore, this material remains too short in the reactor, thus it does not get the time to react optimally. The opposite of short-circuiting flows are stagnant regions. In these areas, the material stays much too long and is almost not mixed, which leads to a loss of effective volume in the reactor. Stagnant regions also lower the performance of the reactor.
It is practically often difficult to analyse the flow visually to identify these two problems. Therefore, it is necessary to draw conclusions from the concentration versus time curve, to see if these imperfections are present. Figure 30 shows how short-circuiting and stagnant regions look like on this C(t)-curve, compared to a practical ideal curve [88] [89].

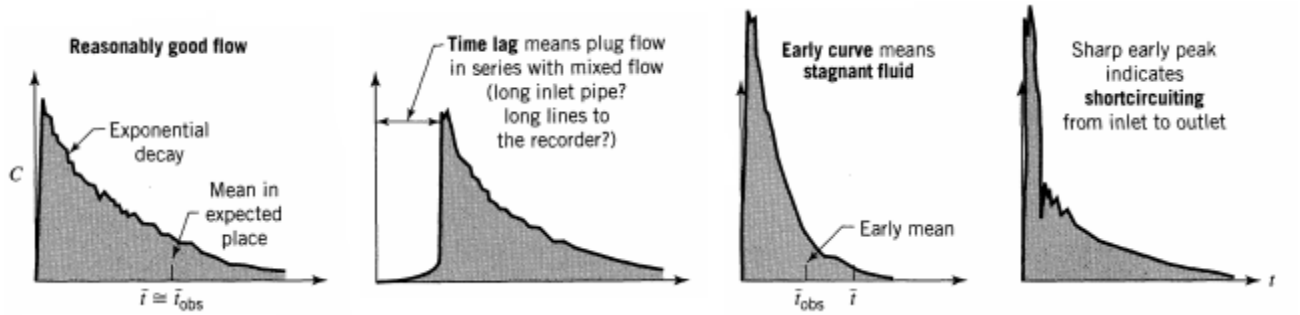

Figure 30: Various problems with effect on RTD in mixed flow [88]*: Left: Practical ideal curve; Middle left: Time lag; Middle right: Stagnant regions; Right: Short-circuiting flow*

The first graph shows the ideal curve when a practical step experiment is conducted. An exponential decay is observed, and the average theoretical residence time ($\bar{t}$) corresponds approximately to the average residence time, calculated out of the practical data obtained from the step experiment ($\bar{t}_{obs}$). Sometimes, a delay between the start of the experiment and the detection of tracer material is observed. In that case, a long inlet pipe to the reactor, or long lines to the recorder could be the cause.

This tubing can be represented as plug flow in series with the actual reactor, which is mixed flow. The plug flow causes the delay of tracer to the mixed flow reactor.
The middle right graph is valid for a reactor with stagnant regions. These zones reduce the reactor volume, causing the practical residence time ($\bar{t}_{obs}$) to be lower than the theoretical residence time $\bar{t}$, leading to a lower efficiency.
Short-circuiting results in a lower flow rate in the reactor volume because a part of the flow leaves the reactor immediately, which increases the practical residence time. The short-circuiting flow has a negligible residence time, and manifests itself as a sharp peak in the beginning as seen on the right graph of Figure 30.

2.4.2 RTD in cascade CSTR setup

When using multiple CSTRs in series, both the cumulative distribution function and the residence-time distribution function will change [90]. The concentration from the effluent of CSTR 1 will be distributed over the volume of CSTR 2. This results in a decreased concentration in the subsequent effluent. The residence time distribution will be the distribution over the whole series. With an increment of CSTRs, the RTD curves approach RTD curves of plug flow, seen in Figure 31. This change is beneficial as the residence time for an equal efficiency in a CSTR is higher than a PFR.

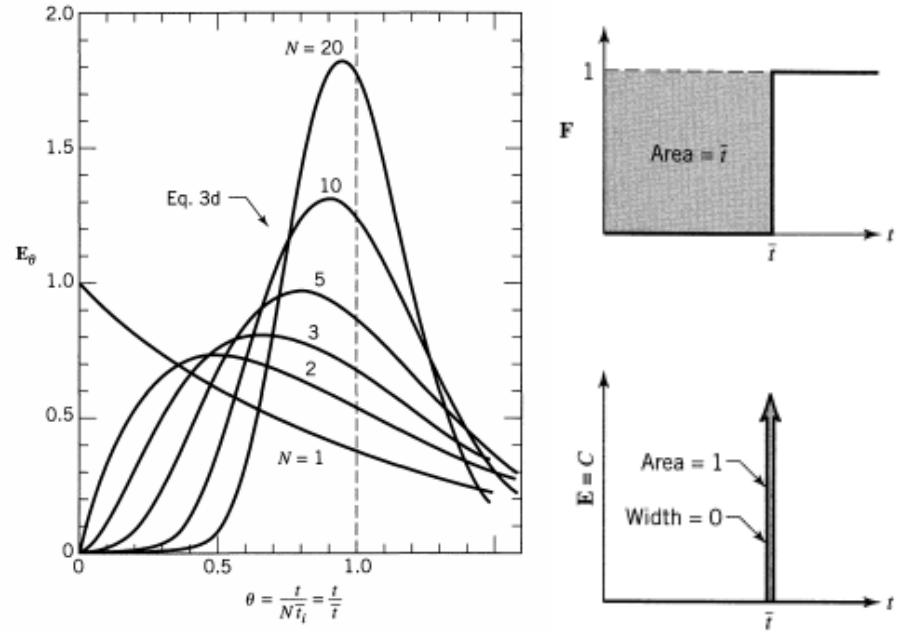

Figure 31: Dimensionless E-curve for N CSTRs in series for a pulse experiment [76] *and E- and F-curves of an ideal PFR* [75]

As a result, a cascade of CSTRs can be approached as a non-ideal PFR. There are two models to characterise the RTD, the axial dispersion model, and the tanks-in-series model. In this Master's thesis, the axial dispersion model is applied as this model is used in all correlations for flow in real reactors [90].

When a step experiment is applied, the border between the tracer and non-tracer fluids dissolves as it passes through the reactor. This non-ideal behaviour, longitudinal diffusion, is called dispersion. The dispersion coefficient D (m^2/s) is a measure for this process. D is ideally 0, and increases as the spreading through the vessel increases. The dispersion is often used as the dimensionless D/μL, where μ is the flowrate, and L the length of the vessel.

There are two cases for the deviation from plug flow: a small deviation, and a large deviation.
A small deviation is defined as a D/μL below 0.01. In this case, a probability plot of a step response

signal is made. This can be seen in Figure 32.

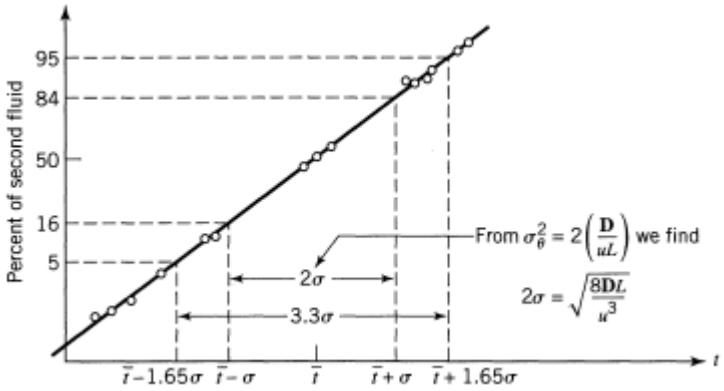

Figure 32: Probability plot for a step experiment [76]

The interval between 16 and 18 percent represent two times the standard deviation σ (in time), the dimensionless σ_θ, defined by $\frac{\sigma}{\bar{t}}$, leads to D/uL with following equation:

$$\sigma_\theta^2 = 2\frac{D}{uL}$$

If D/μL is greater than 0.01, this method cannot be applied as the F curve is not symmetrical anymore and a straight line will not be obtained for the probability plot. In this case, the F curve had to be differentiated to obtain a F_{pulse}-curve.

3 MATERIALS AND METHODS

This section of the Master's thesis explains how the different experiments were carried out, and which materials were used during testing. After a list of the used chemicals, the magnesium activation and initiation tests, the various reactor setups and the solids settling system design are explained. Thereafter, the method of characterising the final Cascade CSTR setup by measuring the residence time distribution is clarified. Subsequently, the reaction characterisation of the Grignard formation and the coupling reactions with acetophenone and benzaldehyde are discussed in more detail. Finally, the sample preparation, method and validation of the HPLC analysis are explained in detail.

3.1 CHEMICALS

Several chemicals were used in this Master's thesis, which are listed in Table 3, sorted according to the area of use.

Table 3: Summary of used chemicals

Chemicals	Supplier	Min. purity or concentration
Reaction solvent		
THF	VWR Chemicals	99.5%
Reaction reagents, products, side products and initiators		
Bromobenzene	Sigma-Aldrich	99%
Magnesium (Powder: 0.06-0.3 mm)	Merck KGaA	98.5%
Acetophenone	Sigma-Aldrich	99%
Benzaldehyde	Sigma-Aldrich	99%
1,1-diphenylethanol	Sigma-Aldrich	98%
Diphenylmethanol	Sigma-Aldrich	99%
Benzene	Merck KGaA	99.9%
Biphenyl	UCB	Pure
Phenylmagnesium bromide solution in THF	Sigma-Aldrich	1.0 M
Iodine, resublimed	UCB	Pure
Quenching solution		
Ammonium Chloride	Merck KGaA	99.8%
Residence time distribution solution		
Potassium Chloride	Merck KGaA	0.1 M

HPLC analysis		
Acetonitrile	VWR Chemicals	99.9%

When using water, always Milli-Q water was used with a conductivity of 0.056 µS/cm at 25 °C.

3.2 REACTOR SETUPS

3.2.1 Pump calibration

3.2.1.1 Chemtrix KiloFlow pumps

In this Master's thesis, Chemtrix KiloFlow® pumps were mainly used, which can be seen in Figure 33. Three pumps were available on the Chemtrix KiloFlow but only pump 2 and 3 were used in the conducted experiments.

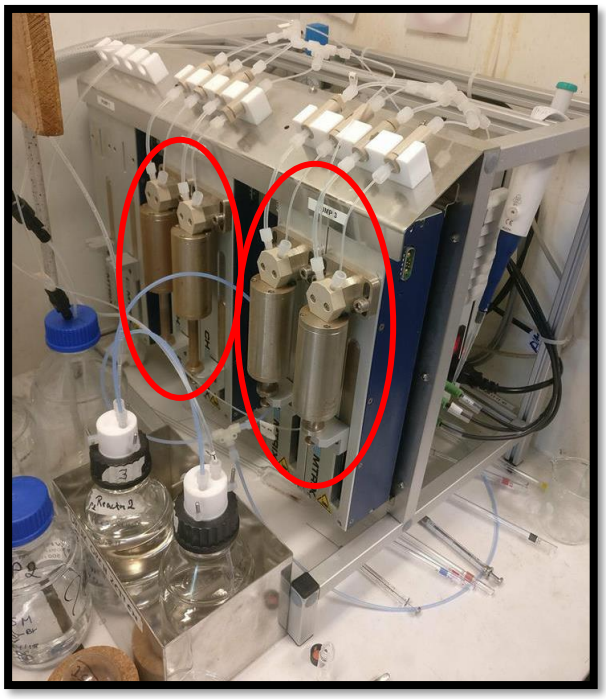

Figure 33: Chemtrix KiloFlow® pumps: (Left circle) Pump 2; (Right circle) Pump 3

Before these two pumps could be representatively used, a flow rate calibration was needed. The calibration was conducted with THF and water. Various flow rates were set, and each time the pumped liquid was collected for two minutes. The collected liquid was weighed on an analytical balance. With the density of the liquid, the flow rate was calculated in ml/min. The calibration curves of pump 2 and 3 with THF are shown in Figure 34, and those with water in Figure 35.

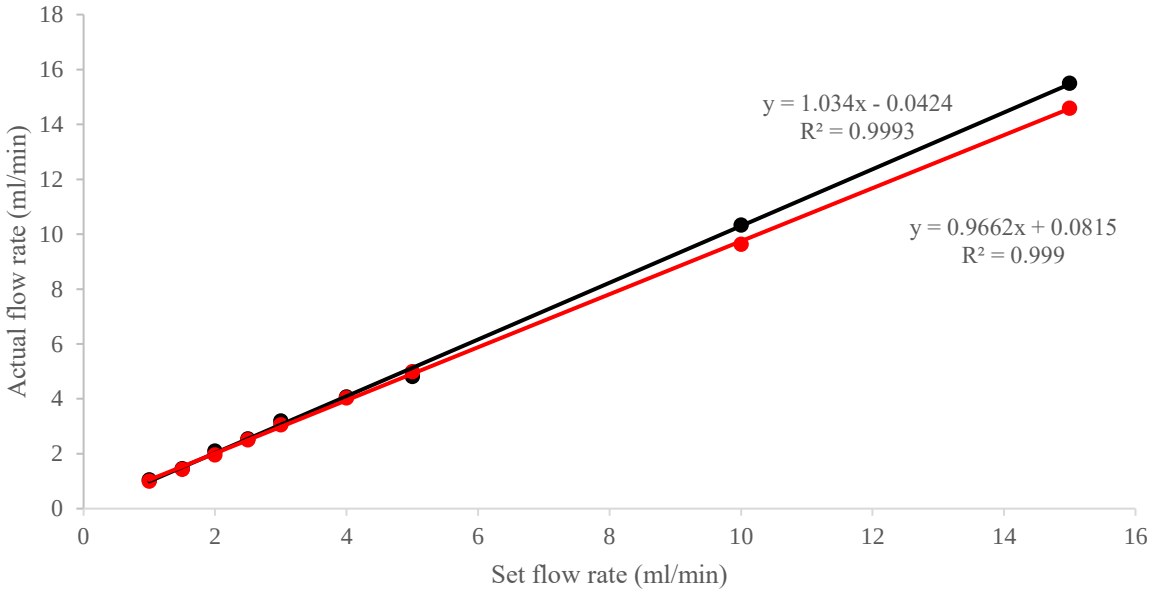

Figure 34: KiloFlow pump calibration with THF for pump 2 (black) and pump 3 (red)

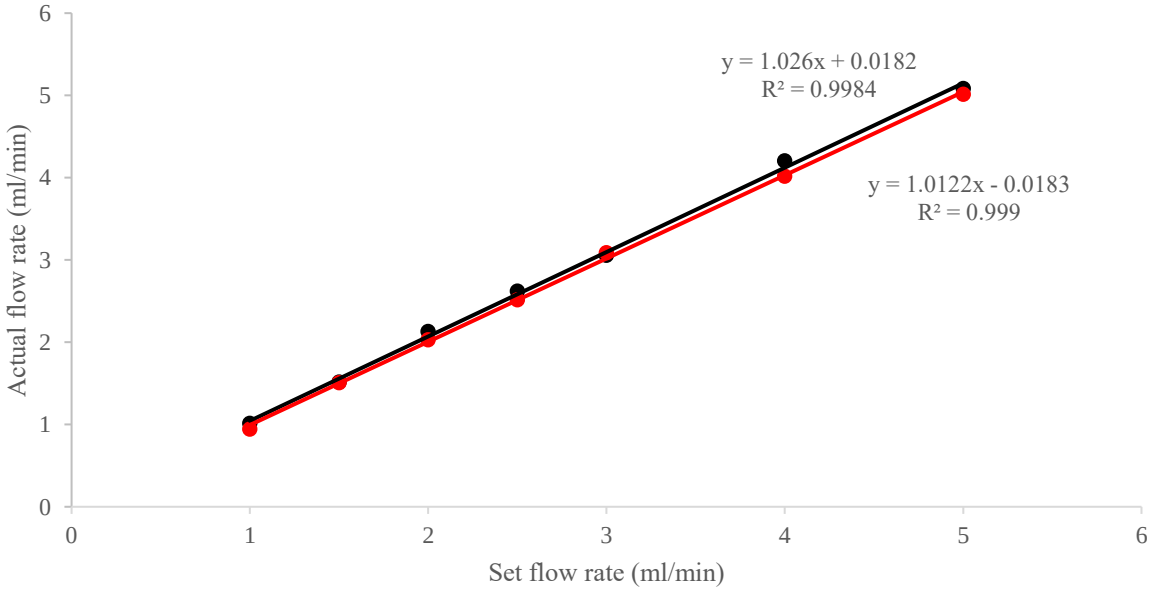

Figure 35: KiloFlow pump calibration with water for pump 2 (black) and pump 3 (red)

A linear trend line was drawn, which represented the flow rate calibration curves. The correct pump flow rate was then set based on these calibration curves.

3.2.1.2 Watson Marlon 120U peristaltic pump

A Watson Marlow 120U peristaltic pump with Marprene peristaltic tubing (2.4 mm ID and 5.6 mm OD) was used for the cascade setup. The calibration curve of this pump when using THF is shown in Figure 36.

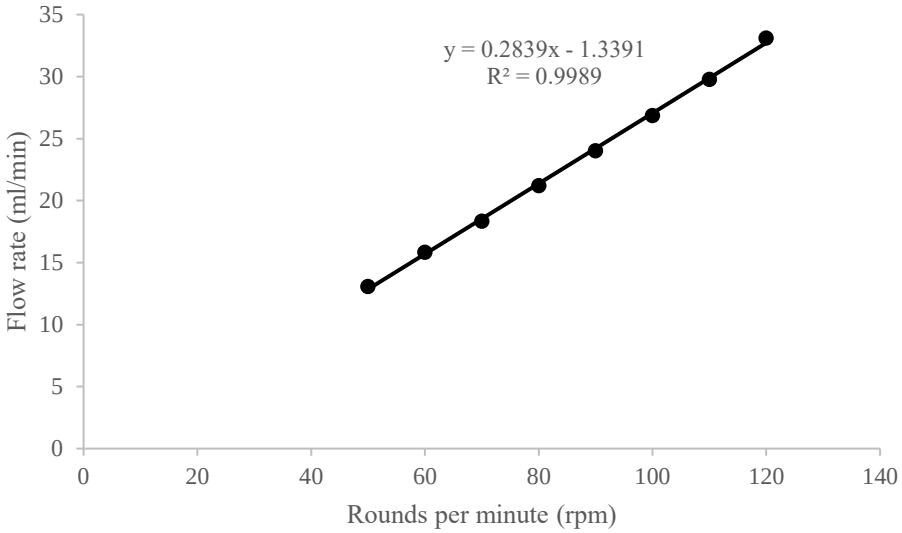

Figure 36: Calibration curve of Watson Marlow 120U (THF)

Again, the correct pump flow rate was set based on this calibration curve.

3.2.2 Reaction activation and initiation setup

After the pump calibration, the best method of magnesium activation and initiation was investigated for the reaction of bromobenzene with magnesium. Several methods to achieve activation and initiation were tested in test tube experiments, which are shown in Table 4.

Table 4: Different magnesium activation experiments

Experiment	Activation technique			
	Iodine in THF	Iodine in THF (heated)	Iodine vapour	Phenylmagnesium bromide addition (100µl)
1	x			
2		x		
3			x	
4	x			x
5				x
6	x		x	x

In experiments 1, 2, 4, and 5, half a gram of fresh magnesium powder was loaded into the test tube together with a trace of iodine. Thereafter, 5 ml of THF was added. In experiment 2, this mixture was heated to the boiling point of THF (66 °C) for a few seconds, and then cooled again.
In experiment 3 and 6, the dry magnesium (also 0.5 g) and iodine were heated and shaken until sublimation of iodine occurred, which created purple vapours (iodine vapour). Hereafter, 5 ml of THF was added.

The main purpose of adding this iodine was to see if the magnesium was activated quickly, which is reflected in a colour change of the solution from yellow to colourless. After the colour change, 1 ml of

bromobenzene was added. When no activation (colour change) had happened after at least 10 minutes, 1 ml of bromobenzene was added to see if this would start the activation. Observed parameters were time of the colour change, and a large exothermic heat release, observed by solvent vapour formation at the magnesium surface. The concentration of bromobenzene in the reaction mixture was 1.56 M and 1.59 M for respectively the initiation method with or without phenylmagnesium bromide addition.

In a second series of test tube experiments, the ideal amount of 1.0 M phenylmagnesium bromide that had to be added to activate the formation of Grignard reagent, was determined. In 0.5 g of magnesium in 5 ml THF and a trace of iodine, 10 µl of the phenyl magnesium bromide solution was added stepwise, until the colour change occurred. The purpose of this test was to see how much phenylmagnesium bromide solution should be added if a switch was needed to larger volumes in subsequent experiments.

3.2.3 Grignard reagent formation in CSTR

A CSTR design was built for carrying out the formation of the Grignard reagent, phenylmagnesium bromide. Then, tests were carried out to gain a better understanding of the parameters that affect the formation of the Grignard reagent. The setup is shown in Figure 37.

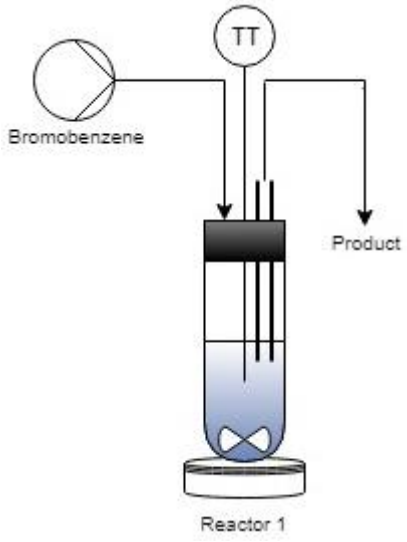

Figure 37: CSTR design

The reactor was a pressure-tight 50 ml Pyrex test tube with a Teflon coated screw cap. An 1/8-inch PFA tubing inlet for the bromobenzene solution was provided, as well as an 1/4-inch PerFluorAlkoxy (PFA) tubing outlet for a magnesium settling pipe which was responsible for the removal of the product, while magnesium was kept in the reactor. More information of the magnesium settling pipe can be found in 3.2.4 Settling pipe design, more specifically the section 3.2.4.1.

Additionally, a Pt100 thermocouple was inserted into the reactor to detect initiation of the reaction. The steady-state temperature of the process could also be measured in this way. A stirring plate with magnetic stirrer was set to 1500 rpm to provide thorough mixing of the heterogeneous reaction mixture.

To perform an experiment, the Pyrex test tube was always flame dried to obtain an anhydrous reactor. The desired amount of magnesium powder was loaded, followed by a trace of iodine. Then, the reactor was flame heated again to create iodine vapours that would activate magnesium a first time. After cooling to room temperature, the magnetic stirrer was added. 3 ml of phenylmagnesium bromide solution (1 M) was added as a second activator. Finally, the reactor was closed with the screw cap and the experiment was started by starting the bromobenzene solution flow.

After 4 times the residence time, a sample was taken for HPLC analysis, and was prepared as discussed in 3.5.1. The components benzene, bromobenzene and Biphenyl were analysed quantitatively. Benzene, the quenched product of phenylmagnesium bromide, was analysed to determine the yield of phenylmagnesium bromide. Bromobenzene was analysed to determine the overall conversion, biphenyl was analysed as a possible side product.

3.2.3.1 Varying concentration of bromobenzene

The first parameter that was varied on the CSTR setup, was the concentration of bromobenzene. In this way, it was also possible to check the steady-state temperature of the reaction at different concentrations. Table 5 shows the set parameters during these experiments.

Table 5: Variating concentrations experiments in CSTR

$C_{Bromobenzene}$ (mole/l)	$m_{magnesium}$ (g)	Ratio Mg:Bromobenzene (mole:mole)	Residence time (min)	Feed rate bromobenzene (ml/min)	Time of sampling (min)
0.3000	0.5833	2	5	2	20
0.4976	0.9675	2	5	2	20
0.6829	1.3279	2	5	2	20

In these experiments, a double ratio of magnesium to bromobenzene was used. One ratio of magnesium to bromobenzene is defined as the maximum amount of magnesium that can react away between the start of the experiment and the moment of sampling. This means that when the sample is taken, maximum 1 equivalent of magnesium has reacted. This way of defining the ratio magnesium to bromobenzene is extended to all experiments.

3.2.3.2 Influence of ratio magnesium to bromobenzene

Next, the influence of the ratio magnesium to bromobenzene was tested. The reaction conditions are shown in Table 6.

Table 6: Influence of ratio magnesium to bromobenzene experiments in CSTR

$C_{Bromobenzene}$ (mole/l)	$m_{magnesium}$ (g)	Ratio Mg:Bromobenzene (mole:mole)	Residence time (min)	Feed rate bromobenzene (ml/min)	Time of sampling (min)
0.4976	0.9675	2	5	2	20
0.4976	1.9349	4	5	2	20
0.4976	2.9024	6	5	2	20

3.2.3.3 Varying residence times

The influence of a variating residence time in the CSTR on the yield of phenylmagnesium bromide was also tested. The experimental conditions are shown in Table 7.

Table 7: Variating residence time experiments in CSTR

$C_{Bromobenzene}$ (mole/l)	$m_{magnesium}$ (g)	Ratio Mg:Bromobenzene (mole:mole)	Residence time (min)	Feed rate bromobenzene (ml/min)	Time of sampling (min)
0.4976	2.9024	6	5	2	20
0.4976	5.8047	6	10	2	40
0.4976	8.7071	6	15	2	60

3.2.3.4 Different feed rate of bromobenzene

Lastly, the possible influence of the feed rate of bromobenzene was tested. Experiment parameters are found in Table 8.

Table 8: Variating feed rates of bromobenzene experiments in CSTR

$C_{Bromobenzene}$ (mole/l)	$m_{magnesium}$ (g)	Ratio Mg:Bromobenzene (mole:mole)	Residence time (min)	Feed rate bromobenzene (ml/min)	Time of sampling (min)
0.4976	2.9024	6	10	1	40
0.4976	4.3749	6	10	1.5	40
0.4976	5.8047	6	10	2	40

3.2.4 Settling pipe design

3.2.4.1 Vertical settling pipe

The design of the settling pipe in the Grignard reagent formation in CSTR experiments consisted of 10 cm 1/4-inch PFA tubing, followed by 40 cm of 1/8-inch PFA tubing. The 1/4-inch tubing was set up vertical, so that magnesium could settle back to the reactor. The 1/8-inch tubing served as a transporting pipe to the waste container or a sampling vial, and therefore had no additional utility as a magnesium settler. During experiments, this design proved to be effective for flow rates up to 2.5 ml/min. This was sufficient for the CSTR experiments, where the flow rates were below 2.5 ml/min.

3.2.4.2 Single angled settling pipe

The second design was called the single angled settling pipe. This design was a copy of the design that was described in the literature (see 2.3.2 Solids settling system). It consisted of an angled piece of glass pipe, which had an angle of 60° away from the vertical piece of glass tubing. The design is shown in Figure 38, and the right settling pipe was used in the Cascade CSTR setup.

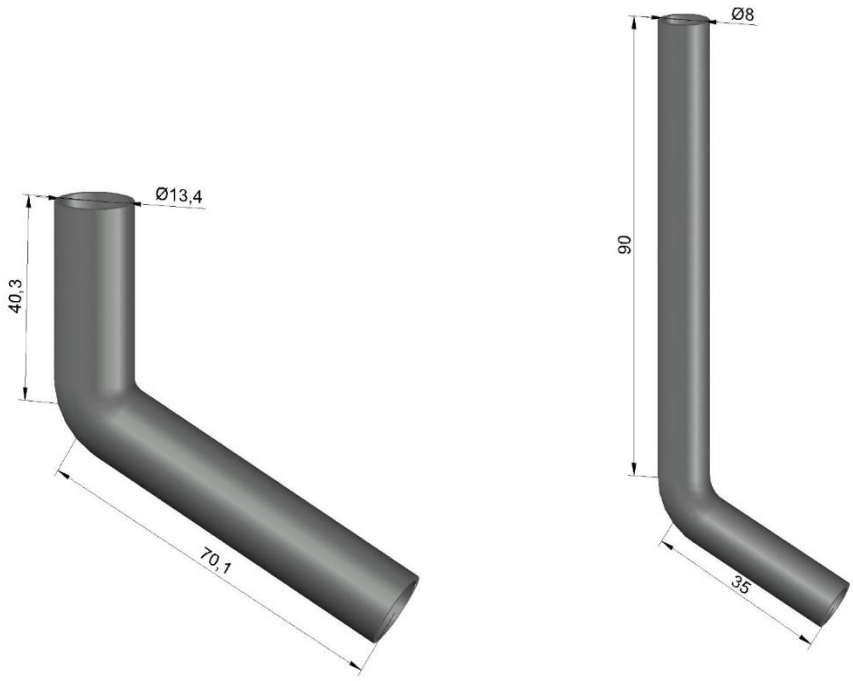

Figure 38: Ideal (left) and used (right) single angled settling pipe with dimensions in mm

The dimensions of this settling pipe were chosen by looking at the dimensions used in the literature, which were already described in Table 2. The most important dimensions are plotted according to the flow rate used in the different reactors, as shown in Figure 39.

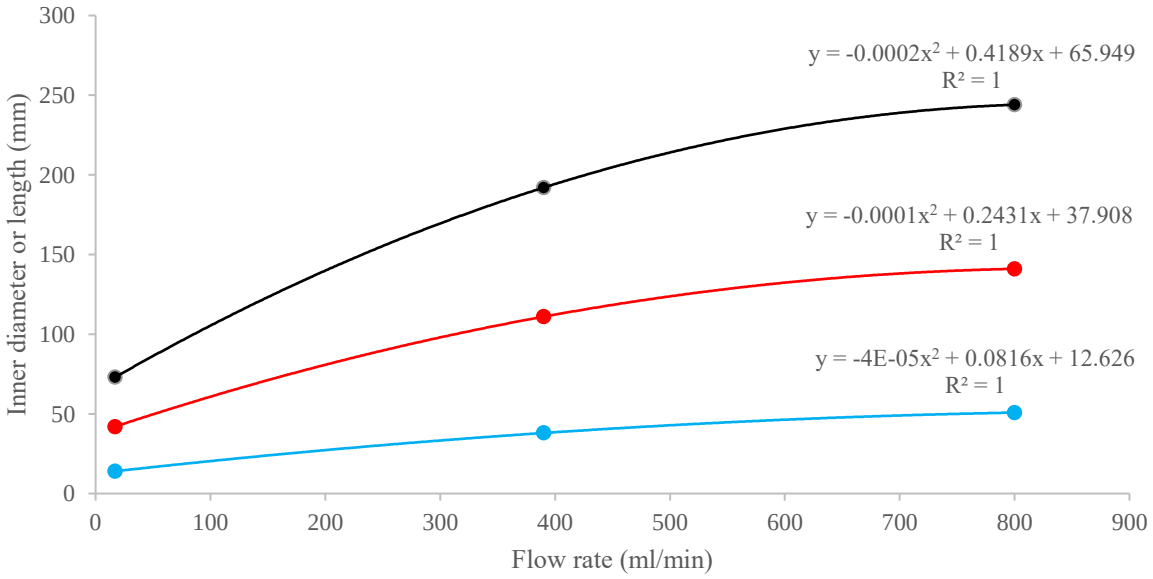

Figure 39: Dimensioning curves for the single and double angled settling pipes used in this Master's thesis, with the settling pipe inner diameter (blue), the vertical tube height to bend (red) and the angled tube length (black)

The trend lines obtained from these points were the basis for the settling pipe dimensions that were used in this Master's thesis. With the cascade CSTR tests carried out with a flow rate of 10 ml/min, the ideal dimensions were found as shown on the left settling pipe in Figure 38.

However, due to the use of small 100 ml round-bottom flasks as a reactor, these dimensions were too large to fit in these flasks. Also, the extrapolation of the dimensions from the literature data cannot be

considered as reliable. Therefore, a reduced model had to be made. The single angled settling pipe dimensions as used in this cascade CSTR setup, are shown on the right settling pipe in Figure 38.

3.2.4.3 Double angled settling pipe

A third model was also tested, which could possibly improve the settling of magnesium. This model was called the double angled settling pipe, because two angled pieces of glass pipe were connected by a vertical piece of glass pipe. The design of this settling pipe is shown in Figure 40, and was also used in the Cascade CSTR setup.

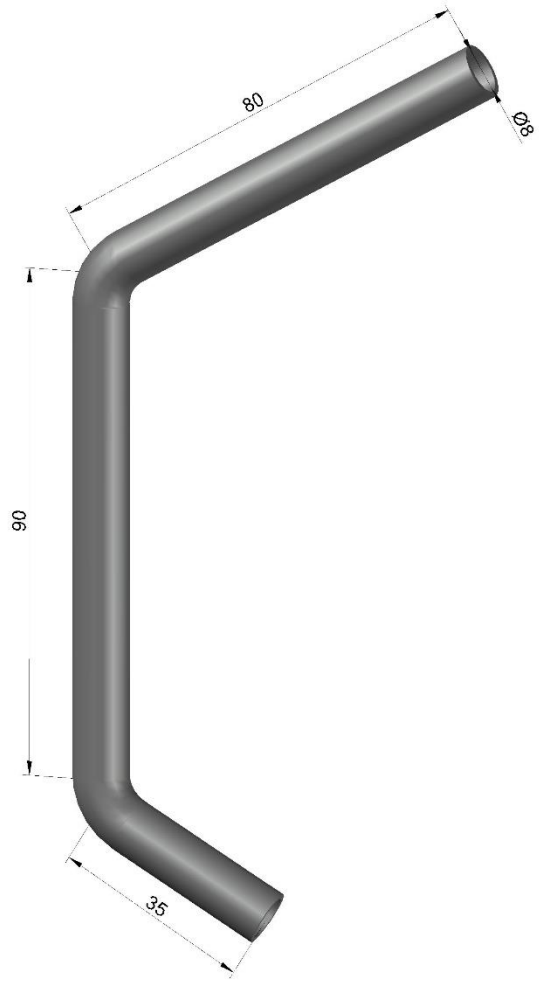

Figure 40: Double angled settling pipe with dimensions in mm

The lower angled and vertical tube dimensions were chosen identically to the single angled settling pipe. The higher angled tube was given a longer length, to compensate for the too short lower angled pipe, which was explained in the section 3.2.4.2. The dimensions of this double angled settling pipe design are shown in Figure 40.

3.2.5 Cascade CSTR setup

After optimising the first reaction in the CSTR setup, the cascade CSTR setup could be tested. The setups that were built are shown in Figure 41 and Figure 42.

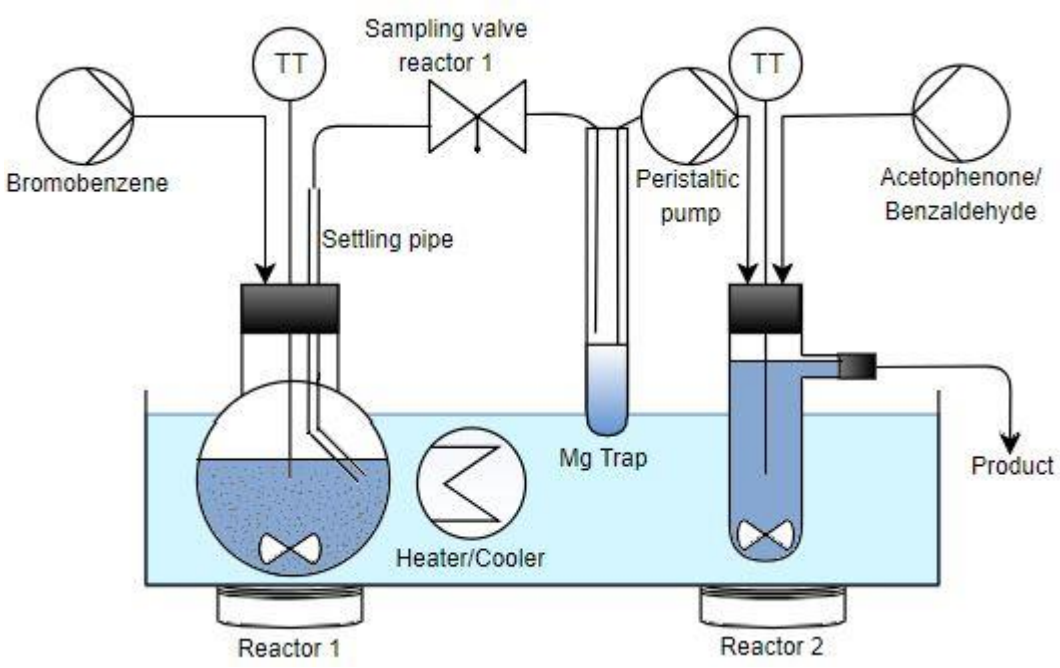

Figure 41: Cascade CSTR setup with single angled settling pipe

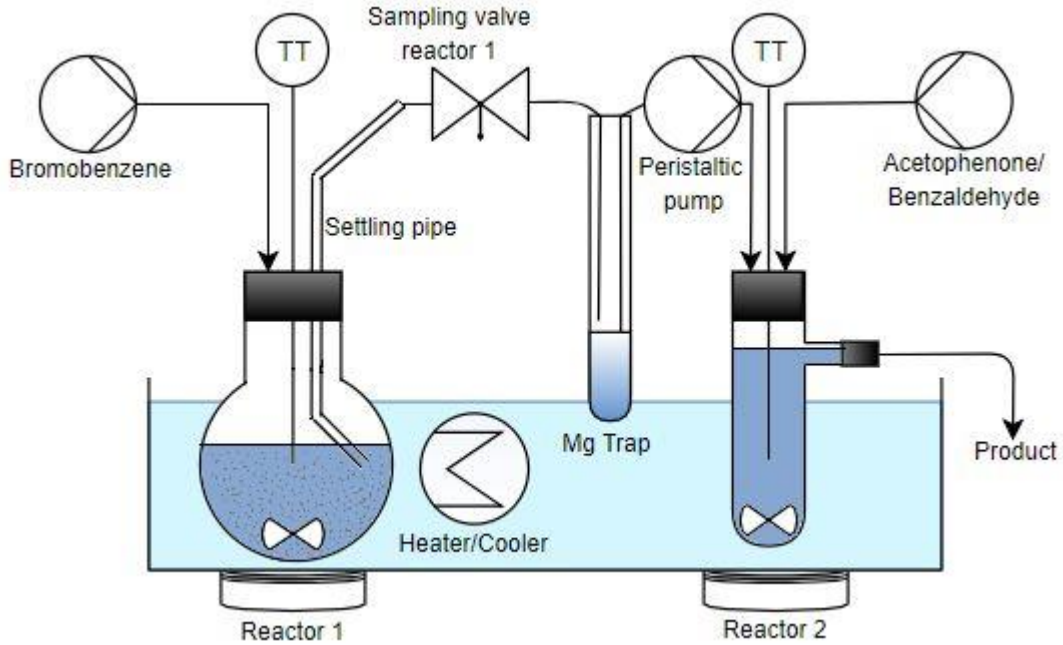

Figure 42: Cascade CSTR setup with double angled settling pipe

All tubing used in these setups was 1/8-inch PFA tubing. The first reactor was a borosilicate glass 100-ml round bottom flask, always containing 50 ml reaction mixture. The second reactor was an overflow reactor built from a wide borosilicate glass test tube (28 mm ID and 110 mm height) and T-piece, containing 55 ml of reaction mixture. Both reactors were stirred with a magnetic stirring bar at 650 rpm. In the first reactor, the desired amount of preloaded magnesium powder reacts with the incoming bromobenzene solution to phenylmagnesium bromide. A Pt100 thermocouple indicates if the initiation has started, and at which steady-state temperature the reactor is at the end. Both the single and double

angled settling pipes were tested in the cascade CSTR setup with reaction 1, to see which was the most efficient to retain magnesium in reactor 1. Additional information on the settling pipe design in this Master's thesis can be found in the section 3.2.4. The inlet of the settling pipe was always positioned to the reactor's wall, because this was the only option in the small CSTR cascade setup. Based on the literature found (see 2.3.2 Solids settling system), a mild vortex was created when mixing reactor 1, as this was the ideal mixing pattern for positioning the entrance of the settling pipe to the reactor's wall.

The liquid product from reactor 1 passes a sampling valve, which can pass the product to reactor 2, or through which a sample can be taken to analyse the composition of the outlet of reactor 1. Between the sampling valve and reactor 2, a long and small pressure tight borosilicate glass test tube (15 mm ID and 70 mm fluid height) is positioned where magnesium can settle that is not retained by the settling pipe. At the end of the test, this magnesium is analysed by microscopy with a Carl Zeiss Axiolab microscope (with an Axiocam 105 Color) to determine the critical particle size that passes the settling pipe. A Watson Marlow 120U peristaltic pump transports the reaction mixture of reactor 1 (and the magnesium trap) to reactor 2, at the same flow rate as that bromobenzene solution is fed. Here, it can react with the acetophenone or benzaldehyde solution. A Pt100 thermocouple indicates the temperature in this reactor. The second sampling takes place at the end of reactor 2. This sampling point has two goals: looking for the presence of magnesium in the final stream by microscopy and finding out the composition of the liquid flow exiting reactor 2.

Cooling of the exothermic reactor system was performed by placing the reactors and magnesium trap in a water bath of which the temperature was set at 41 °C. As a result, the temperature in the first reactor was always 50 °C. The temperature of the water bath was controlled by a Julabo EM heater and a stainless-steel cooling coil, which was cooling with cold tap water.

Before an experiment, all glassware was flame dried. Thereafter, the desired amount of magnesium and a trace of iodine was loaded into the first reactor, followed by flame heating the reactor again to create iodine vapours that would activate magnesium in a first way. After cooling to room temperature, the magnetic stirrer, 47 ml THF and 3 ml of phenylmagnesium bromide solution of 1 M was added as a second activator to trigger immediate reaction initiation.
The experiment was started by turning on the magnetic stirrers, the feeds of bromobenzene and acetophenone/benzaldehyde solution, and the peristaltic pump.

Samples of reactor 1 and 2 were taken after the first reactor and consecutively the second reactor had run for 4 residence times. When testing was done with reaction 1, the components acetophenone, benzene, 1,1-diphenylethanol, bromobenzene and biphenyl were analysed quantitatively. For reaction 2, these were the components benzaldehyde, benzene, diphenylmethanol, bromobenzene and biphenyl.

Three tests were performed on the cascade CSTR setup, two with acetophenone as reagent in the second reactor, and the other with benzaldehyde. The conditions of these tests are shown in Table 9. The residence times of these reactors used in this table were obtained by deriving the average residence time from the Residence time distribution results.

Table 9: Experimental parameters during the cascade CSTR experiments

Parameter	Reaction 1 (with acetophenone)	Reaction 2 (with benzaldehyde)
$C_{Bromobenzene}$ (mole/l)	0.5	0.5
$m_{magnesium}$ (g)	7.2915	7.2915
Ratio Mg:Bromobenzene (mole:mole)	2	2
Residence time reactor 1 (min)	9 min 10 s	9 min 10 s

Feed rate bromobenzene (ml/min)	10	10
Settling pipe	Single angled and double angled	Only double angled
$C_{acetophenone}$ or $C_{benzaldehyde}$ (mole/l)	0.5	0.5
Desired ratio Phenylmagnesium bromide:acetophenone or benzaldehyde (mole:mole)	1	1
Feed rate acetophenone or benzaldehyde (ml/min)	10	10
Residence time reactor 2 (min)	2 min 45 s	2 min 45 s
Sampling time (min)	31	31

3.3 RESIDENCE TIME DISTRIBUTION

To identify the non-ideal behaviour of the flow in the reactors of the Cascade CSTR setup with double angled settling pipe, the residence time distribution of the particles entering those reactors was measured. The negative step technique was used, by a sudden change of feed from a 0.1 M conductive KCl solution to Milli-Q water with a two-way valve. At the end of the reactor system which had to be measured, a conductivity meter (Amber Science Inc. 829 Micro Flow S/S MFD 11/2014) was connected. The condition to apply the negative step was that the conductivity meter had to indicate a constant value, while fresh 0.1 M KCl solution was constantly sent through the setup. When the switch was made, the 'Labview conductivity meter' software was started and measured the conductivity, which was recorded with 1 measurement per second.

Four tests were executed to obtain a characterised system. The first was a reference test to obtain the conductivity of the Milli-Q water and 0.1 M KCl solution, which turned out to be respectively 0.070 µs/cm and 1170 µS/cm at 30 ° C and 10 ml/min. The other three tests are shown in Table 10, and based on the reactor setup that was illustrated in Figure 41.

Table 10: RTD tests experimental conditions

Characterised part	Feed rate reactor 1 (ml/min)	Feed rate reactor 2 (ml/min)	Theoretical residence time (min)	Stirrer (rpm)	Conductivity to be achieved (µS/cm)
First reactor Settling pipe Magnesium trap Peristaltic pump	10 (Milli-Q)	/	5	650	0.070
Second reactor	/	20 (Milli-Q)	2 min 45 s	650	0.070

Whole cascade CSTR	10 (Milli-Q)	10 (0,1 mole/l KCl)	7 min 45 s	650	585.035

It was chosen to feed a 0.1 M KCl solution to reactor 2 with the characterisation of the whole CSTR cascade. In this way, a characterisation of the whole cascade CSTR was possible, while the second reactor still had a flow rate of 20 ml/min. If a Milli-Q feed at reactor 2 would be used, the two residence time distributions of the separate reactors would be mixed, which would lead to complex results.

3.4 REACTION CHARACTERISATION

To characterise a reaction, a constant temperature is necessary. To achieve this, the Mettler Toledo EasyMax 102 was used, a workstation for organic synthesis. The reagents were added to the Easymax reactor with a graduated glass cylinder and a glass funnel. The stirrer was fixed at 400 rpm during all experiments. The temperature of the reaction mixture was controlled automatically, after defining a temperature setpoint. Sampling of these experiments was executed as explained in 3.5.1 Sample preparation.

3.4.1 Reaction to phenylmagnesium bromide

To characterise the first part of the reaction, the formation of the Grignard reagent, five experiments were performed as shown in Table 11. Three experiments, where the temperature was altered, were necessary to determine the k-value and activation energy. Thereafter, two extra experiments were executed: a halving of the concentration of bromobenzene, and a doubling of the amount of magnesium. In this way, the order of the reaction could be deduced.

Table 11: Performed experiments for reaction characterisation of the Grignard formation

Parameter	1	2	3	4	5
Concentration bromobenzene (mole/l)	0.5	0.5	0.5	0.5	0.25
Mass magnesium (g)	1.9444	1.9444	1.9444	3.8888	1.9444
Ratio Mg:Bromobenzene (mole:mole)	2	2	2	4	4
Volume phenylmagnesium bromide (ml)	1.00	1.00	1.00	1.00	1.00
Temperature (°C)	30	20	15	30	30
Time (min)	40	75	96	40	50

Each test, the reactor was flame dried and iodine vapours were created in the presence of the desired amount of magnesium. After cooling, 1.00 ml phenylmagnesium bromide was added to enhance the initiation. The experiment was started when 80 ml of the bromobenzene solutions was added.
The duration of the experiments was determined by monitoring the temperature of the heating/cooling jacket of the Easymax. Due to the exothermic character of the reaction, extensive cooling was required during the reaction. When the reaction was nearly completed, the jacket's temperature would rise and stagnate at the end of the reaction. It was at this point that the sampling was stopped.

3.4.2 Coupling reaction with acetophenone or benzaldehyde

An attempt was made to characterise the second part of reaction 1 and 2, the reaction of phenylmagnesium bromide and acetophenone or benzaldehyde to respectively 1,1-diphenylethanol or diphenylmethanol. Five experiments were carried out: four for the coupling reaction with acetophenone, and one for benzaldehyde. These experiments are shown in Table 12.

Table 12: Performed experiments for reaction characterisation of the coupling reaction with acetophenone

Parameter	1	2	3	4	5
Concentration acetophenone in reactor (mole/l)	0.5	0.06	0.06	0.5	
Concentration benzaldehyde in reactor (mole/l)					0.5
Concentration phenylmagnesium bromide in reactor (mole/l)	0.5	0.06	0.06	0.5	0.5
Temperature (°C)	30	-10	30	-10	30

A test was started by pouring 40 ml of phenylmagnesium bromide solution, which was brought to the experimental temperature, into the temperature controlled reactor containing 40 ml of acetophenone or benzaldehyde solution. To obtain the right concentrations in the reactor, the 40 ml solutions of phenylmagnesium bromide, acetophenone and benzaldehyde had to be twice as concentrated than the concentration needed in the reactor.

3.5 QUANTITATIVE ANALYSIS METHOD

The samples were analysed by a reverse phase HPLC, equipped with an UV-detector and autosampler. The results were used to determine the yield of the desired product, as well as the conversion to side products.

3.5.1 Sample preparation

When running a continuous flow experiment, samples were always taken after 4 times the residence time, to ensure that the system was steady-state, and that no impurities were left in the reactor. Then, a sample of three to four ml was taken, as an assurance to preserve enough product in case of doubtful results. 1.00 ml of the sample was quenched with 1.00 ml of an acidified aqueous NH_4Cl solution (0.26 g/ml) in a 4-ml vial, except for the sample preparations for the reaction kinetics, where 0.50 ml of sample was quenched with 0.50 ml NH_4Cl solution to minimize the disturbance of the batch volume. The quenching created two layers, with on top an organic layer with white precipitate, at the bottom, a transparent aqueous layer. Next, the vial was shaken until 2 transparent layers were obtained. Out of the organic layer, 5.00 or 10.00 µl (depending on the initial concentrations) was diluted with acetonitrile in a 5.00-ml or 10.00-ml volumetric flask. This dilution was necessary to ensure concentrations below 200 ppm as the calibration curves of the components were limited to 200 ppm, as seen in the section 3.5.3.1 Calibration curves. Then, the sample was analysed by HPLC.

3.5.2 HPLC method

The HPLC used for the analysis is an Agilent 1100 series HPLC. The UV detector, able to measure one wavelength at a time, was set at 210 nm to detect all the used components. The column used for the separation, is an Alltima HP C18 5 µm column (250 mm x 4.6 mm ID).

The eluents used for the HPLC analysis were acetonitrile (ACN) and water. Flow rate during analysis was set constantly at 1.00 ml/min. A multi-step gradient was used to separate the components. The multi-step gradients for the components of reaction 1 with acetophenone and reaction 2 with benzaldehyde are respectively shown in Table 13 and Table 14. An example of a chromatogram of reaction 1 and 2 can be found in 6.1 Appendix A: Chromatograms examples, in respectively 6.1.1 Reaction 1 and 6.1.2 Reaction 2. The identification of the components is also shown there.

Table 13: HPLC program for reaction 1

	Time (min)	%ACN	%H_2O
1	0.00	40	60
2	4.00	40	60
3	15.00	60	40
4	19.00	100	0
5	24.00	100	0
6	28.00	40	60
7	31.00	40	60

Table 14: HPLC program for reaction 2

	Time (min)	%ACN	%H_2O
1	0.00	50	50
2	10.00	50	50
3	12.00	90	10
4	14.00	90	10
5	16.00	50	50
6	19.00	50	50

Each sequence of samples started and ended with a flush program, followed by a 100% acetonitrile wash of 10 minutes. The multi-step gradient of the flush program is shown in Table 15.

Table 15: HPLC flush program

	Time (min)	%ACN	%H_2O
1	0.00	40	60
2	4.00	100	0
3	13.00	100	0
4	17.00	40	60
5	20.00	40	60

3.5.3 Validation and processing of the HPLC results

3.5.3.1 Calibration curves

In order to find the calibration curves of the components, samples of 5, 10, 20, 35, 50, 75, 100, 125, 150, 175 and 200 ppm were made in acetonitrile. There were two different samples of each concentration. One for the reaction with a ketone, containing the two reagents bromobenzene and acetophenone, the (quenched) intermediate benzene, the product 1,1-diphenylethanol, and a possible side product biphenyl. The other sample was for the reaction with the aldehyde, containing the two reagents bromobenzene and benzaldehyde, the (quenched) intermediate benzene, the product diphenylmethanol, and a possible side product biphenyl. The samples of each reaction were made from a 5000-ppm stock solution in acetonitrile containing the components of that reaction. From this stock, the desired amount was then transferred to a 5-ml volumetric flask, which was then diluted with acetonitrile.

The equations for each component can be found in Table 16 and Table 17. These were calculated by performing a linear regression analysis, combined with a 95% confidence interval.

*Table 16: Equations for the calibration curves of reaction 1, with y the peak area in mAU*min and x the concentration in ppm*

Reaction 1	Equation	R^2
Acetophenone	$y = 44.002x + 200.22$	0.9982
Benzene	$y = 26.764x + 175.14$	0.996
1,1-diphenylethanol	$y = 77.988x + 85.093$	0.9997
Bromobenzene	$y = 47.877x + 30.026$	0.9997
Biphenyl	$y = -0.2191x^2 + 140.02x + 126.92$	0.9995

*Table 17: Equations for the calibration curves of reaction 2, with y the peak area in mAU*min and x the concentration in ppm*

Reaction 2	Equation	R^2
Benzaldehyde	$y = -0.0784x^2 + 66.482x + 65.868$	0.9998
Diphenylmethanol	$y = 78.959x + 138.31$	0.9993
Benzene	$y = 25.719x + 194.63$	0.9954
Bromobenzene	$y = 47.958x + 19.917$	0.9999
Biphenyl	$y = 126.67x + 281.95$	0.999

After carrying out the linear regression, almost each of these curves had a linear range of 5 ppm to 200 ppm as can be seen in 6.2 Appendix B: Calibration curves. The calibration curves of biphenyl in the first reaction and benzaldehyde in the second reaction were an exception, as they had a quadratic relation. This was calculated with the 95% confidence interval, it showed that no linear relation was present. Therefore, the quadratic values of the peak area were tested and approved by the 95% confidence interval for linearity, meaning they both have a quadratic relation. For biphenyl in the second reaction, the linear regression with 95% confidence interval excluded concentrations above 50 ppm. This

From these results it appears that the detection of biphenyl is influenced by the other components as one equation is linear, and the other is quadratic. However, as seen in Figure 43, for relatively low concentrations, both curves will give the same result. Because biphenyl is a side product that will form in relatively low concentrations compared to the end product, both equation will be sufficient.

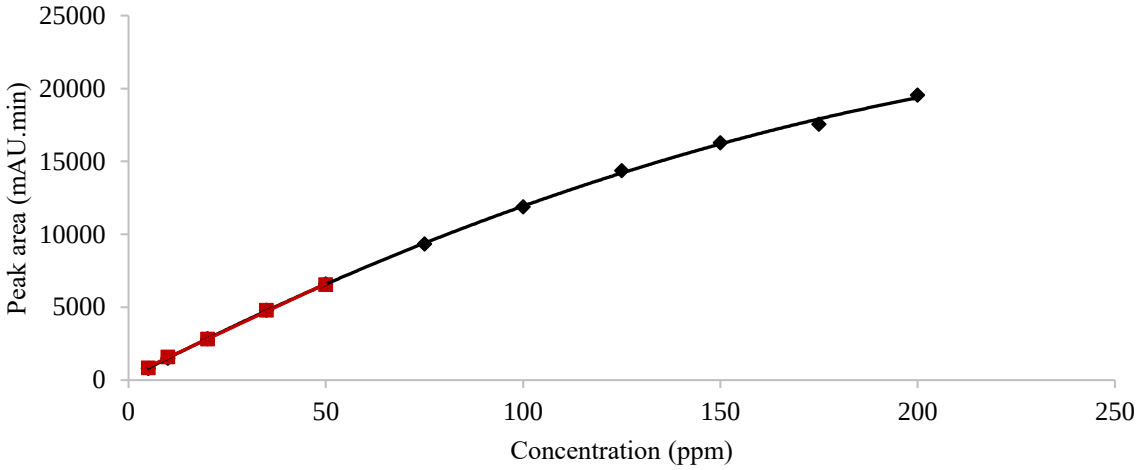

Figure 43: Comparison of biphenyl in reactions 1(black) and 2 (red)

Although all calibration curves for the same components in the different reactions are proven viable, and the independency of the components were tested positively, for further calculation, the equation of the corresponding reaction will be used.

3.5.3.2 Detection limit, accuracy, repeatability and reproducibility

The **detection limit** is the lowest concentration of a component of which the value is still reliable and quantitative. To acquire this value, 8 samples of the lowest concentration of 5 ppm were made. The detection limit is defined as three times the standard deviation on these results.

The **accuracy** is defined as the difference between the actual value and the calculated value from the calibration curve. It shows the trueness of the acquired results. For this validation, 8 samples of 50 ppm were made of each reaction. The average difference will be the accuracy.

The **repeatability** was designed to give an idea of the agreement between successive results of the same quantity and their deviation. 8 samples of 50 ppm of each reaction were made, the repeatability is defined as the standard deviation of these samples.

The **reproducibility** differs from the repeatability as the circumstances must be variable. To achieve this variability, 8 days long, one sample of 50 ppm of each reaction is made by either Cornelissen D. or Debrie R. from a freshly made stock solution. The reproducibility is the standard deviation on these samples.

For each validation method two stock solutions were made of 5000 ppm in acetonitrile, one for each reaction. From this, the appropriate amount was then transferred in a 5-ml volumetric flask to dilute to 5 or 50 ppm. This flask was then diluted to 5 ml with acetonitrile.

The graphs of each component can be found in 6.3 Appendix C: Validation curves. The summary table can be seen in Table 18.

Table 18: Detection limit, accuracy, repeatability and reproducibility

	Detection limit (ppm)	Accuracy (ppm/%)	Repeatability standard deviation (ppm)	Reproducibility standard deviation (ppm)	Detection limit standard deviation (ppm)	Accuracy standard deviation (ppm)
Acetophenone	0.59	1.86/3.71	0.84	0.42	0.20	0.11
Benzene	0.17	3.52/7.07	0.56	0.92	0.06	0.19
1,1-diphenylethanol	0.44	1.62/3.22	0.60	0.61	0.15	0.11
Bromobenzene	0.28	-0.35/-0.70	0.59	2.32	0.09	0.11
Biphenyl	0.28	1.35/2.71	0.55	0.31	0.09	0.10
Benzaldehyde	0.24	1.08/2.16	0.18	3.07	0.08	0.29
Diphenylmethanol	0.32	-1.01/-2.01	0.33	1.06	0.11	0.10
Benzene	0.44	3.28/6.51	0.63	0.49	0.15	0.30
Bromobenzene	0.36	-1.51/-3.03	0.65	1.08	0.12	0.78
Biphenyl	0.53	-1.05/2.10	0.35	0.49	0.18	0.78

It can be concluded that the detection limit overall is relatively low. When diluting the samples, the goal is to dilute till 50 - 100 ppm when calculating with the maximal concentration possible for each component. It is possible that with a high conversion, the detection limit for bromobenzene is reached, but the most important components to analyse are both alcoholic end products for the complete reactions, and benzene for the first part of the reactions. If bromobenzene, acetophenone, benzaldehyde of biphenyl cannot be detected, this too is a good indication for a high conversion with less side products (if no other side products were formed) and the actual product would be measured quantitively.

The accuracy varies from -1.51 ppm to 3.52 ppm, or from 3% less (bromobenzene) to 7% more (benzene) than the actual values. Especially for benzene in both reaction, this accuracy must be kept in mind for the results.

The repeatability with a maximum below 1 ppm in deviation is very well. The reproducibility has a slightly larger deviation with 3.07 ppm for benzaldehyde, but is still acceptable.

Another important factor is that no trend is visual in the analysed samples, as can be seen in 6.3 Appendix C: Validation curves.

3.5.3.3 Recovery

The measured concentration of a component is often not the real concentration in the reactor. The sample preparation could lead to an over- or an underestimation. The fraction of the component of interest that is detected is defined as the recovery. This is an important parameter as the sample solution of THF is quenched with an aqueous solution were 30 g THF per 100 g water is soluble [91].

To measure the recovery, first 0.5 ml sample from a cascade Grignard experiment (matrix) and 0.5 ml pure THF (instead of a 1.0 ml sample) is processed according to the normal analysis procedure as

described in 3.5.1 Sample preparation. In the same way, 7 more samples are made.
Secondly, 0.5 ml sample from a cascade Grignard experiment (matrix) is spiked with 0.5 ml 50000 ppm stock solution of the reaction components to be considered. This is then further processed as described in 3.5.1. Again, 7 more samples are made in the same way. This method was conducted for the two reactions.

The recovery is the average of the differences between the spiked sample and the unaffected sample, over the spike concentration. The recovery is shown in Table 19, expressed in percentages. The results of each sample did not show any trend during the analysis, which can be verified in 6.3 Appendix C: Validation curves in the section 6.3.3 Recovery reaction 1 and 2.

Table 19: Recovery of each component

	Recovery (%)	Standard deviation (%)
Acetophenone	103.34	3.37
Benzene	126.55	2.59
1,1-diphenylethanol	122.50	3.05
Bromobenzene	130.67	3.48
Biphenyl	130.60	3.18
Benzaldehyde	114.53	1.64
Diphenylmethanol	108.59	3.11
Benzene	126.55	2.59
Bromobenzene	130.67	3.48
Biphenyl	130.60	3.18

The recovery is always greater than 100%, which could be predicted as THF dissolves in the aqueous layer, but the components are more compelled to the organic layer. This leads to an increase of concentration as roughly the same amount of components reside in less solvent. Without the recovery, the result would be significantly overrated.

3.5.3.4 Influence of matrix

The recovery that was explained above, was tested by using the matrix as it appeared in Grignard experiments. The influence of this matrix on the recovery, was therefore examined as well.

For each reaction, a synthetic stock solution of 5000 ppm in THF was made with the components that were analysed in this reaction. Of each stock, a sample was taken 3 times, and analysed according to the conventional sample preparation. After HPLC analysis, the results were calculated by applying the recovery that was found above. The results are shown in Table 20, and are compared with the matrix samples, which are all 5000 ppm (by applying the recovery). The results of each sample did not show any trend during the analysis, which can be verified in 6.3 Appendix C: Validation curves, more specifically 6.3.4 Influence of matrix for reaction 1 and 2.

Table 20: Sampling preparation method with synthetic stock

	Average concentration with recovery applied on synthetic stock (ppm)	Standard deviation (ppm)	Overestimation (+) or underestimation (-) of results (%)
Acetophenone	6086	0.94	21.73
Benzene	5189	0.83	3.78
1,1-diphenylethanol	4759	0.63	-4.82
Bromobenzene	4411	0.48	-11.79
Biphenyl	4628	0.61	-7.43
Benzaldehyde	4983	1.55	-0.33
Diphenylmethanol	5571	1.60	11.42
Benzene	5332	1.70	6.63
Bromobenzene	4458	1.35	-10.85
Biphenyl	4452	1.78	-10.96

When the recovery is applied on a synthetic sample from a synthetic stock solution (only THF and analysed components) instead of a matrix sample (from a Grignard experiment), it gives wrong results which deviate a lot from the 5000 ppm that had to be obtained. Therefore, the recovery can only be used when samples are taken from Grignard experiments, and not when synthetic solutions are used.

3.5.3.5 Degradation

During the validation, it was observed that both the stock solution in acetonitrile of acetophenone and benzaldehyde decreased in time, leading to an increase in benzene as a partial degradation product. The degradation was observed for 8 days to conclude the shelf life of the HPLC samples. At day one, a 5000-ppm stock solution in acetonitrile of each reaction was made. Every day, a 50-ppm sample of each reaction was made from these stocks, to visualise the degradation. The results are displayed in Figure 44 and Figure 45.

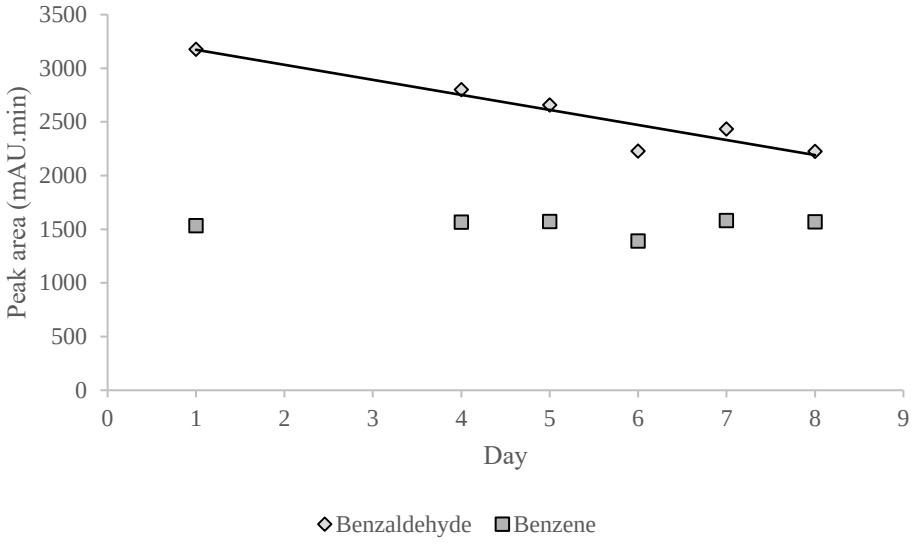

Figure 44: Degradation of benzaldehyde

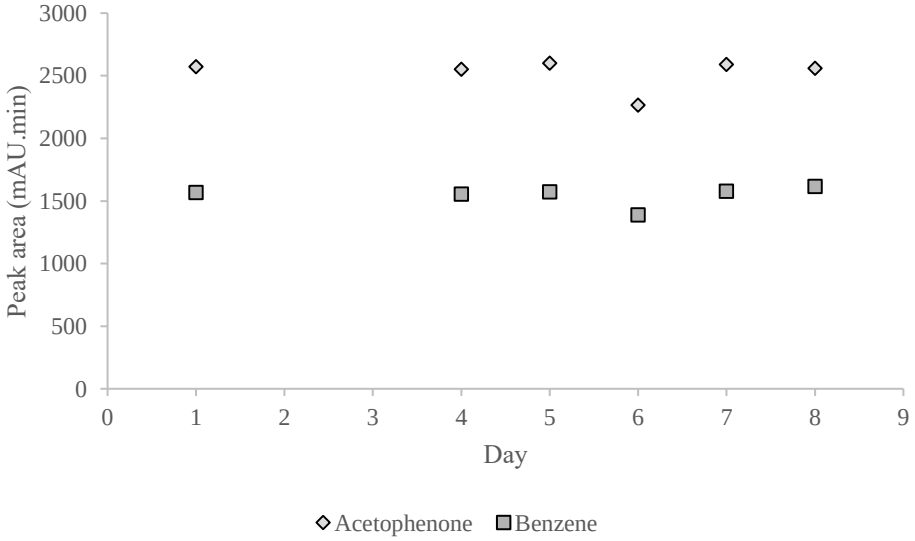

Figure 45: Degradation of acetophenone

It is obvious that benzaldehyde degrades starting at day one. Samples containing benzaldehyde are therefore only quantitative the day of the experiment. Acetophenone did not degrade over the period of 8 days. The observed degradation must have been with a sample older than this. This leads to the conclusion that a sample of reaction one can be reanalysed the next day, even the next week, without the danger of degrading product.

4 RESULTS AND DISCUSSION

4.1 TESTING MAGNESIUM ACTIVATION AND REACTION INITIATION

Different magnesium activation and initiation methods are tested to find an applicable method on lab scale. The results of these tests are shown in Table 21. When magnesium activation does not happen instantly, the solution is shaken for 10 minutes to see if a delayed activation would occur.

Table 21: Overview of magnesium activation and reaction initiation experiment results

Experiment	Activation technique	Description of execution
1	Iodine in THF	No activation after 10 min of shaking At 10 min: Addition of 1 ml pure bromobenzene At 13.5 min: magnesium activation and initiation At 16 min: Moderate reaction with weak convection patterns of magnesium (T<50 °C) No gas formation
2	Iodine in THF (heated to 66 °C, boiling point of THF, then cooled again to room temperature)	No activation after 16 min of shaking, but gradual transition from dark to light yellow At 16 min: Addition of 1 ml pure bromobenzene Instant activation and slow reaction (initiation) No convection patterns of magnesium (T<30°C) No gas formation
3	Iodine vapour	No activation after 10 min of shaking At 10 min: Addition of 1 ml pure bromobenzene Instant activation and heavy reaction (initiation) with intense convection patterns of magnesium (50<T<66 °C, $T_{boiling}$ of THF) No gas formation
4	Iodine in THF + Phenylmagnesium bromide addition	After 1 min: Addition of 100 µl 1.0 M phenylmagnesium bromide in THF solution Instant activation At 2 min: Addition of 1 ml pure bromobenzene and almost unremarkable initiation At 3 min: Heavy reaction with boiling of solution (gas formation)

5	Phenylmagnesium bromide addition	After 1.5 min: Addition of 100 µl 1.0 M phenylmagnesium bromide in THF solution Instant activation At 2 min: Addition of 1 ml pure bromobenzene Instant heavy reaction (initiation) and boiling of solution (gas formation)
6	Iodine vapour + Iodine in THF + Phenylmagnesium bromide addition	After 1 min: Addition of 100 µl 1.0 M phenylmagnesium bromide in THF solution Instant activation At 2 min: Addition of 1 ml pure bromobenzene Instant very heavy reaction and boil over of test tube (extreme gas formation)

As can be seen in the table, the magnesium is always activated. This activation is not always instantaneous (experiment 1) and does not always happen before the addition of bromobenzene (experiment 1, 2 and 3). However, when bromobenzene is added, a direct activation is observed in experiment 2 and 3, which suggests that there is already some (slight) activation.
Reaction initiation is also visually obtained directly after the addition of bromobenzene in each test, except for experiment 1 and 4. However, it is assumed that the initiation has already taken place here, but that the reaction starts very slowly because the magnesium was already activated.
Differences in reaction intensity are also observed. Experiment 2 shows a slow reaction, without convection patterns of magnesium or gas formation of THF. The intensity of the reaction (convection patterns of magnesium and gas formation) increases gradually in experiment 1, 3, 4, 5 and 6, going from a hot (<50 °C) solution with magnesium convection patterns to an extreme gas formation of the solvent THF, of which the volume increases to more than 5 times the starting volume (6 ml), causing the test tube to overflow.
Lastly, it is noted that magnesium is shaken for 16 minutes before bromobenzene is added in experiment 2. The reason is that the solution gradually changes from dark to pale yellow, which is not visible in any other experiment. This could thus indicate partial activation of the magnesium.

It is concluded that the combination of iodine vapour, iodine in THF and phenylmagnesium bromide addition (experiment 6) gives the most intense activation and initiation technique on lab scale for the reaction that forms phenylmagnesium bromide. The qualities of the three separate techniques probably amplify each other to one instantaneous initiation technique. The iodine vapour technique not only activates the magnesium when the test tube with magnesium is heated, but also dries the equipment (in this case the test tube). Phenylmagnesium bromide also exerts a water-removing effect, because it is injected after the solvent THF is poured in the test tube, it makes the solvent anhydrous. These two reasons that ensure an anhydrous environment are a decisive factor that has already been discussed in the section 2.1.5 [40] [41]. The iodine that is solved in THF is mainly used to visually observe the activation of magnesium.

The activation and initiation by iodine vapour, phenylmagnesium bromide addition and the combination of iodine in THF and phenylmagnesium bromide are also equivalent initiation methods. They may not provide the most intense reaction, but the initiation happens instantaneously, which is desired in the industry. However, the industrial relevance of these techniques should be considered. For example, the use of iodine vapour is more difficult and costly in industry than at lab scale, where

the iodine vapours are simply created by holding the sublimated iodine (in the reactor) above a flame until purple vapours were formed. Therefore, an addition of phenylmagnesium bromide can be more interesting.

Reaction initiation with non-heated and heated iodine in THF (experiment 1 and 2, respectively) works, but does not result in a good reaction intensity. The presence of water may form a problem since these techniques do not work water-removing. Furthermore, the solvation of iodine by THF can also have a negative influence on the magnesium activation. Therefore, these initiation methods are not recommended.

Because such an instantaneous and intense activation and initiation takes place when using technique 6, there is no danger for the accumulation of bromobenzene in the continuous-flow reactors used in this Master's thesis which could lead to a runaway reaction. Therefore, this technique is further used in all reactor setups.

To investigate how much 1.0 M phenylmagnesium bromide solution had to be added to 0.5 g of magnesium and 5 ml of THF with a trace of iodine, phenylmagnesium bromide solution is added in 10 µl increments. After a total addition of 100 µl, there is magnesium activation. This amount of phenylmagnesium bromide is important in scaling up experiments.

Further research on the initiation methods on a larger scale would be useful, since an industrially relevant method should eventually be developed. Also, more repetitions on the different initiation methods should be conducted, to determine their reliability. Optionally, it can also be investigated how much the activation energy of the Grignard reagent formation decreases with each initiation method. Finally, it would be interesting to look if the amount of 1.0 M magnesium bromide solution to be added depends on the volume of solvent or the mass of magnesium. Ideally, these experiments all take place in an inert nitrogen environment, so that water in the air cannot have an influence on the initiation.

4.2 GRIGNARD REAGENT FORMATION TESTS

In the experiments performed in one CSTR, the influence of both the concentration of bromobenzene and magnesium, as well as the residence time and feed rate are examined. The results will be discussed in the following paragraphs. When interpreting the results, it should be kept in mind that the tests are performed with a constant feed rate, and varying reaction volume (except for the feed rate experiments). The influence of the reaction volume itself is not examined and could be an interesting parameter for future research.

4.2.1 Influence of concentration bromobenzene

First, the relation between the concentration of bromobenzene to its conversion and the yield of Grignard reagent is examined. The ratio magnesium to bromobenzene and the residence time are kept constant at 6:1 and 5 min, respectively. The results are shown in Figure 46.

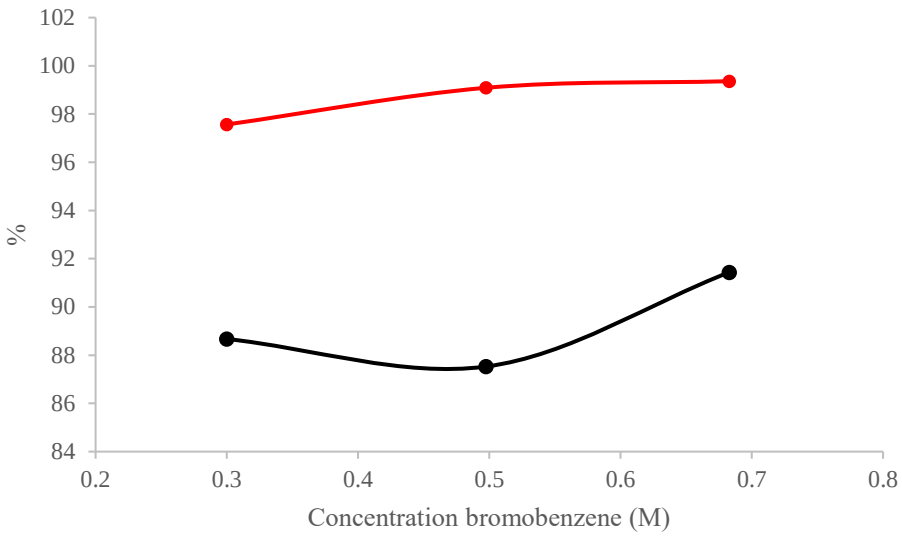

Figure 46: Influence of the concentration of bromobenzene to the conversion (red) and yield (black)

The graph does not show a trend with an increasing concentration. On top, the yields of 88,67%, 87,53% and 91,44% for 0.3 M, 0.5 M and 0.7 M bromobenzene, respectively, are within the standard deviation of the reproducibility of 0.92 ppm (1.84%) for benzene, which is the quenched product of phenylmagnesium bromide. Therefore, no clear decision can be made from the results of the yield phenylmagnesium bromide.

The conversion of bromobenzene with the test at a concentration of 0.3 M shows that the reaction rate could be just too slow relative to the residence time of 5 min, as there is 2,43% unreacted bromobenzene present. On top, the temperature of each experiment increases with increasing concentration (48.7 °C, 52.4 °C and 56.9°C for 0.3 M, 0.5 M and 0.7 M, respectively), and thus increasing the reaction rate as well. This leads to an increase in the bromobenzene conversion as well. The varying temperature is an extra factor, but except for the reaction rate of bromobenzene, it seems that the reaction is not influenced. With an increasing temperature, it is expected to form more side products because the reaction rate increases as described in section 2.1.8.1 [51] [52] [53]. However, the difference between the yield and the conversion for the highest concentration and temperature is the smallest, with 8,57% side products. This argument must also be approached carefully, since no conclusive decisions can be made from the yield of phenylmagnesium bromide.

Possibly, the effect of the bromobenzene concentration on the Grignard formation reaction in a CSTR could be better investigated by testing a wider range of concentrations. In that case, the differences between the conversion bromobenzene and yield phenyl magnesium bromide could be bigger, which could lead to an unequivocal conclusion. However, the concentration should not be higher than 0.7 M without external reactor cooling, as the exothermicity of the reaction could cause the reaction mixture to boil.

4.2.2 Ratio magnesium to bromobenzene

During the experiments of an alternating ratio magnesium to bromobenzene, the concentration of bromobenzene and the residence time are kept constant at 0.5 M and 5 min, respectively. The results for the measured conversions and yields are shown in Figure 47.

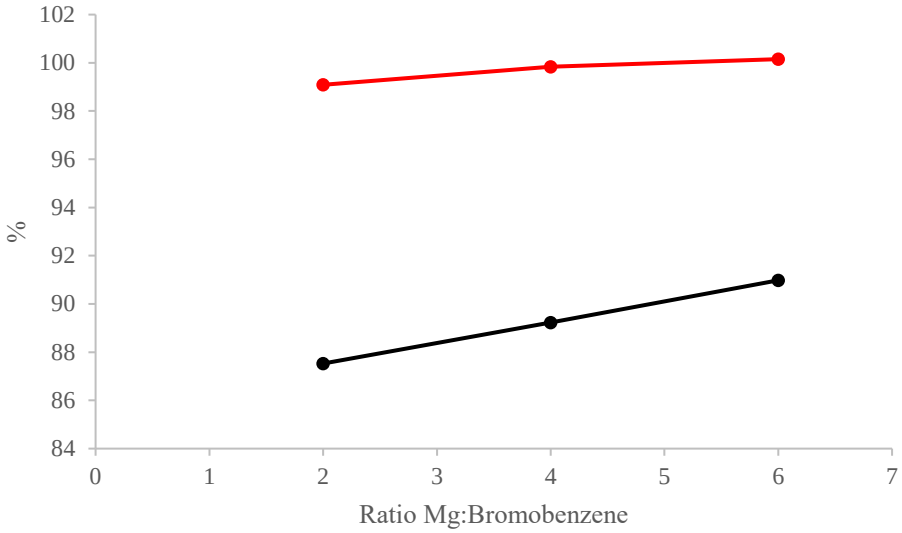

Figure 47: Influence of the ratio magnesium to bromobenzene to the conversion (red) and yield (black)

It appears that an increasing ratio of magnesium influences the reaction rate. With a ratio of 2:1, the reaction is not finished yet with a conversion of 99.09%. The ratios 4:1 and 6:1 respectively have a conversion of 99.84% and 100%. This conclusion contradicts the previously assumed pseudo zeroth-order for magnesium in the reaction rate as discussed in section 2.2 Reaction kinetics [54]. The most likely cause may be the use of magnesium powder instead of turnings, used in their research. However, the formation of less side product is an expected result. By increasing the ratio, it is less likely for 2 molecules of bromobenzene to react with each other by Wurtz coupling, reducing at least one side product: biphenyl. Other possible side products are phenol, diphenyl ether, and diphenyl-benzene by oxidation of phenylmagnesium bromide, although these products aren't verified with a HPLC analysis. Further research into the quantification and identification of these by-products is therefore advised.

The yields are 87.53%, 89,53% and 90,98% for ratios Mg: bromobenzene of 2:1, 4:1 and 6:1 respectively, shown by the steeper black curve. From this graph, it can be concluded that an increase of ratio magnesium to bromobenzene results in less side products, although this result should be approached with caution as the standard deviation for the reproducibility of benzene quantification is 1.84% and the total increase is only 3.45%.

4.2.3 Residence time

Although the reaction kinetic results in section 4.3.1 show the relation between residence time and the conversion and yield, these tests are performed prior to the decision to thoroughly examine the reaction kinetics. The concentration of bromobenzene and ratio of magnesium to bromobenzene are kept constant at 0.5 M and 6:1, respectively. The results can be observed in Figure 48.

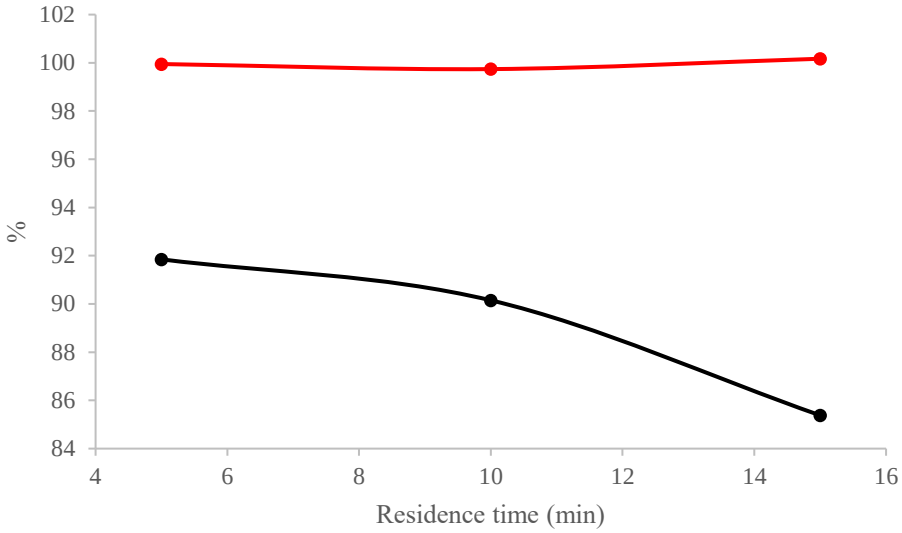

Figure 48: Influence of residence time to the conversion (red) and yield (black)

The graph shows a decrease in yield over time, while all three tests reach complete conversion. The decrease in yield leads to the conclusion that the product phenylmagnesium bromide degrades during the process, resulting in side products. This degradation is most likely due to the degradation reaction with oxygen, since the reactor was not purged with nitrogen [43].
This conclusion makes the residence time in the first reactor an important parameter to maximize the yield of the cascade when no purging with nitrogen is provided. It is therefore recommended to conduct future experiments under nitrogen atmosphere, to obtain a maximum yield of phenylmagnesium bromide.

4.2.4 Feed rate

Different feed rate experiments are performed to examine the influence of possible hot-spots at the inlet of the reactor. The results are presented in Figure 49. During the experiments, the concentration of bromobenzene, the ratio magnesium to bromobenzene and the residence time are kept at constant values of 0.5 M, 6:1 and 10 min, respectively.

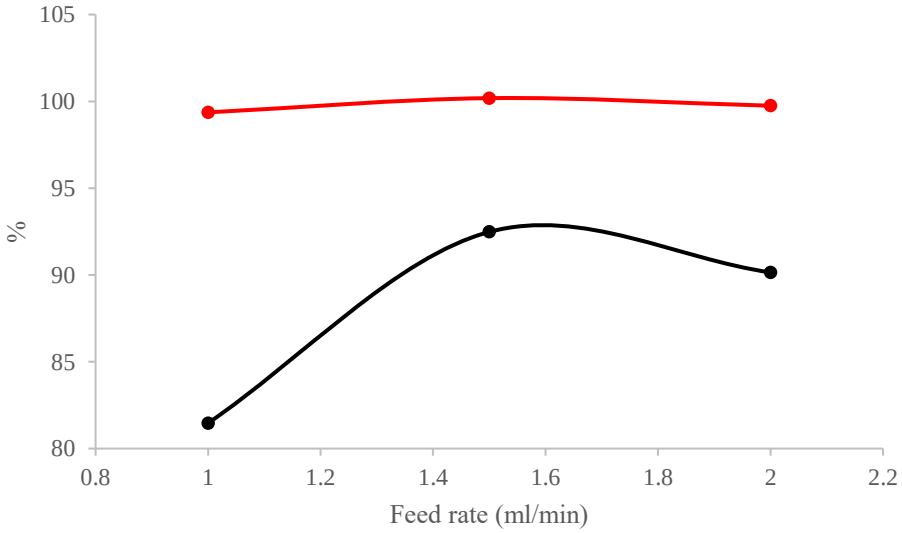

Figure 49: Influence of the feed rate to the conversion (red) and yield (black)

Except for the conversion of 99,37% with a feed rate of 1 ml/min, all conversions are 100%. However, the yield shows great differences. Taking the standard deviation of benzene quantification into account (1,84%), the experiments with feed rate 1.5 ml/min and 2 ml/min have similar yields, 92,48% and 90,14%, respectively. The feed rate of 1 ml/min results in a yield of 81,47%.

The results show biphenyl percentages of 0.07%, 0.05% and 0.03% for 1 ml/min, 1.5 ml/min and 2 ml/min, respectively (not shown in Figure 49). These yields of biphenyl are too low to cause the large deviations of the yields, seen in Figure 49. Increased Wurtz coupling due to hot-spots at the inlet is therefore excluded. The increased formation of side products could be a result of the reaction volume. The reaction volumes were 10 ml, 15 ml and 20 ml, respectively, for the experiments of 1 ml/min, 1.5 ml/min and 2 ml/min with a constant reactor volume of 50 ml. Therefore, more air is present in the reactor, increasing the oxidation of the Grignard reagent which can cause the significant decrease of the phenylmagnesium bromide yield at a feed rate of 1 ml/min.

Therefore, it cannot be concluded that a feed rate is the cause of the yield of only 81.47 % for phenylmagnesium bromide. Future experiments should examine the influence of the reaction volume to make a conclusive decision for these experiments. The temperature of these experiments should be kept constant as well, as these experiments have an increasing temperature with an increasing feed rate as well (38.5 °C, 43.3 °C and 45.3 °C for 1, 1.5 and 2 ml/min, respectively), introducing another varying factor in these experiments. Also, a wider range of feed rates should be tested, so that a better trend would be visible in the results.

4.3 Reaction kinetics

The reaction characterisation is of great value. On top of the obtained activation energy and reaction order, the acquired reaction rate is important for the process intensification as the obtained reaction rate gives insight in the ideal residence time for the reaction. All these experiments are performed in a batch reactor, with a set temperature, controlled by the Easymax. For each experiment, samples are taken at appropriate times and quenched directly with diluted NH_4Cl.

4.3.1 Grignard reagent formation

The reaction of bromobenzene to magnesium is monitored by collecting samples during a time period as described in section 3.4.1. The result of the experiment of 20°C and 0.5 M bromobenzene and a magnesium to bromobenzene ratio of 2:1 is shown in Figure 50.

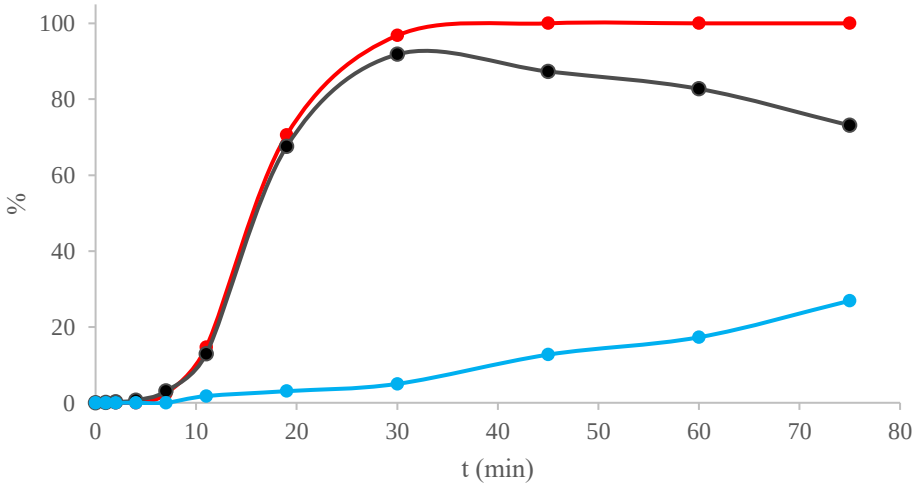

Figure 50: Conversion of bromobenzene (red), yield of phenylmagnesium bromide (black) and the formation of side products during the experiment of 20 °C and 0.5 M bromobenzene

First of all, the degradation observed in 4.2.3 is clearly visible in this experiment as well. The conversion increases to a maximal value at 30 minutes reaction time and a maximum yield of phenylmagnesium bromide of about 92% is reached at 30 min reaction time. As the time increases, yield of this product decreases, and side or degradation products are formed up to 26.90% in a time period of only 65 min. After 11 minutes, the first degradation and/or side products are observed.

This rather fast degradation shows the importance of the adjusted residence time in the first reactor. A possible cause could be the reaction with oxygen as described in section 2.1.5 [30] [42]. To be certain, future experiments should be performed in an inert, nitrogen- or argon-environment and should result in no degradation over time.

Figure 51 shows that the side products are formed at a constant rate during the reaction, at 15 °C, 0.5 M bromobenzene and a ratio of 2:1 magnesium.

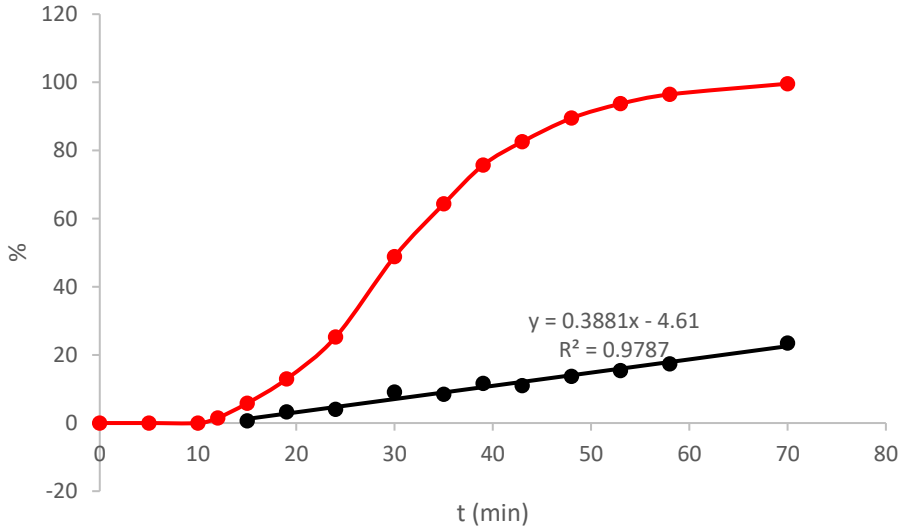

Figure 51: Formation of side products (black) and conversion (red) during the reaction of bromobenzene with magnesium

This experiment shows a formation of 23.79 % side products, and is a clear example of the linear increase of the formation of side products with time. A shorter experiment (0.5 M bromobenzene and a ratio of 4:1 magnesium to bromobenzene) showed at 100% conversion after 28 min only 8.00% side products. From these results it can be concluded that the formation of side products occurs evenly throughout the experiments, since the experiment shown in Figure 51 shows 9% formation of side products at 30 minutes. If the presence of air cannot be prevented, it is advised to perform a fast reaction, meaning a high temperature, concentration of bromobenzene and mass of magnesium that requires a low residence time to decrease the side products.

4.3.1.1 Determination of reaction order

At first, the order of the reaction is established by halving the concentration of magnesium and halving the concentration of bromobenzene to 0.25 M, performed at 30 °C. The results are shown in Figure 52 and Figure 53.

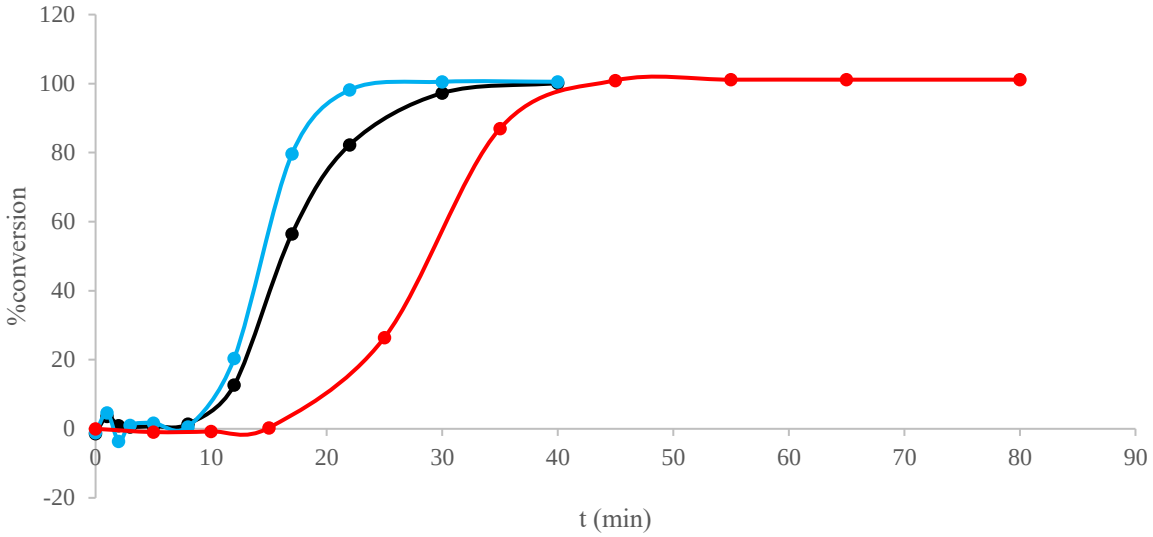

Figure 52: Conversion of bromobenzene for the experiment with 0.5 M bromobenzene and ratio 4:1 (blue), 0.5 M bromobenzene and ratio 2:1 (black), and 0.25 M bromobenzene and ratio 4:1 (red)

The blue curve represents the test with the ratio 4:1 magnesium to bromobenzene and a concentration of 0.5 M for bromobenzene. This curve can be compared to the black curve, where the mass of magnesium is halved, and to the red curve where the concentration of bromobenzene is halved.

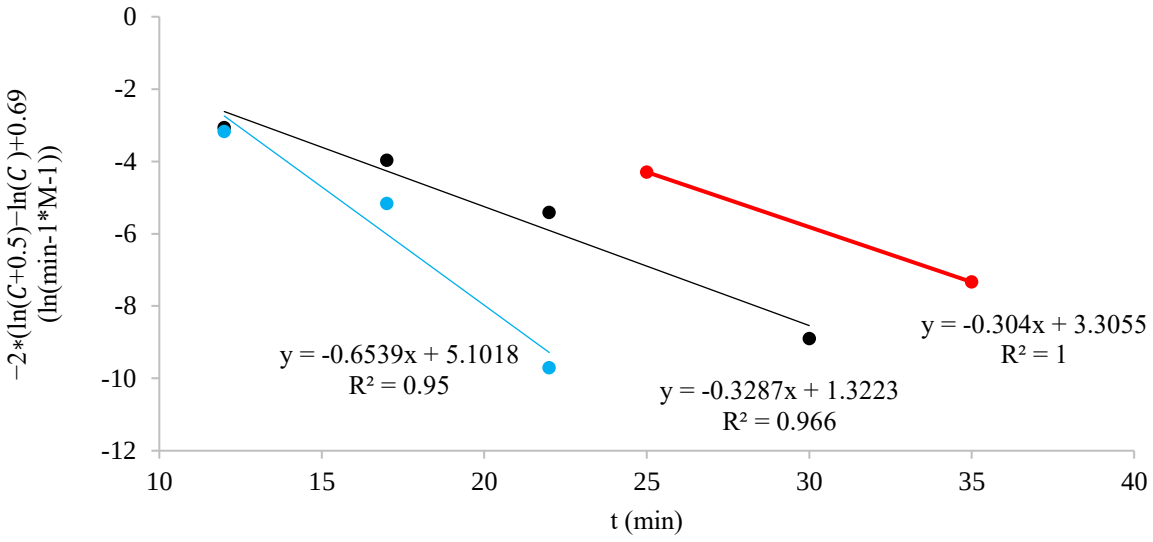

Figure 53: Variation of the concentration of magnesium (blue relative to black) and the concentration of bromobenzene (blue relative to red)

From these graphs, the rate constant k can be obtained:

$$-r_A = \frac{dC_a}{dt} = k * C_A * C_B$$

with $C_B = (0.5 + C_A)$, C_B the concentration of magnesium and C_A the concentration of bromobenzene.

Solving this equation leads to the curves shown in Figure 46 with the equation:

$$-2 * (\ln(C_A + 0.5) - \ln(C_A) + 0.69 = -k * t + [-2 * (\ln(C_{A,0} + 0.5) - \ln(C_{A,0}) + 0.69]$$

Or simplified:

$$y = -k * t + cte$$

When halving the concentration of magnesium and bromobenzene, the rate constant halves as well, more precisely, with a factor of 0.504 and 0.465, respectively. Although it was believed at first to be a first-order reaction for bromobenzene, the results clearly showed a second-order relation. Therefore, the equations above were applied.

A possible explanation of the second-order result instead of the expected first-order reaction with an excess of magnesium could be the different type of magnesium as described in section 2.2 Reaction kinetics [54]. They concluded that the activated sites on magnesium are limited. These reactive sites increase in area as the activated magnesium reacts with the organic halide. The reactive area is not increased by initiating new sites during the reaction.

As the volume/area ratio of powder is less than the volume/area ratio of turnings, the magnesium particles are faster diminished, and new sites are necessary. The ratio of 2:1, even 4:1 could therefore be too little to become an excess compared to the concentration of bromobenzene and result in a pseudo zeroth-order for magnesium.

4.3.1.2 Determination of k_0 and E_a

After confirming the order of the reaction, the temperature can be altered to acquire the activation energy E_a and the pre-exponential factor k_0. Three different temperatures are tested with a concentration of 0.5 M bromobenzene and a magnesium to bromobenzene ratio of 2:1. The results are displayed in Table 22.

Table 22: Rate constants for reaction temperatures of 15, 20 and 30 °C

T (K)	k ($min^{-1}*M^{-1}$)	R^2
288	0.1538	0.9762
293	0.2013	0.9008
303	0.3849	0.9894

The rate constants are obtained analogous to the rate constants of the determination of the reaction order. These results are then converted to a $\ln(k)(\frac{1}{T})$-graph, which is shown in Figure 54.

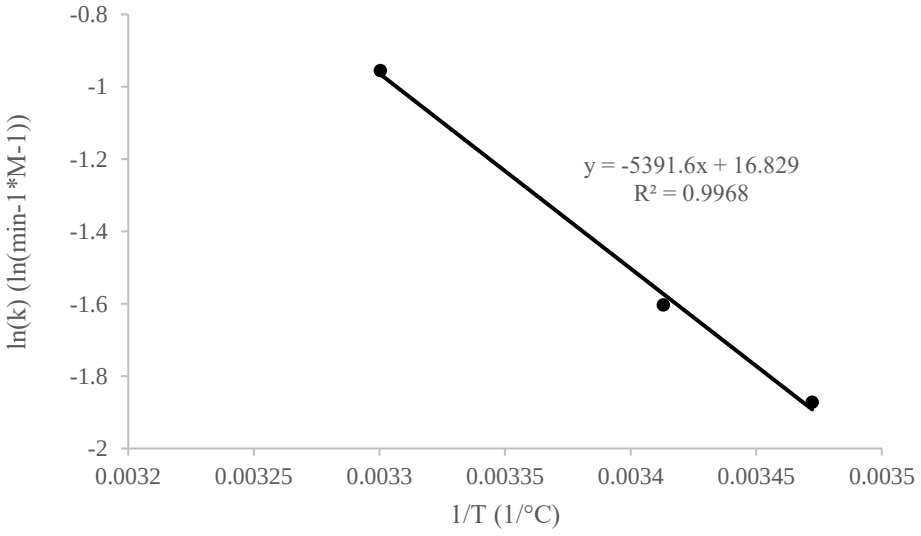

Figure 54: ln(k)(T^{-1}) -graph for the reaction of bromobenzene with magnesium

The activation energy and pre-exponential factor can now be acquired as the equation in the graph stands for:

$$\ln(k) = \frac{-E_a}{R} T^{-1} + \ln(k_0)$$

The activation energy is:

$$E_a = R * 5391.6$$
$$E_a = 8.31 * 5391.6 \ \frac{J}{mol}$$
$$E_a = 44\,828.3 \ \frac{J}{mol}$$

The pre-exponential factor is:

$$\ln(k_0) = 16.829$$
$$k_0 = e^{16.829}$$
$$k_0 = 2.04 * 10^7 \ min^{-1} M^{-1}$$

The activation energy of the reaction of bromobenzene and magnesium is 44,8 kJ/mol, and the pre-exponential factor is $2.04*10^7$ min^{-1} M^{-1}. With these values and the Arrhenius equation $k = k_0 e^{\frac{-E_a}{R*T}}$, the rate constant for each temperature can be calculated. As a result, the reaction rate can be calculated for different concentrations as well with the equation $-r_A = \frac{dC_a}{dt} = k * C_{Bromobenzene} * S_{Magnesium}$.

4.3.1.3 Calculating the required residence time for cascade tests

The reaction rate for the cascade tests can also be calculated from the reaction rate equation. The conditions of the first reactor in these cascade tests are a temperature of 50 °C, a ratio magnesium to bromobenzene of 2:1 and a bromobenzene feed concentration of 0.5 M with 7.2915 g of magnesium (3.2.5).

A method to estimate the residence time needed in the first reactor to obtain 100% conversion of bromobenzene, is by using the Arrhenius equation. It is visible in Figure 52 that in a reaction time of about 32 minutes at 30 °C (black curve) the reaction is completed (100% bromobenzene conversion). With the Arrhenius equation: $k = k_0 e^{\frac{-E_a}{R*T}}$, the reaction rate is increased with a factor of 3.01 when the reaction is carried out at 50 °C (compared with the test at 30 ° C). The required reaction time at 50°C would be 10 min 39 sec, when the same amount of magnesium is used.

However, in the cascade tests 7.2915 g of magnesium is used. In the reaction characterisation tests at 30 °C with a 2:1 ratio magnesium to bromobenzene, only 1.9444 g magnesium is used (3.4.1). Because the area of magnesium S_{Mg} is first order, the reaction is 3.75 times faster in the cascade tests. Thus, the required residence time decreases to 2 min 50 sec for a 100 % conversion of bromobenzene in the first reactor. When the same calculations are executed for a 99% conversion of bromobenzene, a residence time of 2 min 13 sec is needed. It can be concluded that a much smaller residence time is required in the first cascade reactor, which now has a residence time of 9 min 10 (3.2.5).

4.3.2 Reaction of phenylmagnesium bromide with acetophenone and benzaldehyde

For the characterisation of the second part of the reaction, the experiments shown in Table 23 are performed. These experiments are performed analogous to the previous experiments of 4.3.1: carried out in a batch reactor, with a set temperature, controlled by the Easymax. For each experiment, samples are taken at appropriate times and quenched directly with diluted NH_4Cl.

Table 23: Experiments performed for the characterisation of the reaction of phenylmagnesium bromide to acetophenone

Parameter	1	2	3	4	5
Concentration acetophenone in reactor (mole/l)	0.5	0.06	0.06	0.5	
Concentration benzaldehyde in reactor (mole/l)					0.5
Concentration phenylmagnesium bromide in reactor (mole/l)	0.5	0.06	0.06	0.5	0.5
Temperature (°C)	30	-10	30	-10	30
Duration experiment (min)	22	20	50	5	1

The reaction of the first experiment happens too fast to collect enough samples for a characterisation, as the first sample showed a conversion of 100% for phenylmagnesium bromide.
Both the concentration and temperature are drastically decreased in the second experiment to ensure enough reaction time, only this time, the reaction goes too slow to characterise with a conversion of phenylmagnesium bromide of 5% after 20 minutes.
Test 3 and 4 give nearly instantaneous conversion so it was concluded that conversion of the formed phenylmagnesium bromide would definitely be instantaneous at the intended temperature and concentration in the cascade tests (50 °C and 0.5 M, relatively). Furthermore, no degradation is observed, within the experimental time of 50 minutes for the third experiment.

The characterisation of benzaldehyde results in an even heavier reaction than the reaction to acetophenone. Benzaldehyde is therefore likely even more reactive than acetophenone.
Because of the extremely fast reaction rate of both reactions with acetophenone and benzaldehyde with temperatures (30 °C) below the intended 50 °C in the cascade setup, reaction will not be kinetically controlled in the envisaged reactor setup and further kinetic experiments are not performed.

The high reactivity of the coupling reaction makes this reaction an excellent candidate to be performed in a flow process. If this reaction is performed in large batch reactors, the time to empty and clean the reactor in between would take most of the time. On top, the released heat would need an extreme amount of cooling, or careful dosing is necessary, increasing the time per batch. These disadvantages would not occur when working in smaller flow reactors. Further research into the optimization of this reaction in a flow reactor is therefore certainly recommended.

4.4 RESIDENCE TIME DISTRIBUTION

The results of the residence time distribution experiments are discussed in the following paragraphs. The first section (4.4.1) is the RTD of the first reactor with both the double angled settling pipe and the magnesium trap. The section 4.4.2 is the RTD of solely the second CSTR. Lastly, the section 4.4.3 is the distribution measured for the reagent of the bromobenzene solution entering the first reactor (measured with a negative step experiment from 0.1 M KCl to milli-Q water as described in 3.3). The setups can be consulted in the section 3.2.

Before these results are discussed, an important comment should be made. While the reactors and the cascade are characterised as if they contain microfluid (0.1 M KCl solution), it is important to know that the first reactor operates as a macrofluid when the Grignard reaction is carried out in the reactor setup. This was also cited in the literature in the section 2.4. However, this deviation is much smaller than the deviation caused by the retention of magnesium by the solids settling system when only looking at the magnesium concentration. The concentration of magnesium in product flow of reactor 1 (after the magnesium trap) is highly different from the concentration in the reactor. Furthermore, the concentration of magnesium in the reactor itself is also different over time because of the one-time

addition of magnesium. This RTD measures solely the RTD of the liquid phase, the solid movement is not taken into account.

4.4.1 Cascade reactor 1

The result of the first residence time distribution experiment is displayed in Figure 55, obtained by dividing the measured conductivity by the maximum conductivity at the start.

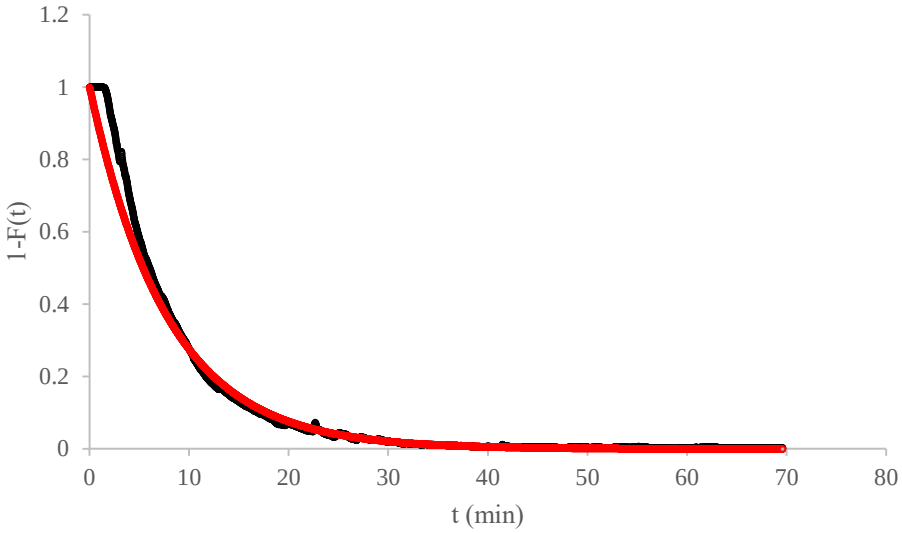

Figure 55: '1-F(t)'-curve for the measured (black) and ideal (red) for the negative step experiment for reactor 1

The black curve is the data recovered from the experiment, the red curve is the fitted equation, plotted with the software Eureqa Pro.

This 1-F(t)-graph for a negative step experiment results in:

$$1 - F(t) = e^{-0.129t}$$

with an R^2 of 0.997.

F(t) is defined as the cumulative distribution function, shown in Figure 56.

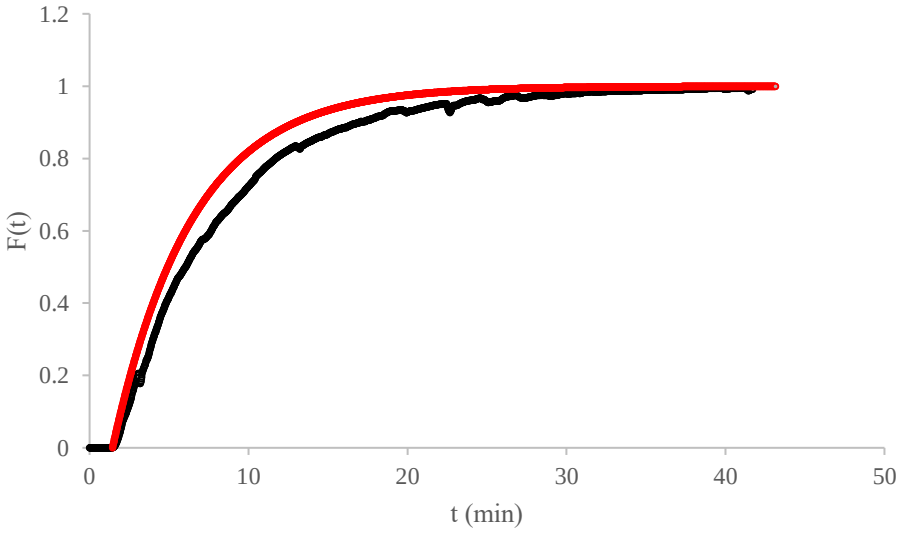

Figure 56: Measured (black) and ideal (red) F(t)-graph for reactor 1

F(t) leads to the residence time $\bar{t}$ as described in the literature section 2.4.1 [87]:

$$F(t) = 1 - e^{-0.129t}$$

$$E(t) = \frac{dF(t)}{dt} = \frac{d(1 - e^{-0.129t})}{dt} = 0.129 * 0.879^{t}$$

$$\bar{t} = \int_0^\infty t\, E(t)\, dt = \int_0^\infty t * 0.129 * (0.879)^{t}\, dt = 7.75\,\text{min} = 7\,\text{min}\,45\,sec$$

The residence time of the first reactor is 7 min 45 sec, which is more than the intended 5 minutes. On top, there is a time lag due to the PFR nature in the setup of reactor 1, seen on the bottom left in Figure 56, as the curve is constant during the first 1 min 25 sec.
The total residence time of the first part of the cascade is 9 min 10 sec, almost twice the intended residence time. The time lag is caused by the settling pipe and the used tubing, operating as a PFR. The increased time, derived from the F(t)-curve is caused by the magnesium trap. This result is expected as the set flow is based on the 50 ml of solution in the first reactor, not taking into account the extra volume of the magnesium trap which may not be stirred, but is slightly mixed due to the incoming feed.

The increased time due to the settling pipe and the magnesium trap is not a big issue as there is no air available in the settling pipe to degrade the formed Grignard reagent (discussed in 4.3.1). The magnesium trap is pressure-tight, the oxygen present in the trap is therefore limited.

The difference between the measured and ideal F(t)-curve for a residence time of 5 minutes is displayed by shifting the equation, $F(t) = 1 - e^{-\frac{t}{\bar{t}}} = 1 - e^{-\frac{t}{5}}$, until after the constant part of the graph.
The difference between the residence times in the CSTRs (excluding the PFR-part) of 7 min 45 sec and 5 min respectively for the measured and ideal graphs is visible as the $F(t)_{measured}$-curve takes longer to reach the cumulative value of 1.

The variance σ_t^2, a measurement for the spread around the average, is obtained with following equation:

$$\sigma_t^2 = \int_0^\infty (t - \bar{t})^2 E(t)\, dt = \int_0^\infty (t - 9.17)^2 * 0.129 * (0.879)^{t}\, dt = 62.1$$

The dimensionless dispersion D/µL is determined with the equations:

$$\sigma_\theta^2 = \frac{\sigma_t^2}{\bar{t}^2} = \frac{62.1}{8.92^2} = 0.74$$

$$\sigma_\theta^2 = 2\left(\frac{D}{\mu L}\right) + 8\left(\frac{D}{\mu L}\right)^2 = 0.74$$

$$\frac{D}{\mu L} = 0.20$$

A dispersion above 0.1 is considered as big dispersion. The first reactor has, with a dispersion of 0.20, a CSTR nature as expected.
The E(θ)-curve is shown in Figure 57.

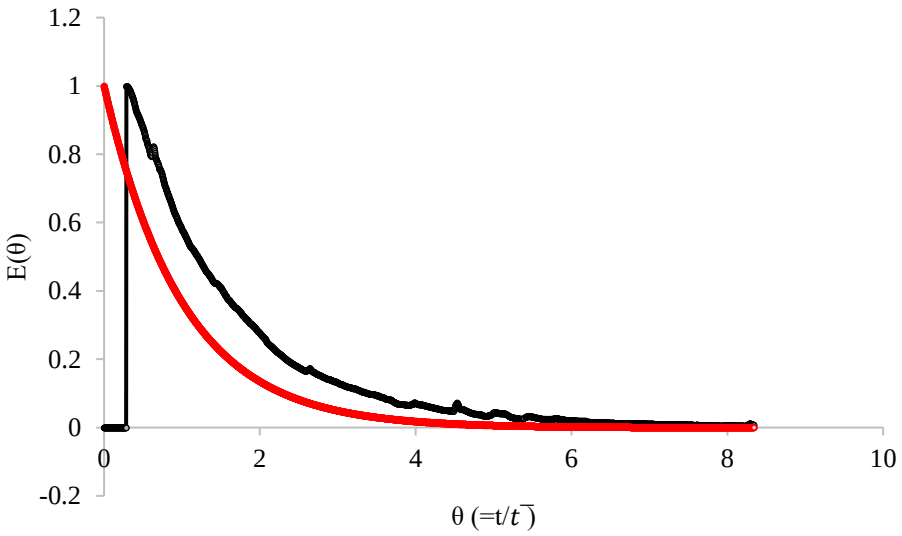

Figure 57: E(θ)-curve for the ideal CSTR (red) and the measured RTD (black) for reactor 1

An ideal PFR would show a small peak, symmetrical with the first part of the measured curve. The measured curve drops rather slow with a slope comparable to the ideal red curve. This verifies the previous conclusion of a CSTR character.

4.4.2 Cascade reactor 2

In Figure 58, the result of the second residence time distribution experiment can be observed. This graph is acquired analogous to the Figure 55.

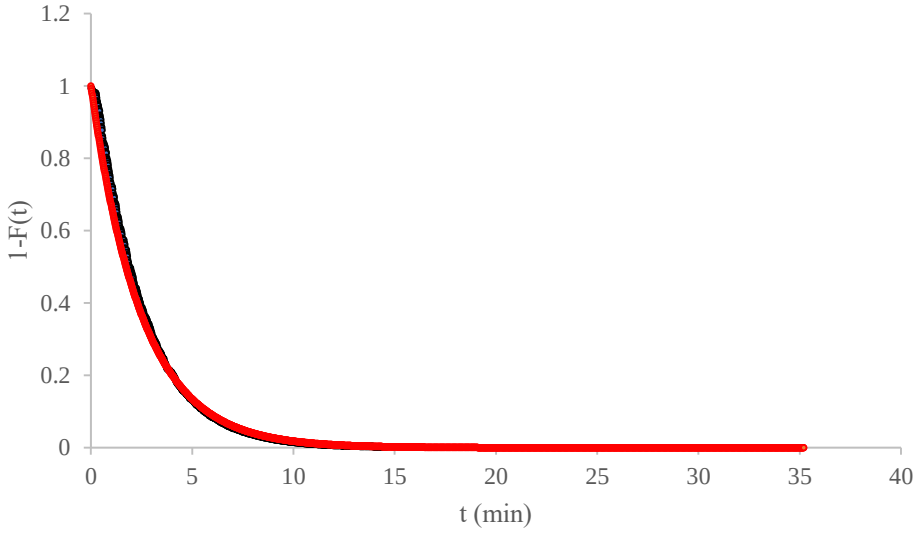

Figure 58: '1-F(t)'-curve for the measured (black) and ideal (red) for the negative step experiment for reactor 2

The black curve is the curve acquired by the measured data points, the red curve is the curve plotted by Eureqa Pro.

The cumulative distribution function F(t) for the second reactor is $1 - e^{-0.401t}$ with an R^2 of 0.994.

$$F(t) = 1 - e^{-0.401t}$$

$$E(t) = \frac{dF(t)}{dt} = \frac{d(1 - e^{-0.401t})}{dt} = 0.401 * (0.670)^t$$

$$\bar{t} = \int_0^\infty t\, E(t)\, dt = \int_0^\infty t * \ 0.401 * (0.670)^t \, dt = 2.494\, min$$

The residence time of the second reactor is 2 min 30 sec, which is close to the intended theoretical residence time of 2 min 45 sec. This could be a consequence of a small stagnant region within the reactor. There is however also a small time lag of 15 seconds. The total residence time of the second reactor is therefore equal to the intended 2 min 45 sec, although this time lag is not desirable. On top, the residence time of this reaction is of less importance as the reaction rate is much faster as discussed in section 4.3.2. The residence time in the CSTR is solely to ensure an adequate cooling as the reagent is directly diluted in the reaction volume.
However, due to the fast reaction rate of the second reaction, it is recommended to investigate the use of a PFR instead of a CSTR as a second reactor in the future. The side products could be reduced due to the absence of oxygen in the PFR-part of the cascade and the residence time could be decreased.

The F(t)-graph is shown in Figure 59.

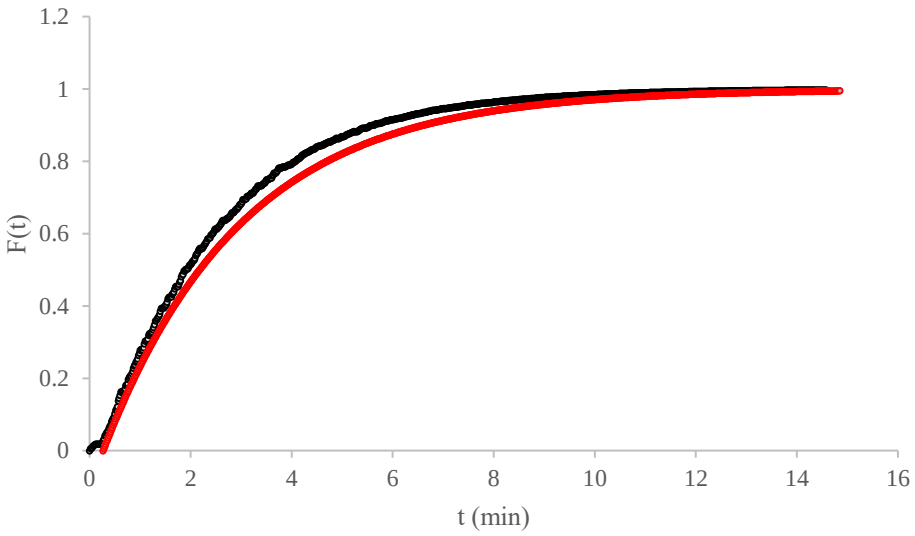

Figure 59: Measured (black) and ideal (red) F(t)-graph for reactor 2

From the measured and ideal curve $F(t) = 1 - e^{-\frac{t}{2.75}}$ in Figure 59, it is clearly that the second CSTR on its own has a nearly ideal flow. Although there is a time lag of 15 sec due to the used tubing, a smaller residence time in the CSTR itself can be observed as the measured curve is a little steeper compared to the ideal curve.

The variance is obtained with following equation:

$$\sigma_t^2 = \int_0^\infty (t - \bar{t})^2 E(t)\, dt = \int_0^\infty (t - 2.75)^2 * \ 0.401 * (0.670)^t \, dt = 6.31$$

D/µL, determined with the equations:

$$\sigma_\theta^2 = \frac{\sigma_t^2}{\bar{t}^2} = \frac{631}{2.75^2} = 0.83$$

$$\sigma_\theta^2 = 2\left(\frac{D}{\mu L}\right) + 8\left(\frac{D}{\mu L}\right)^2 = 0.83$$

$$\frac{D}{\mu L} = 0.22$$

The dispersion is 0.22. Thereby, the second reactor has a CSTR nature as well, also as expected.

The E(θ)-curve for the second reactor is shown in Figure 60.

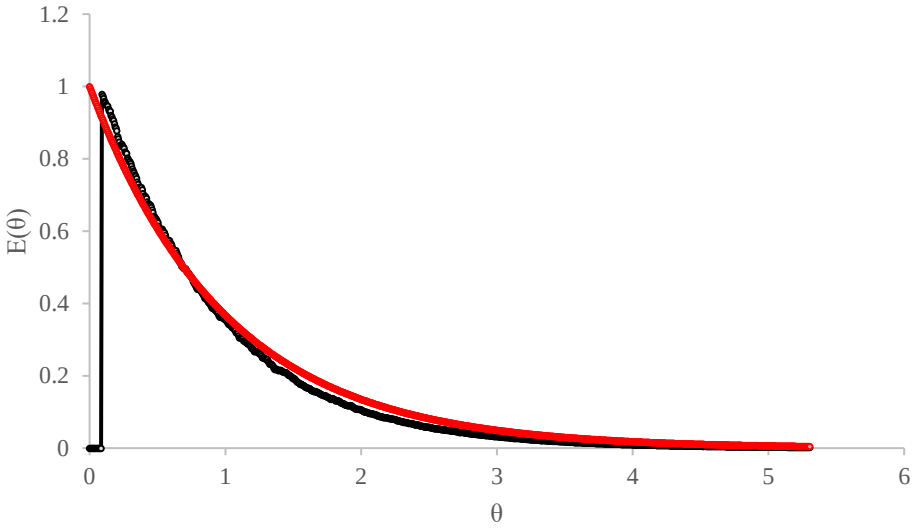

Figure 60: E(θ)-curve for the ideal CSTR (red) and the measured RTD (black) for reactor 2

Like the first reactor, the measured curve drops with a slope comparable to the ideal red curve. The CSTR nature is here verified too. The time lag is smaller due to the absence of a settling pipe. Only the used tubing creates a little PFR behaviour.

4.4.3 Cascade both reactors

In Figure 61, the result of the residence time distribution experiment for the cascade of both CSTRs is shown. This graph is acquired analogous to the Figure 55 and Figure 58. In reactor 1, a 0.1 KCl solution is switched to milli-Q water. In reactor 2, the feed remains 0.1M KCl.

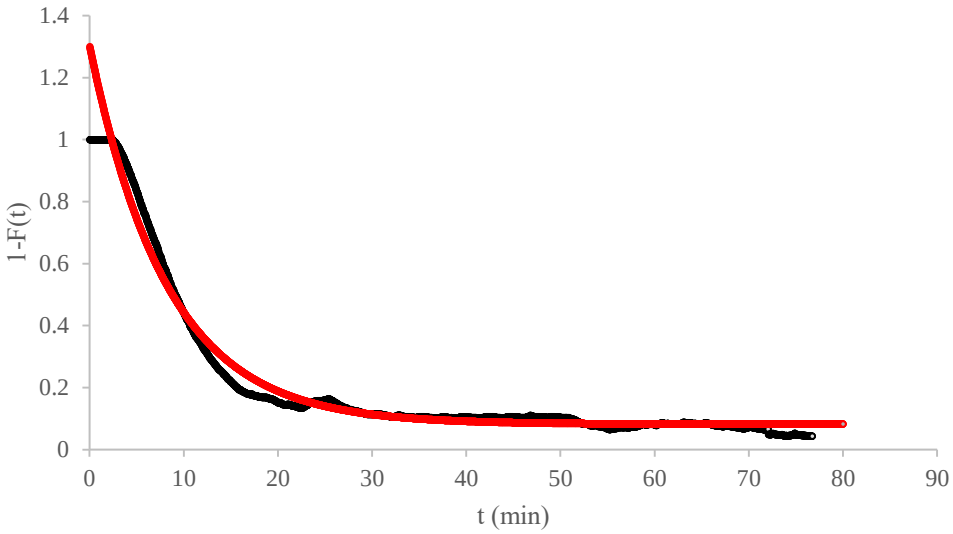

Figure 61: '1-F(t)'-curve for the measured (black) and ideal (red) for the negative step experiment for the cascade

Again, the black curve is the curve acquired by the measured data points, the red curve is the curve plotted by Eureqa Pro.

The cumulative distribution function F(t), derived with Eureqa Pro is $1-(0.0828+1.22e^{-0.122t})$ with an R^2 of 0,974.

$$F(t) = 1-(0.0828+1.22e^{-0.122t})$$

$$E(t) = \frac{dF(t)}{dt} = \frac{d(1-(0.0828+1.22e^{-0.122t}))}{dt} = 0.149 * 0.885^t$$

$$\bar{t} = \int_0^\infty t\,E(t)\,dt = \int_0^\infty t * 0.149 * 0.885^t\,dt = 10\,min$$

The residence time of the cascade is 10 min. This result is expected as the sum of the residence times of reactor 1 and 2 without the time lag (7 min 45 sec and 2 min 30 sec) is 10 min 15 sec. The deviation of 15 seconds could be due to the imperfect fittings of the measured curves. Overall, this experiment confirms the residence times derived from the separate experiments.
The total residence time, including the time lag of 2 min 32 sec, of the cascade setup is 12 min 32 sec. The increased time is a consequence of the connection between the magnesium trap and the second reactor, extra tubing with a PFR nature.
Due to the imperfect fitting, the more correct Riemann sum is calculated for the surface under the E(θ)-curve, which results in a residence time of 11 min 40 sec. This is comparable to the sum of the total residence time including the time lags of reactor 1 and 2 which is 11 min 55 sec (9 min 10 sec and 2 min 45 sec).
Using the Riemann sum is more precise, especially with this curve which fluctuates a lot. The total residence time of 11 min 40 sec is therefore considered more reliable.

The measured curve can be compared with 2 ideal curves. It can be compared with the ideal F(t)-curve obtained by using the theoretical residence times, which are 5 min and 2 min 45 sec for the first and second reactor, respectively. The second and most useful option is to compare the measured F(t)-curve with the ideal F(t)-curve obtained by using the calculated residence times from reactor 1 and 2 (without time lag), which are 7 min 45 sec and 2 min 30 sec for the first and second reactor respectively. These 3 F(t)-curves are shown in Figure 62.

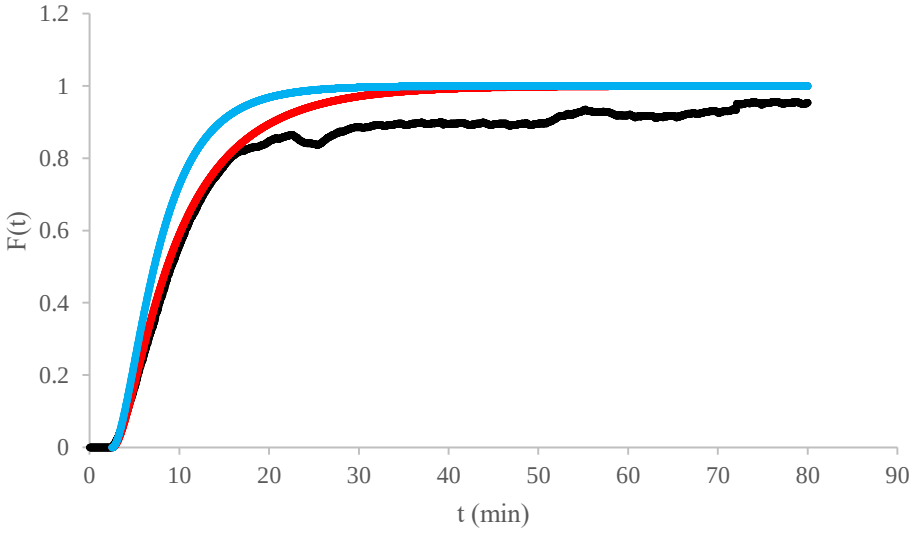

Figure 62: Measured (black), theoretical residence times ideal (blue) and calculated residence times ideal (red) F(t)-graph for the cascade

Again, the ideal curves are shifted until after the time lag due the PFR nature of the settling pipe and tubing, which is 2 min 32 sec for the cascade setup. The ideal curves are presented with the equation $F(t) = \left(1-e^{-\frac{t}{7.75}}\right)\left(1-e^{-\frac{t}{2.50}}\right)$ for the calculated residence times (red curve), and $F(t) =$

$\left(1-e^{-\frac{t}{5}}\right)\left(1-e^{-\frac{t}{2.75}}\right)$ for the theoretical residence times (blue curve). As can be seen in the figure, the blue curve does not match the black curve well, which is expected as the theoretical residence times are used here.

In the whole cascade setup, the higher residence time of 11 min 40 sec than the intended 10 min can be observed, caused by the full setup of reactor 1 with its settling pipe and magnesium trap. The curve does not completely coincide with the ideal curve towards the end of the experiment. A deviation in flow rate may be the cause. As a result, a perfect 1: 1 volume ratio is not achieved, so that the end conductivity (defined as 585 µS/cm) would be different. Specifically, in this case, the 0.1 M KCl pump in reactor 2 pumps faster than the peristaltic pump which fed the content of reactor 1.

When calculating the variance, it is important to know that the more precise total residence time of the Riemann sum cannot be used together with the formula that Eureqa plotted. This would give erroneous results. Therefore, the total residence time that was obtained from the calculations with the curve obtained from Eureqa should be used. However, it must be considered again that this curve did not perfectly match the measured points. The variance can be obtained with following equation:

$$\sigma_t^2 = \int_0^\infty (t-\bar{t})^2 E(t)\,dt = \int_0^\infty (t-12.53)^2 * 0.149 * 0.885^t\,dt = 104.8$$

D/µL can be determined with the equations:

$$\sigma_\theta^2 = \frac{\sigma_t^2}{\bar{t}^2} = \frac{104.8}{12.53^2} = 0.67$$

$$\sigma_\theta^2 = 2\left(\frac{D}{\mu L}\right) + 8\left(\frac{D}{\mu L}\right)^2 = 0.67$$

$$\frac{D}{\mu L} = 0.19$$

The dispersion in the cascade of CSTRs is large, however, it is slightly smaller than the separate reactors. This result is expected as a cascade of CSTRs reduces the dispersion and improves the PFR nature of the setup.

The E(θ)-curves are shown in Figure 63. Again, the blue and red curve are generated when using the theoretical and calculated residence times, respectively. The black dots represent where the measured E(θ)-curve would be. Due to difficulties during the processing of the results, no curve could be made. The blue and red curve begin after the time lag of the cascade results, to be able to compare the curves.

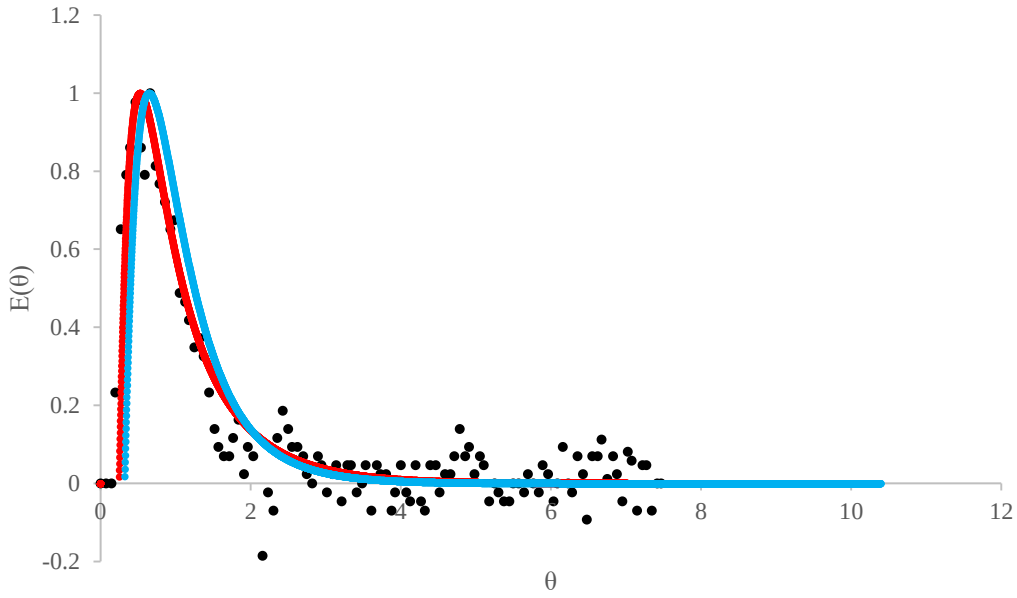

Figure 63: Measured (black), theoretical residence times ideal (blue) and calculated residence times ideal (red) E(θ)-graphs for the cascade

It can be observed that the black E(θ)-graph approximates the red curve better than the blue curve. Again, this is expected since the red curve is generated by using the calculated residence times. The black points coincide well with the red curve, which means that the cascade is also considered reasonably ideal.
Although the cascade has slightly less dispersion than the separate reactors (0.20 for reactor 1, 0.22 for reactor 2 and 0.19 for the cascade), the E(θ)-graph clearly proves the big dispersion and CSTR nature of the setup as the curve has a rather large slope, compared to the first part of the peak. This result is within the expectations as the second reactor is not identical, but smaller. The PFR nature due to the cascade setup is therefore less forthcoming as would be acquired with two identical CSTRs with the same residence time. This is confirmed by the blue curve, as it gives a slightly sharper peak and therefore has more PFR nature because the residence times of the two reactors are closer together.

4.5 CASCADE CSTR SETUP

4.5.1 Solids settling system

The efficiency of the solids settling system of the cascade CSTR setup is tested with reaction 1. Both the single and double angled settling pipe are examined. The test conditions can be found in section 3.2.5 and the dimensions of the settling pipes can be found in section 3.2.4. Microscopy images of the particles that are settled in the magnesium trap during the experiment (which is positioned after the settling pipe) are shown in Figure 64.

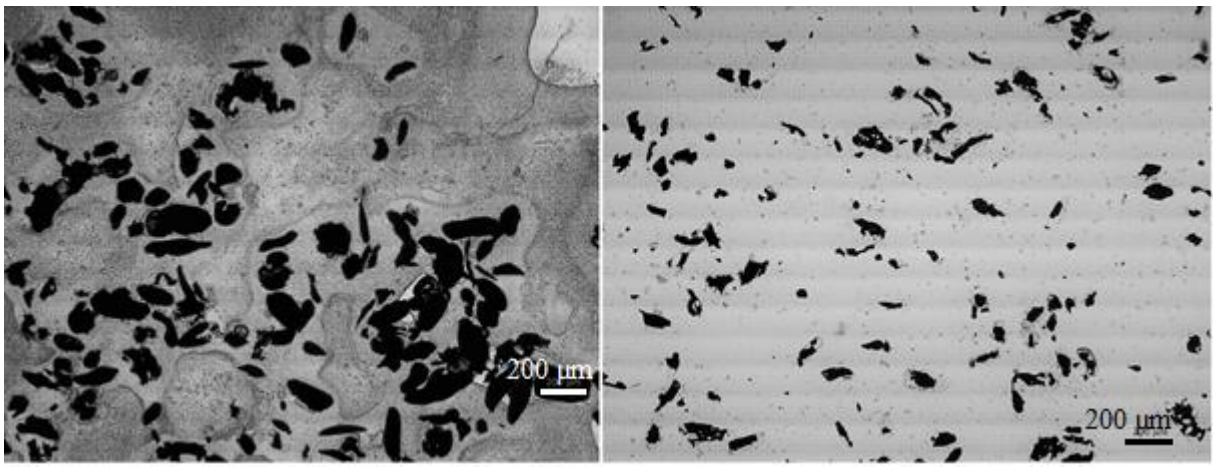

Figure 64: Mg particles captured in Mg trap with single (left) and double (right) angled settling pipe

The scaling mark at the bottom right of the figures indicates 200 µm, which is the most visible in the right picture. Both pictures are taken at the same magnification. A clear difference in particle size can be noticed, while these pictures are taken right after the experiment. In this way, a possible difference due to shrinkage of the particles by reaction could be excluded.
When the single angled settling pipe is used in the cascade CSTR setup, magnesium particles up to 340 µm are observed in the magnesium trap. When using the double angled settling pipe, the largest particles are only 200 µm in size.

It can be concluded that the double angled settling pipe is clearly more efficient. Therefore, this design is also used for the other cascade test, where the reaction was carried out with benzaldehyde (see 3.2.5 for test conditions). The double angled settling pipe works much better than the single angled settling pipe because of the compensation for the under-dimensioning (explained in 3.2.4 Settling pipe design) by adding another upper angled section of pipe. The upper angled section of pipe at the double angled settling pipe provides an extra settling effect for the magnesium particles. The magnesium particles that move vertically upwards in the settling pipe are forced to make an angle of 60°. For particles above 200 µm, the change of direction is too abrupt, leading to a collision with the wall of the upper part of the settling pipe. Due to a loss of kinetic energy, they no longer reach the end of the settling pipe, causing them to settle in the upper part of the pipe and ultimately back into the reactor. This mechanism is clearly observed during the experiments. Particles smaller than 200 µm could also collide with the wall and lose kinetic energy. However, the microscopy images show that this loss is not big enough to settle all of them.
Upscaling to larger reactors would make the implementation of a better settling pipe easier. The dimensions of the settling pipe could then be chosen without the magnesium settling pipe being limited by the small reactor design on lab scale. Further research is advised.

After choosing the most efficient settling pipe, which was the double angled settling pipe, the final flow of the cascade CSTR setup is also checked for the presence of magnesium particles to analyse the efficiency of the magnesium trap during the cascade test performed with acetophenone. Microscopic images of these particles are shown in Figure 65. The concentration of these particles on this image is not representative for the concentration of particles in the final product flow, because these particles have settled for 5 days in a 1 l collection beaker. If the sample is directly analysed after the experiment, there are virtually no particles to be seen. It is positive that very little amounts of magnesium come along with the final product flow, since this magnesium can create hydrogen when the product flow is quenched.

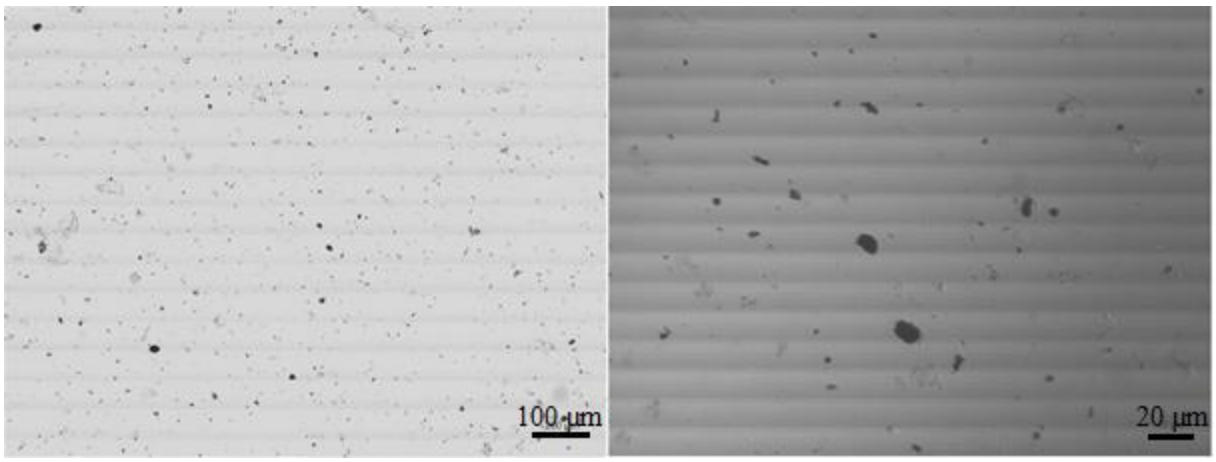

Figure 65: Settled Mg particles in final cascade CSTR product flow: (left) 10x; (right) 40x

The scaling mark at the bottom right of the figures indicates 100 µm for the left picture, and 20 µm for the right one. Compared to the right image in Figure 64, the particles are much smaller. The largest particles in the magnesium trap are 200 µm, while in the final product flow, a maximum size of 25 µm is noticed. Smaller particles thus cannot be stopped with the magnesium trap.

It can be concluded that the magnesium trap has a large influence on the retention of magnesium particles which are not stopped by the double angled settling pipe. In fact, it is a crucial component, allowing the smaller particles to settle. The non-stirred volume in the magnesium trap has very little flow, so that the smaller particles (>25 µm) are not resuspended or kept in suspension and remain on the bottom of the magnesium trap.
Since in the cascade CSTR setup only a test tube is used as magnesium trap, a lot of improvement is still possible to design a more efficient magnesium trap. The design that is presented in the literature (Figure 23) can be a starting point for further research.

4.5.2 Conversions and yields in the cascade CSTR

At the time of sampling, reaction mixtures from reactor 1 and 2 are collected to analyse the compositions of these flows. Both reaction 1 and 2 are performed in the cascade to compare the reactivity and yield between a ketone and aldehyde with the Grignard reagent. The test conditions and sampling time can be found in 3.2.5. The results of these tests are shown in Table 24.

Table 24: Results of cascade CSTR tests

	Reaction 1 (acetophenone)	Reaction 2 (benzaldehyde)
Reactor 1		
Conversion bromobenzene (%)	99.25	98.93
Yield phenylmagnesium bromide (%)	90.88	92.73
Temperature of reaction mixture (°C)	50.0	50.0
Steady-state? (volume = constant)	Yes	Yes
Reactor 2		
Additional conversion bromobenzene (%)	0.05	0.49

Conversion acetophenone/benzaldehyde (%)	90.81	91.37
Temperature of reaction mixture (°C)	43.7	44.5
Steady-state? (volume = constant)	Yes	Yes
Overall		
Total yield 1,1-diphenylethanol (%)	70.41	
Total yield diphenylmethanol (%)		Not quantifiable

With 99.25% for the first reaction and 98.93% for the second reaction, an almost complete conversion of bromobenzene is observed in the first reactor. Also, taking the standard deviation of the reproducibility into account, nearly the same amount is converted to the desired phenylmagnesium bromide, with 90.88%. and 92.73% for reaction 1 and reaction 2, respectively. These results are as expected from all preliminary tests (4.2 and 4.3). The temperature of the reactor mixture can be kept perfectly at 50 °C, which is the target temperature.
In the exit flow of reactor 2, an additional 0.05% and 0.49% conversion of bromobenzene is observed for reaction 1 and 2, respectively. This additional conversion is probably obtained by the small entrained magnesium particles. The conversion of acetophenone in reaction 1 and benzaldehyde in reaction 2 are nearly the same (90.81 for acetophenone and 91.37 for benzaldehyde).
Overall, the total Grignard reaction with acetophenone gives a 70.41% yield of 1,1-diphenylethanol in the cascade CSTR setup. However, the total Grignard reaction with benzaldehyde was not quantifiable, due to heavy fronting in the diphenylmethanol peak. A first approach to total steady-state (constant volume) is also obtained during all tests and in each reactor.

Although the first reactor works great and the liquid volume of the reactor is kept constant, the surface of magnesium is constantly shrinking and reacting so that no real steady-state was obtained (reaction rate depends on magnesium surface, explained in 4.3.1.1).
Reactor 2 also shows no deviations, other than the temperature in this reactor which does not reach the targeted 50 °C. Because the magnesium trap and reactor are not completely submerged in the hot water bath, the reaction mixture cannot be heated to 50 °C despite the exothermic nature of the coupling reaction. This lower temperature of 43.7 °C and 44.5 °C for reaction 1 and 2 respectively can result in a slower conversion of acetophenone and benzaldehyde. From section 4.3.2 however, it appeared that the reaction went extremely fast when tested at 30 °C, so it can be concluded the temperature was high enough. The temperature of the reaction mixture is 0.8 °C higher in reaction 2 than in reaction 1, which may indicate the higher reactivity of benzaldehyde. Steady-state can also be achieved in this reactor, provided that the flow coming from the first reactor has a constant composition. Further research into a method of continuously adding magnesium to reactor 1 in the same amount as it disappears is therefore recommended to achieve a real steady-state process. Not only the amount of magnesium that shrinks during the reaction should be taken into account, but also the magnesium that is entrained by the settling pipe to the consecutive magnesium trap and reactor 2. If the first reactor can operate in a real steady-state (constant volume and composition of exit flow), this can also easily be achieved in reactor 2.

The total yield of the desired final product of reactions 1 and 2 cannot be compared with each other, because heavy fronting of the diphenylmethanol peak was observed. The calculated yield was far too high (higher than the yield of phenylmagnesium bromide in the first reactor), and therefore unrealistic. The chromatogram with the diphenylmethanol peak, which is circled in red, is shown in Figure 66.

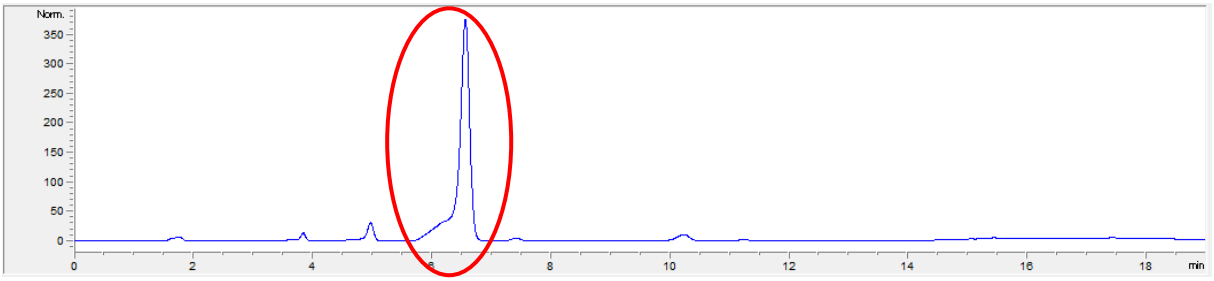

Figure 66: HPLC chromatogram of sample from reactor 2 (reaction 2)

The fronting of this peak can be a result of a poor analysis by the HPLC. This possibility cannot be excluded since the HPLC column may be negatively affected throughout the Master's thesis, since fronting is also observed during some other samples in the last weeks. Another possibility may be that an unexpected side product is formed in the second part of reaction 2, which is not taken into account during the establishment of a good HPLC method for reaction 2.

Due to the unexpected problems with the diphenylmethanol quantification, no quantitative result can be applied to the total yield of this product. Therefore, it is recommended to do several repetitions of this test, to see if the problem persists. In the case of deterioration of the HPLC column, the cause must be identified. If it concerns a side product, this substance must be identified and the HPLC method for reaction 2 must be adjusted to provide good separation of the peaks.

The result of the reaction 1 with acetophenone is quantitative, so conclusions can be drawn here. While 90.81% of acetophenone has reacted in reactor 2, only 70.41% 1,1-diphenylethanol is observed in the final product flow. Not all acetophenone is converted to the desired end product, so it can be concluded that one or more side products are formed. Possible side reactions enolization or a reduction(opposite to the addition reaction which yields 1,1-diphenylethanol) are most likely not the cause, since almost no benzene was found in the HPLC analysis, while this benzene would be the by-product of the enolization or reduction [32]. Another possibility is that the acidic quench with NH_4Cl elicits an elimination reaction which converts a part of the 1,1-diphenylethanol to 1,1-diphenylethylene by forming a double bond, which is conjugated with the two phenyl rings. However, this possible explanation must be approached very carefully, since the weak acid may not be able to carry out this elimination reaction.
When using benzaldehyde, this enolization and reduction reaction cannot take place. An elimination with the formation of a double bond is also excluded. This makes an elimination reaction for acetophenone less likely. If there is a side product formed during the reaction of benzaldehyde and acetophenone, it would most likely be a similar side reaction. The (possible) side products should still be identified. Since the second part of the reaction is not further investigated in this Master’s thesis, further research can be done on the suppression of these side products.

In general, it can be concluded that the continuous cascade CSTR is working properly. The reaction volumes in the reactors remain constant, making it a first step towards a fully steady-state system which could be achieved by continuous addition of magnesium.

5 CONCLUSION

In this Master's thesis, the design and characterisation of a cascade of CSTRs for a Grignard reaction is examined. The research consists of 5 substudies. First, different reaction initiation methods for the Grignard formation reaction are studied based on literature. In this way, a fast and predicable method could be selected which can be applied in the consecutive tests. Secondly, the Grignard formation reaction is examined in a CSTR on the influence of both the concentration of bromobenzene and magnesium, as well as the residence time and feed rate. Thirdly, a cascade CSTR setup with an accompanying solids settler is designed and tested with the 2 selected Grignard reactions. Thereafter, this cascade CSTR setup is characterised by measuring the residence time distribution. Finally, the kinetics of Grignard reagent formation starting from bromobenzene and magnesium powder is characterised, from which k_0, E_a and the order of the reaction could be derived.

The initiation tests show that the combination of iodine vapour, iodine in THF and phenylmagnesium bromide addition ensure the most instantaneous and intense initiation. While iodine vapour activates the magnesium, it also exerts a water-removing effect on the reactor and the magnesium. Addition of phenylmagnesium bromide provides a water-removing effect on the reaction medium as well, by a hydrolysis reaction with the water dissolved in the solvent. These two techniques ensure that water can no longer exert a negative influence on the reaction initiation, resulting in instantaneous initiation. Iodine in THF is mainly used as an indicator, it visualizes the magnesium activation.
The activation and initiation by iodine vapour, phenylmagnesium bromide addition and the combination of iodine in THF and phenylmagnesium bromide are also equivalent initiation methods. They may not provide the most intense initiation, but the initiation happens instantaneously, which is desired in the industry. Reaction initiation with non-heated and heated iodine in THF works, but the reaction went too slow.

Two important conclusions can be drawn from the Grignard formation tests. Firstly, a higher magnesium to bromobenzene ratio ensures a better yield of phenyl magnesium bromide, while the conversion of bromobenzene remains approximately the same. This means that less side products are formed with an increasing ratio of magnesium. When varying the residence time, a linear degradation of phenylmagnesium bromide is observed in time. This degradation is an important factor in optimizing the yield in the cascade CSTR setup and is probably caused by reaction with oxygen. However, no unambiguous trend on the yield is observed during the variation of the feed rate and concentration of bromobenzene.

Both the Grignard reaction with acetophenone and benzaldehyde were tested in the designed cascade CSTR setup, at a total flow rate of 1.2 l/h. The cascade test with acetophenone and benzaldehyde both obtain a 91% yield of phenylmagnesium bromide and 99% conversion of bromobenzene in the first reactor at 50 °C. In the second reactor, a 91% conversion of acetophenone/benzaldehyde is achieved at 43.7 and 44.5 °C, respectively. No accumulation is observed in reactor 1 and 2, as the volume in these reactors remained constant during testing.
In the final flow which exits reactor 2, a total yield of 70% 1,1-diphenylethanol is achieved when the Grignard reaction is carried out with acetophenone. The Grignard reaction is also carried out with benzaldehyde, but this result is not quantitatively interpretable due to heavy fronting of the diphenylmethanol peak in the HPLC chromatogram. A likely cause of this fronting is a side product that coincides with the diphenylmethanol peak, but degradation of the HPLC column is not excluded. Further, a solids settling system had to retain the magnesium in the first reactor. No particles above 25 µm are found in the final product flow, and the double angled settling pipe is proved effective up to particles of 200 µm. The single angled settling pipe is less efficient, allowing particles up to 350 µm to pass through.

The residence time distribution experiments consist of three experiments: characterisation of the first reactor including the settling pipe and magnesium trap, the second reactor and the cascade CSTR setup. The first reactor shows a total residence time of 9 min 10 sec, including a time lag of 1 min 25 sec. This time lag is caused by the PFR nature of the settling pipe. The total residence time is higher than the intended 5 min because the theoretical residence time is determined for the reactor solely, while the extra volume in the settling pipe and magnesium trap is not taken into account.
The second reactor shows nearly ideal CSTR behaviour, with a small time lag of 15 sec. The residence time (without time lag) of 2 min 30 sec is close to the intended theoretical residence time of 2 min 45 sec. Reactor 1 and 2 have a dispersion of 0.20 and 0.22 respectively, verifying the CSTR nature.
The cascade of CSTRs has a total residence time of 11 min 40 sec, including a time lag of 2 min 32 sec. The increased time lag is a result of the tubing throughout the cascade. The total residence time of the cascade setup is approximately the sum of the separate residence times of reactor 1 and 2 including the time lags, which is 11 min 55 sec. The dispersion of the cascade is slightly lower with a value of 0.19 which is expected as the second, smaller, reactor in series causes a slightly more PFR nature, resulting in a lower dispersion.

The reaction characterisation of the reaction with bromobenzene and magnesium powder results in a second-order reaction defined by the equation $-r_A = k_0 * e^{\frac{-E_a}{R*T}} * C_{Bromobenzene} * S_{Magnesium}$, with a k_0 of $2.04*10^7$ $min^{-1}*(mole/l)^{-1}$ and an E_a of 44828.3 J/mol.
Unlike magnesium turnings above a ratio of 2:1 magnesium to bromobenzene, where the surface area of magnesium became pseudo zeroth-order, the order of the reaction with magnesium powder up to a ratio of 4:1 is found to be a second-order. The difference between turnings and powder is mainly the volume. As the number of initiation sites are finite, and the reactive area increases by growth of site, turnings have more reactive area per initiation site. Even a ratio of 4:1 for powder could therefore be too little to obtain a pseudo zeroth-order for magnesium.

There are 3 objectives in this Master's thesis. The first objective, making an effective solids settling system that is incorporated internally in the first reactor, is achieved. The double angled settling pipe is incorporated in the first reactor. Only particles under 25 μm are found in the final product flow.
The second objective is to obtain a total yield of 90% of the desired product in the final flow of the cascade CSTR setup. This objective is not achieved, as only 70% yield of the desired product is obtained in the final flow of the cascade CSTR setup. However, the first reactor achieves a 91% yield.
The third objective, maintaining a constant volume and steady-state in the cascade CSTR setup, is achieved for the liquid reactants. A constant volume in all reactors of the cascade could be maintained, but a continuous addition of magnesium to obtain steady state proved impractical on lab scale with this cascade setup.

Future perspectives

Although the cascade setup designed in this Master's thesis works, it can still be improved as it is only a first approach. The characterisation of the second part of the reaction, addition to acetophenone or benzaldehyde, could give more insight in the residence time necessary in the second reactor and most probably reduce it. It is also advised to investigate the possibility and difference of a PFR instead of a CSTR as a second reactor.

Further research on the possible side products of the reaction of phenylmagnesium bromide with acetophenone and benzaldehyde is a crucial part to optimize the second reactor of the cascade setup, as the yield in the first reactor is much higher than the yield in the second reactor. Particularly their origin and reduction should be investigated. Inertification of the system, for example by a nitrogen atmosphere, should also be considered since phenylmagnesium bromide degrades under the influence of oxygen.

The settling pipe and magnesium trap are effectively, but there is still little magnesium in the final flow present. A bigger diameter or larger bottom part of the settling pipe might improve the retention due to the under-dimensioning of the settling pipes used in this Master's thesis. A different design for the trap could withhold smaller particles, where the design used in the literature can be a starting point.

Further research on the initiation methods on a larger scale would be useful, since an industrially relevant method should eventually be developed. Also, more repetitions on the different initiation methods should be conducted, to determine their reliability. Optionally, it can also be investigated how much the activation energy of the Grignard reagent formation decreases with each initiation method. Finally, it would be interesting to look if the amount of 1.0 M magnesium bromide solution to be added depends on the volume of solvent, or the mass of magnesium. Ideally, these experiments all take place in an inert nitrogen environment, so that water in the air cannot have an influence on the initiation.

The results to investigate the relation between feed rate and concentration of bromobenzene to the conversion and yield when conducting the Grignard reagent formation in a CSTR are inconclusive. Together with the influence of the volume in the reactor, these two parameters could be examined more thoroughly to form an unambiguous conclusion. When varying one parameter, these tests should be carried out with the same reaction volume. It is advised to perform the experiments with a constant temperature because it influences the reaction rate and therefore the results. Reactor inertification is also recommended here, due to the degradation of phenyl magnesium bromide.

Lastly, as no real steady-state is applied due to a one-time addition of magnesium in the first reactor at the beginning of a test, an alternative with continuous addition of magnesium would result in the intended steady-state. This could be a hopper with a screw drive motor (like an injection moulder in the plastic industry), preferably airtight and inert.

BIBLIOGRAPHY

[1] E. Yardeni, D. Johnson, and M. Quintana, "Global Economic Briefing: Industrial Production," 2018.

[2] M. Wackernagel and W. Rees, *Our Ecological Footprint: Reducing Human Impact on the Earth - Mathis Wackernagel, William Rees*. 1998.

[3] W. Tjan, R. R. Tan, and D. C. Y. Foo, "A graphical representation of carbon footprint reduction for chemical processes," *J. Clean. Prod.*, vol. 18, no. 9, pp. 848–856, Jun. 2010.

[4] H. Drotloff, "Reduction of Emissions by Chemical Industry from the German Emission Control Act to the Industrial Emission Directive (IED)," *Procedia Technol.*, vol. 12, pp. 637–642, 2014.

[5] M. R. Hoffmann, "Chemical pollution of the environment: past, present and future.," *Ciba Found. Symp.*, vol. 175, pp. 23-31-41, 1993.

[6] M. E. Porter and C. Van Der Linde, "Toward a New Conception of the Environment-Competitiveness Relationship The Link from Regulation to Promoting Innovation," *J. Econ. Perspect. —*, vol. 9, no. 4, pp. 97–118, 1995.

[7] A. I. Stankiewicz and J. A. Moulijn, "Process Intensification: Transforming Chemical Engineering," *Chem. Eng. Prog.*, vol. 96, no. 1, pp. 22–33, 2000.

[8] A. Stankiewicz* and J. A. Moulijn, "Process Intensification," 2002.

[9] M. J. Pedersen, T. L. Holm, J. P. Rahbek, T. Skovby, M. J. Mealy, K. Dam-Johansen, and S. Kiil, "Full-Scale Continuous Mini-Reactor Setup for Heterogeneous Grignard Alkylation of a Pharmaceutical Intermediate," *Org. Process Res. Dev.*, vol. 17, no. 9, pp. 1142–1148, Sep. 2013.

[10] Y. Mo and K. F. Jensen, "A miniature CSTR cascade for continuous flow of reactions containing solids," *React. Chem. Eng.*, vol. 1, no. 5, pp. 501–507, Sep. 2016.

[11] Janssen Global Services, "About Us | Janssen." [Online]. Available: http://www.janssen.com/about. [Accessed: 25-Mar-2018].

[12] KULeuven, "Lab4U - (Bio-)chemische procestechnologie – Lab4U." [Online]. Available: https://iiw.kuleuven.be/onderzoek/lab4U. [Accessed: 25-Mar-2018].

[13] UCLL, "Lab4U | UCLL." [Online]. Available: https://www.ucll.be/onderzoek/algemene-info/expertisecellen/lab4u. [Accessed: 25-Mar-2018].

[14] Alfa Aesar, "91-01-0 - Benzhydrol, 99% - Diphenylcarbinol - Diphenylmethanol - A12884 - Alfa Aesar." [Online]. Available: https://www.alfa.com/en/catalog/A12884/. [Accessed: 25-Mar-2018].

[15] S. Lomel, L. Falk, J. M. Commenge, J. L. Houzelot, and K. Ramdani, "The Microreactor: A Systematic and Efficient Tool for the Transition from Batch to Continuous Process?," *Chem. Eng. Res. Des.*, vol. 84, no. 5, pp. 363–369, May 2006.

[16] D. M. Roberge, L. Ducry, N. Bieler, P. Cretton, and B. Zimmermann, "Microreactor Technology: A Revolution for the Fine Chemical and Pharmaceutical Industries?," *Chem. Eng. Technol.*, vol. 28, no. 3, pp. 318–323, Mar. 2005.

[17] A. Weiler and M. Junkers, "Using Microreactors In Chemical Synthesis: Batch Process versus Continuous Flow.," *Pharm. Technol.*, vol. 47, pp. s6–s11, 2009.

[18] P. Watts and S. J. Haswell, "The application of micro reactors for organic synthesis," *Chem. Soc. Rev.*, vol. 34, no. 3, p. 235, Feb. 2005.

[19] N. Kockmann and D. M. Roberge, “Harsh Reaction Conditions in Continuous-Flow Microreactors for Pharmaceutical Production,” *Chem. Eng. Technol.*, vol. 32, no. 11, pp. 1682–1694, Nov. 2009.

[20] R. Porta, M. Benaglia, and A. Puglisi, “Flow Chemistry: Recent Developments in the Synthesis of Pharmaceutical Products,” *Org. Process Res. Dev.*, vol. 20, no. 1, pp. 2–25, Jan. 2016.

[21] G. S. Silverman and P. E. Rakita, *Handbook of Grignard Reagents*. 270 Madison Avenue, New York: Marcel Decker, 1996.

[22] W. (William) Hoyle, Royal Society of Chemistry (Great Britain). Process Technology Group., and Royal Society of Chemistry (Great Britain). Speciality Chemicals Sector., *Pilot plants and scale-up of chemical processes II*. Cambridge: Royal Society of Chemistry, 1999.

[23] E. A. William H. Brown, Christopher S. Foote, Brent L. Iverson, *Organic Chemistry*. 2012.

[24] “Grignard Reaction.” [Online]. Available: http://www.namereactions.org/grignard-reaction/. [Accessed: 31-Mar-2018].

[25] E. J. Little and M. M. Jones, “A complete table of electronegativities,” *J. Chem. Educ.*, vol. 37, no. 5, p. 231, 1960.

[26] H. M. Walborsky and M. Topolski, “The Surface Nature,” *J. Am. Chem. Soc.*, vol. 114, no. 3, pp. 3455–3459, 1992.

[27] H. M. Walborsky and A. E. Young, “Cyclopropanes. XVI. An Optically Active Grignard Reagent and the Mechanism of Grignard Formation1,2,” *J. Am. Chem. Soc.*, vol. 86, no. 16, pp. 3288–3296, 1964.

[28] J. C. de Souza-Barboza, J.-L. Luche, and C. PBtrier, “Retention of Optical Activity in Babbier Reactions,” *Tetrahedron Lett.*, vol. 28, no. 18, pp. 2013–2016, 1987.

[29] C. E. Teerlinck and W. J. Bowyer, “Reactivity of magnesium surfaces during the formation of Grignard reagents,” *J. Org. Chem.*, vol. 61, no. 3, pp. 1059–1064, 1996.

[30] L. J. Westrum, “Grignard knowledge : Alkyl coupling chemistry with inexpensive transition metals,” *Fine Chem.*, no. November/December, pp. 10–13, 2002.

[31] J. Tammiku-Taul, P. Burk, and A. Tuulmets, “Theoretical study of magnesium compounds: The Schlenk equilibrium in the gas phase and in the presence of Et2O and THF molecules,” *J. Phys. Chem. A*, vol. 108, no. 1, pp. 133–139, 2004.

[32] S. Yamabe and S. Yamazaki, *Theoretical Studies of the Addition of RMgX to Carbonyl Compounds*. 2008.

[33] A. Tuulmets, B. T. Nguyen, and D. Panov, “Grignard reaction with chlorosilanes in THF: A kinetic study,” *J. Org. Chem.*, vol. 69, no. 15, pp. 5071–5076, 2004.

[34] E. C. Ashby, “A detailed description of the mechanism of reaction of Grignard reagents with ketones,” *Pure Appl. Chem.*, vol. 52, no. 3, pp. 545–569, 1980.

[35] K. Maruyama and T. Katagiri, “Mechanism of the Grignard reaction,” *J. Phys. Org. Chem.*, vol. 2, no. 3, pp. 205–213, Apr. 1989.

[36] T. Holm, “Mechanism of the Grignard Addition Reaction IV. Reaction of Butylmagnesium Compounds with Methyl Acetate in Diethyl Ether and Tetrahydrofuran,” *Acta Chemica Scandinavica*, vol. 20. pp. 2821–2828, 1966.

[37] N. Bartolo, J. Read, E. Valentín, and K. Woerpel, “Reactions of Allylmagnesium Halides with Carbonyl Compounds: Reactivity, Structure, and Mechanism,” *Synthesis (Stuttg).*, vol. 49, no. 15, pp. 3237–3246, Aug. 2017.

[38] E. C. Ashby, I. G. Lopp, and J. D. Buhler, “Mechanisms of Grignard Reactions with Ketones. Polar vs. Single Electron Transfer Pathways,” *J. Am. Chem. Soc.*, vol. 97, no. 7, pp. 1964–

1966, 1975.

[39] A. Aouissi, S. S. Al-Deyab, and H. Al-Shahri, “The cationic ring-opening polymerization of tetrahydrofuran with 12-tungstophosphoric acid,” *Molecules*, vol. 15, no. 3, pp. 1398–1407, 2010.

[40] M. Kumasaki, T. Mizutani, and Y. Fujimoto, “The solvent effects on grignard reaction,” *IChemE*, no. 153, pp. 1–5, 2007.

[41] K. E. Stares and D. al Ende, “The safe scale-up of a Grignard reaction using in-situ reaction monitoring technique,” pp. 62–71.

[42] C. Walling and S. A. Buckler, “The Reaction of Oxygen with Organometallic Compounds. A New Synthesis of Hydroperoxides,” *J. Am. Chem. Soc.*, vol. 77, pp. 6032–6038, 1955.

[43] F. Huntoon, M, P. Masucci, and E. Hannum, “Oxidation of the Grignard Reagent,” *J. Am. Chem. Soc.*, vol. 33, no. 1904, pp. 2650–2654, 1920.

[44] A. A. Grachev, A. O. Klochkov, and V. I. Shiryaev, “Continuous synthesis of organomagnesium compounds,” *Russ. J. Appl. Chem.*, vol. 85, no. 4, pp. 629–638, 2012.

[45] B. J. Wakefield, *Organomagnesium Methods in Organic Chemistry*. 1995.

[46] L. J. Guggenberger, “The structures of the ethyl grignard reagent in diethyl ether and a troponoid photo-oxidation product,” 1965.

[47] U. Tilstam and H. Weinmann, “Activation of Mg metal for safe formation of Grignard reagents on plant scale,” *Org. Process Res. Dev.*, vol. 6, no. 6, pp. 906–910, 2002.

[48] T. S. Eckert, “An improved preparation of a Grignard reagent,” *J. Chem. Educ.*, vol. 64, no. 2, p. 179, 1987.

[49] A. Mendel, “Reaction of p-(dimethylamino)bromobenzene with ‘activated’ magnesium,” *J. Organomet. Chem.*, vol. 6, no. 1, pp. 97–99, 1966.

[50] S. V. Ley and C. M. R. Low, “Preparation of Activated Magnesium,” Springer, Berlin, Heidelberg, 1989, pp. 33–38.

[51] F.-D. Odufalu, P. Chacha, G. Mudda, and A. Iskandar, “Reaction Rate - Chemistry LibreTexts.” [Online]. Available: https://chem.libretexts.org/Core/Physical_and_Theoretical_Chemistry/Kinetics/Reaction_Rates/Reaction_Rate. [Accessed: 10-Apr-2018].

[52] Royal Society of Chemistry, “Rate of reaction – the effects of concentration and temperature,” no. 207890, pp. 73–75.

[53] “Le Chatelier’s Principle.” [Online]. Available: https://chem.libretexts.org/Core/Physical_and_Theoretical_Chemistry/Equilibria/Le_Chatelier’s_Principle. [Accessed: 10-Apr-2018].

[54] H. Simuste, D. Panov, A. Tuulmets, and B. T. Nguyen, “Formation of phenylmagnesium halides in toluene,” *J. Organomet. Chem.*, vol. 690, no. 12, pp. 3061–3066, 2005.

[55] O. Levenspiel, “Chemical Reaction Engineering - Third Edition,” in *3th edition*, 3rd ed., vol. 19, Corvallis: John Wiley & Sons, 1999, pp. 261–264.

[56] E. Erdik and F. Eroğlu, “Kinetics and mechanism of the C-S coupling reactions of aryl Grignard reagents with aryl arenesulfonates,” *Open Chem.*, vol. 6, no. 2, pp. 237–244, Jan. 2008.

[57] J. F. (John F. Richardson, D. G. (Donald G. Peacock, and J. M. (John M. Coulson, “1.2 Classification of reactors and choice of reactor type,” in *Coulson & Richardson’s Chemical Engineering. Vol. 3: Chemical & Biochemical reactors & Process control*, Pergamon, 1994, p. 776.

[58] S. Suresh and S. Sundaramoorthy, “2.2 Chemical Reactors: An Introduction,” in *Green Chemical Engineering: An Introduction to Catalysis, Kinetics, and Chemical Processes*, Boca Ration: CRC Press, 2015, pp. 67–72.

[59] M. Beccari and U. Romano, “6.3 Chemical Reactors,” in *Encyclopaedia of hydrocarbons*, Volume 5., Roma: ENI, 2005, pp. 351–368.

[60] P. Trambouze and J.-P. Euzen, “1.4 Reactor Types,” in *Chemical Reactors: From design to operation*, Paris: TECHNIP, 2004, pp. 23–30.

[61] O. Levenspiel, “Introduction to Reactor Design,” in *Chemical Reaction Engineering - Third Edition*, 3rd ed., vol. 19, Corvallis: John Wiley & Sons, 1999, pp. 83–89.

[62] A. Cybulski, *Fine chemicals manufacture : technology and engineering*. Elsevier, 2001.

[63] E. Heinzle, “Introduction to Ideal Reactors,” 2009.

[64] K. G. Denbigh and J. C. R. (James C. R. Turner, “Batchwise and continuous reactors,” in *Chemical reactor theory : an introduction*, 3rd ed., Cambridge University Press, 1984, pp. 1–14.

[65] The Essential Chemical Industry, “Chemical reactors,” 2013. [Online]. Available: http://www.essentialchemicalindustry.org/processes/chemical-reactors.html. [Accessed: 08-Apr-2018].

[66] S. Catalano, S. Wesorick, and K. Kaplan, “Semi-Batch.” [Online]. Available: http://encyclopedia.che.engin.umich.edu/Pages/Reactors/Semi-Batch/Semi-Batch.html. [Accessed: 15-Apr-2018].

[67] O. Levenspiel, “Ideal Reactors for a Single Reaction,” in *Chemical Reaction Engineering - Third Edition*, 3rd ed., vol. 19, Corvallis: John Wiley & Sons, 1999, pp. 90–96.

[68] O. Levenspiel, “Holding Time and Space Time for Flow Reactors,” in *Chemical Reaction Engineering - Third Edition*, 3rd ed., vol. 19, Corvallis: John Wiley & Sons, 1999, pp. 109–110.

[69] G. Malhotra, “Batch vs. Continuous Processing: A Choice,” *Pharm. Process.*, 2005.

[70] S. Catalano, S. Wesorick, K. Kaplan, T. Plegue, and J. Holland, “Continuous Stirred Tank Reactors.” [Online]. Available: http://encyclopedia.che.engin.umich.edu/Pages/Reactors/CSTR/CSTR.html. [Accessed: 12-Apr-2018].

[71] C. D. de Gooijer, W. A. M. Bakker, H. H. Beeftink, and J. Tramper, “Bioreactors in series: An overview of design procedures and practical applications,” 1996.

[72] K. De Gooijer, “CASCADES OF BIOREACTORS,” Landbouwuniversiteit Wageningen, 1995.

[73] S.-W. Wong, S. M. Changi, R. Shields, W. Bell, B. McGarvey, M. D. Johnson, W.-M. Sun, T. M. Braden, M. E. Kopach, R. D. Spencer, G. Flanagan, and M. Murray, “Operation Strategy Development for Grignard Reaction in a Continuous Stirred Tank Reactor,” *Org. Process Res. Dev.*, vol. 20, no. 2, pp. 540–550, Feb. 2016.

[74] P. V. Danckwerts, “Continuous flow systems: Distribution of residence times,” *Chem. Eng. Sci.*, vol. 2, no. 1, pp. 1–13, Feb. 1953.

[75] O. Levenspiel, “Basics of Non-Ideal Flow,” in *Chemical Reaction Engineering - Third Edition*, 3rd ed., vol. 19, Corvallis: John Wiley & Sons, 1999, pp. 257–260.

[76] H. S. Fogler and M. N. Gürmen, “Distributions of Residence Times for Chemical Reactors,” in *Elements of Chemical Reaction Engineering*, 5th ed., Ann Arbor: Prentice Hall, 2008, pp. 867–868.

[77] D. Sievers, E. Kuhn, M. Tucker, J. Stickel, and E. Wolfrum, “Residence Time Distribution Measurement and Analysis of Pilot-Scale Pretreatment Reactors for Biofuels Production: Preprint,” 2013.

[78] E. Loffill, R. M. Alkhaddar, D. A. Phipps, and M. G. Faram, “Development of residence time distribution measurement techniques to improve reliability and accuracy,” *NOVATECH 2010*, 2010.

[79] O. Levenspiel, “Experimental Methods (Nonchemical) for Finding E,” in *Chemical Reaction Engineering - Third Edition*, 3rd ed., vol. 19, Corvallis: John Wiley & Sons, 1999, pp. 261–264.

[80] H. S. Fogler and M. N. Gürmen, “Measurement of the RTD,” in *Elements of Chemical Reaction Engineering*, 5th ed., Ann Arbor: Prentice Hall, 2008, pp. 871–873.

[81] K. ASTERIADOU, T. HASTING, M. BIRD, and J. MELROSE, “PREDICTING CLEANING OF EQUIPMENT USING COMPUTATIONAL FLUID DYNAMICS,” *J. Food Process Eng.*, vol. 30, no. 1, pp. 88–105, Feb. 2007.

[82] F. Trachsel, A. Günther, S. Khan, and K. F. Jensen, “Measurement of residence time distribution in microfluidic systems,” *Chem. Eng. Sci.*, vol. 60, no. 21, pp. 5729–5737, Nov. 2005.

[83] W. Lin, C. E. Weinell, P. F. B. Hansen, and K. Dam-Johansen, “Hydrodynamics of a commercial scale CFB boiler-study with radioactive tracer particles,” *Chem. Eng. Sci.*, vol. 54, no. 22, pp. 5495–5506, Nov. 1999.

[84] A. Mezo, J. Mottershead, and D. Jones, “Residence Time Distribution Measurements | Coanda Research & Development,” 2016. [Online]. Available: https://coanda.ca/blog/residence-time-distribution-measurements/. [Accessed: 31-Mar-2018].

[85] M. Schmal, “Pulse tracer experiment,” in *Chemical Reaction Engineering: Essentials, Exercises and Examples*, London, UK: Taylor & Francis Group, 2014, pp. 290–291.

[86] O. Levenspiel, “Relationship between the F and E Curves,” in *Chemical Reaction Engineering - Third Edition*, 3rd ed., vol. 19, Corvallis: John Wiley & Sons, 1999, pp. 265–266.

[87] H. S. Fogler and M. N. Gürmen, “Mean residence time,” in *Elements of Chemical Reaction Engineering*, 5th ed., Ann Arbor: Prentice Hall, 2008, pp. 879–881.

[88] O. Levenspiel, “Compartment Models,” in *Chemical Reaction Engineering - Third Edition*, 3rd ed., vol. 19, Corvallis: John Wiley & Sons, 1999, pp. 283–288.

[89] H. S. Fogler and M. N. Gürmen, “Simple Diagnostics and Troubleshooting Using the RTD for Ideal Reactors,” in *Elements of Chemical Reaction Engineering*, 5th ed., Ann Arbor: Prentice Hall, 2008, pp. 892–895.

[90] O. Levenspiel, “The Tanks-In-Series Model,” in *Chemical Reaction Engineering - Third Edition*, 3rd ed., vol. 19, Corvallis: John Wiley & Sons, 1999, pp. 321–323.

[91] American Chemical society, “Common Organic Solvents: Table of Properties.” [Online]. Available: https://www.organicdivision.org/orig/organic_solvents.html. [Accessed: 29-Apr-2018].

6 APPENDIX

6.1 APPENDIX A: CHROMATOGRAMS EXAMPLES

6.1.1 Reaction 1

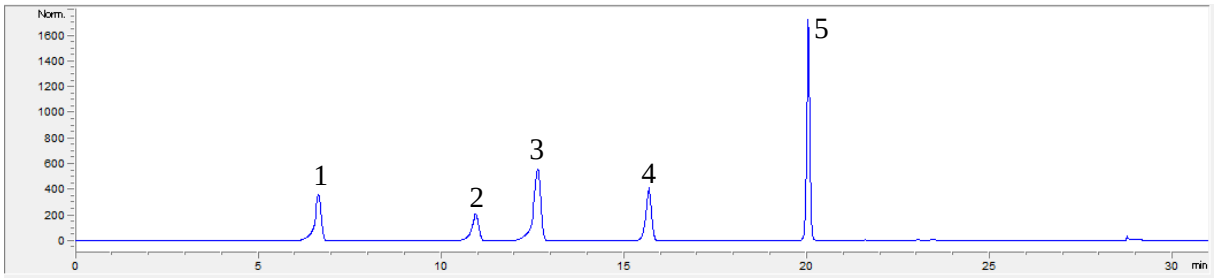

Figure 67: HPLC chromatogram example of reaction 1

1: Acetophenone
2: Benzene
3: 1,1-diphenylethanol
4: Bromobenzene
5: Biphenyl

6.1.2 Reaction 2

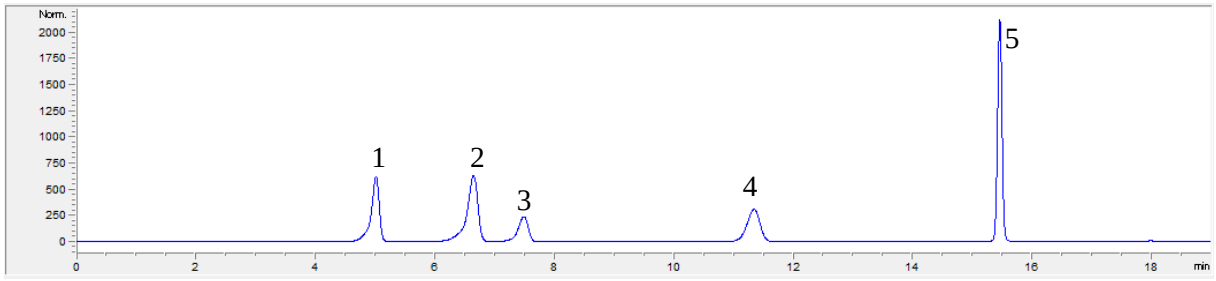

Figure 68: HPLC chromatogram example of reaction 2

1: Benzaldehyde
2: Diphenylmethanol
3: Benzene
4: Bromobenzene
5: Biphenyl

6.2 APPENDIX B: CALIBRATION CURVES

6.2.1 Reaction 1

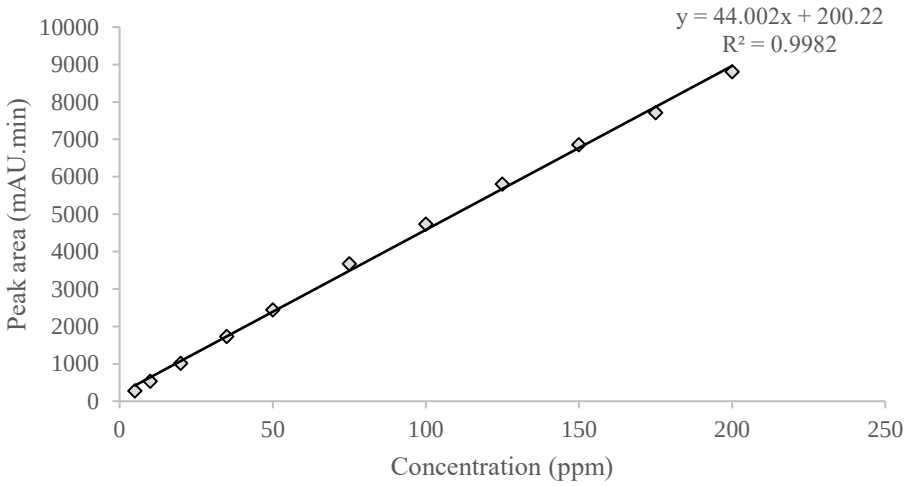

Figure 69: Calibration curve of acetophenone in reaction 1

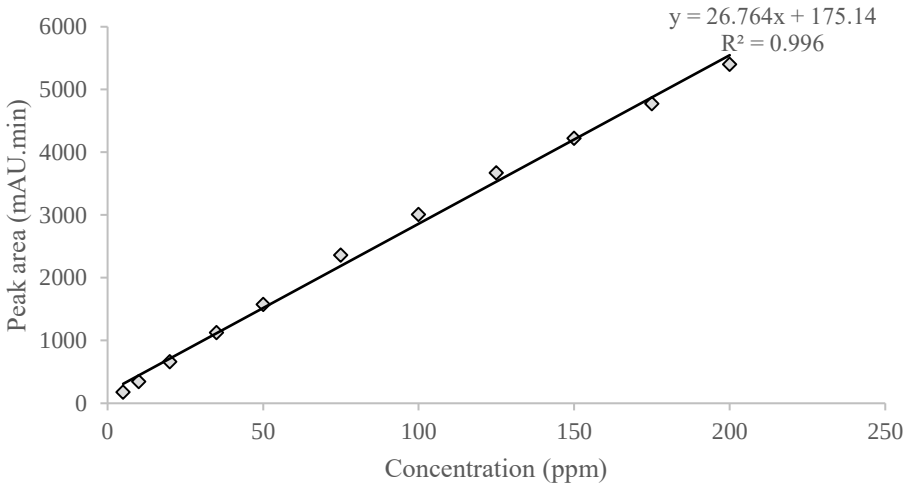

Figure 70: Calibration curve of benzene in reaction 1

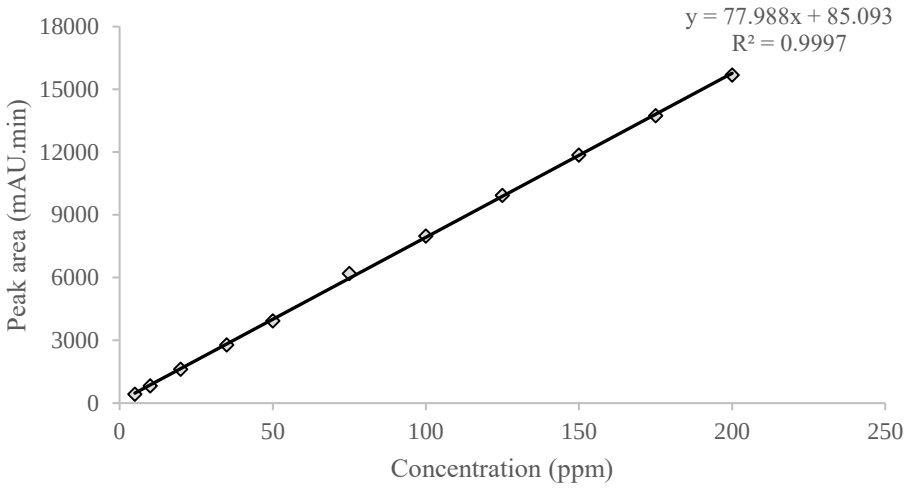

Figure 71: Calibration curve of 1,1-diphenylethanol in reaction 1

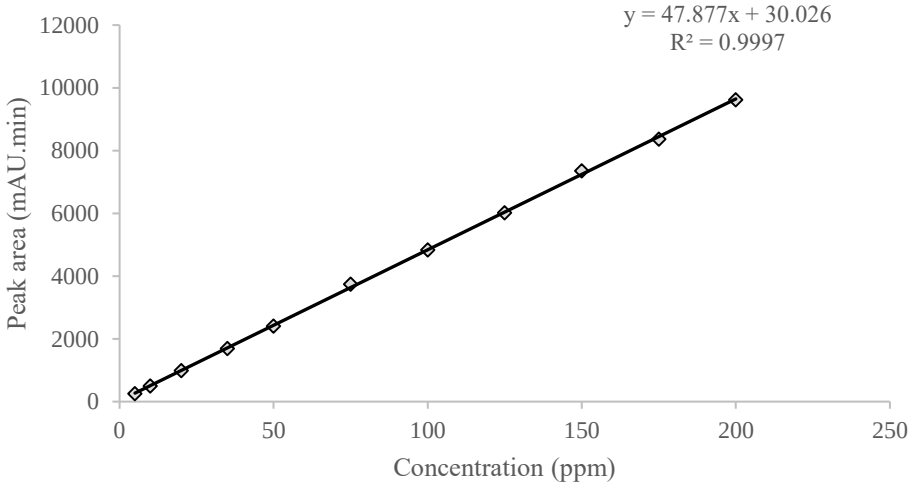

Figure 72: Calibration curve of bromobenzene in reaction 1

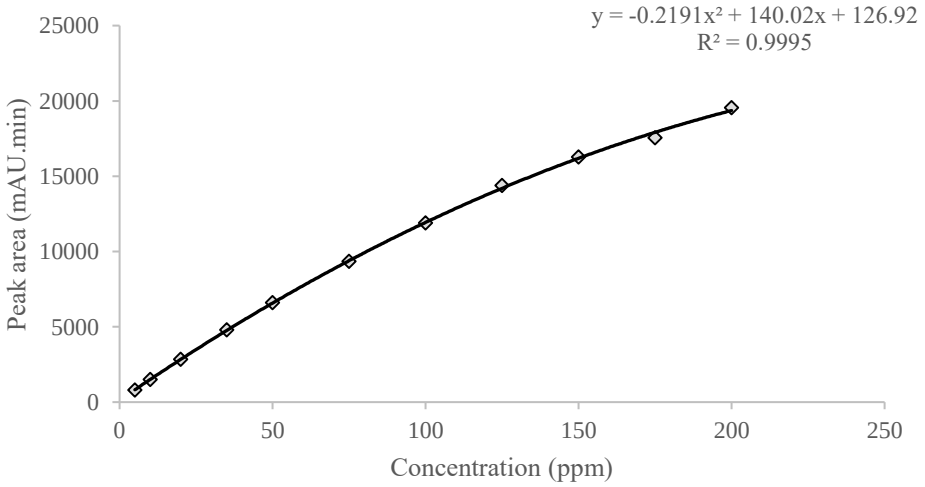

Figure 73: Calibration curve of biphenyl in reaction 1

6.2.2 Reaction 2

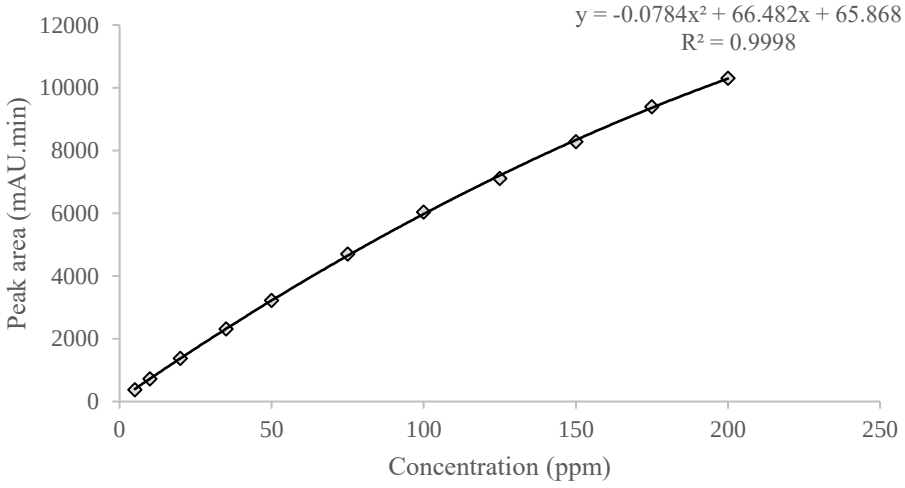

Figure 74: Calibration curve of benzaldehyde in reaction 2

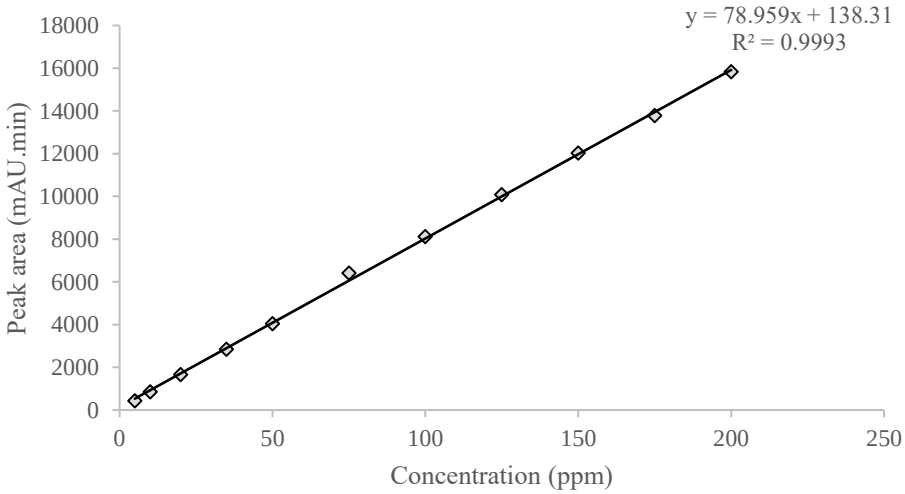

Figure 75: Calibration curve of diphenylmethanol in reaction 2

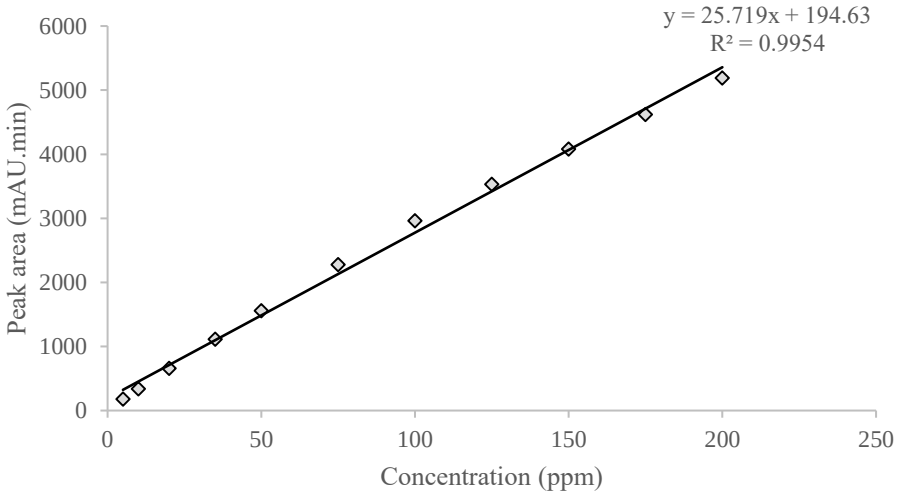

Figure 76: Calibration curve of benzene in reaction 2

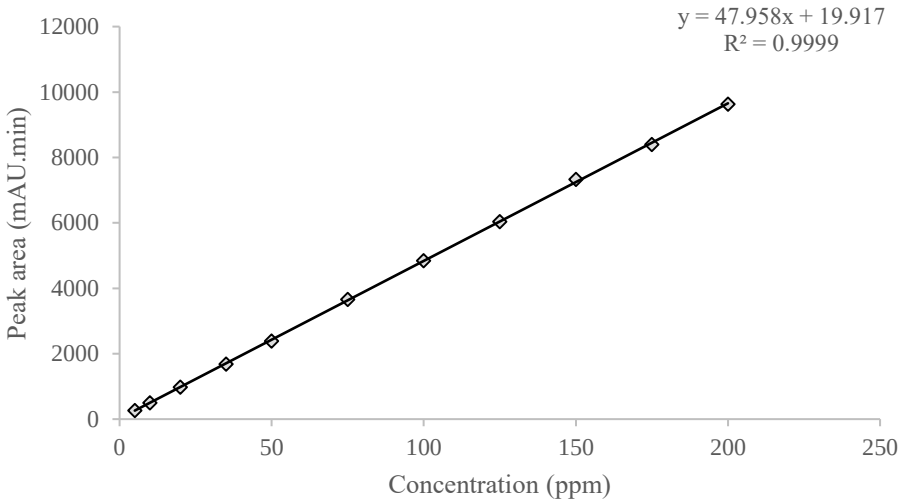

Figure 77: Calibration curve of bromobenzene in reaction 2

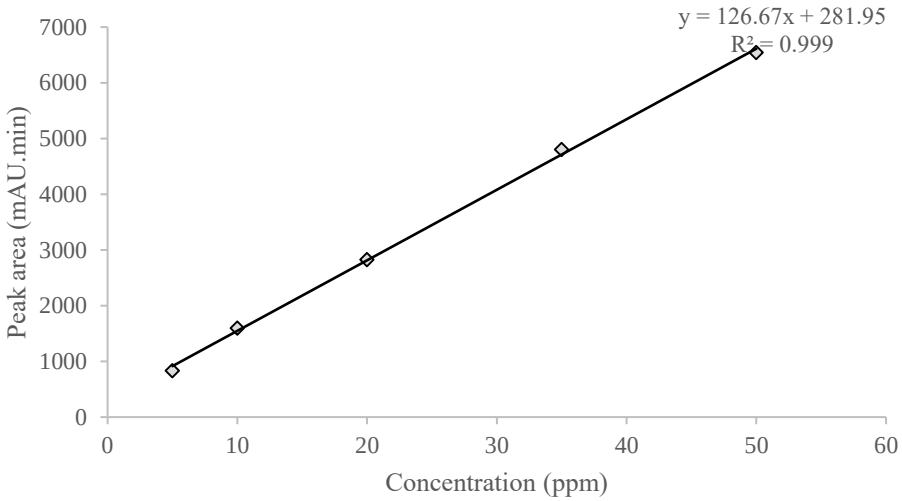

Figure 78: Calibration curve of biphenyl in reaction 2

6.3 APPENDIX C: VALIDATION CURVES

6.3.1 Reaction 1

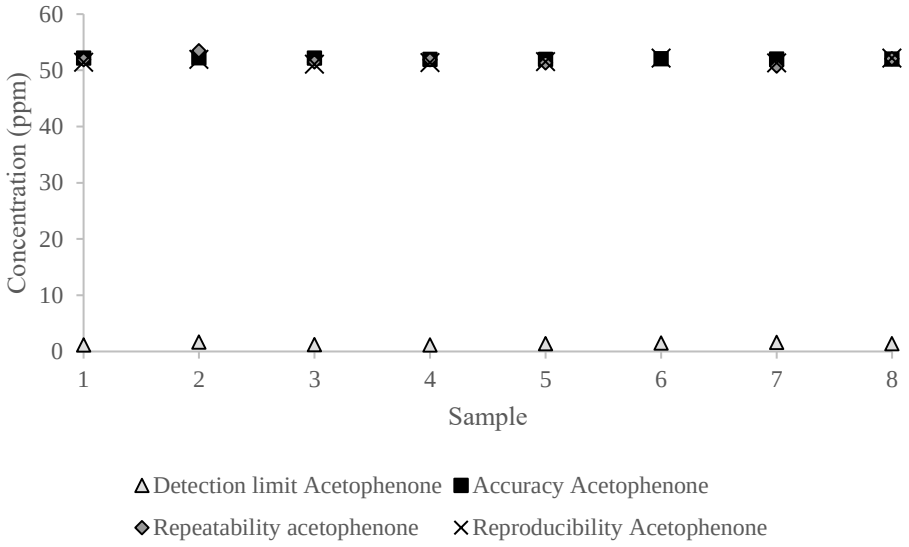

Figure 79: Validation curves of acetophenone in reaction 1

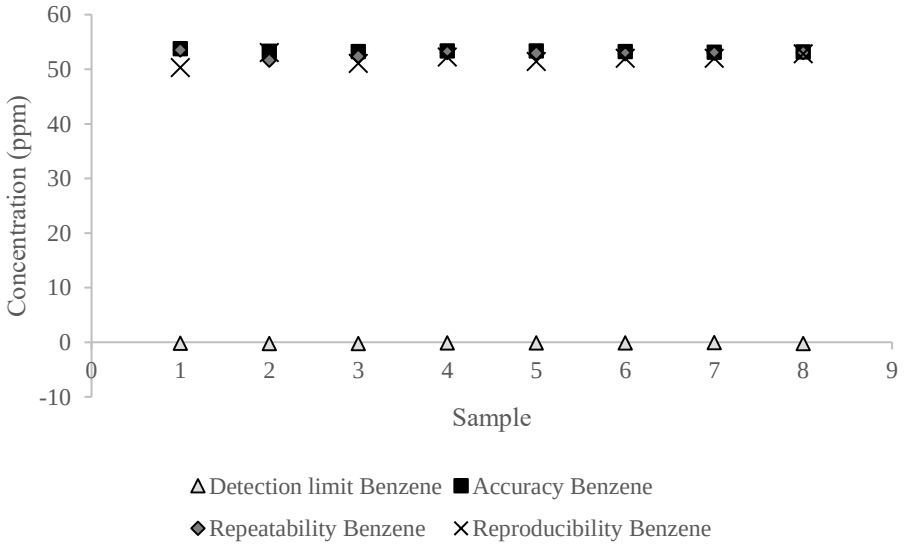

Figure 80: Validation curves of benzene in reaction 1

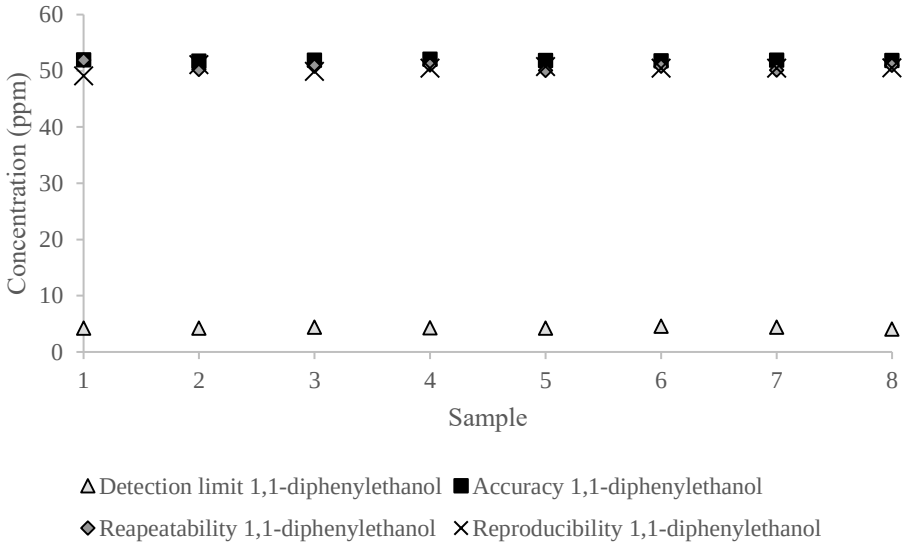

Figure 81: Validation curves of 1,1-diphenylethanol in reaction 1

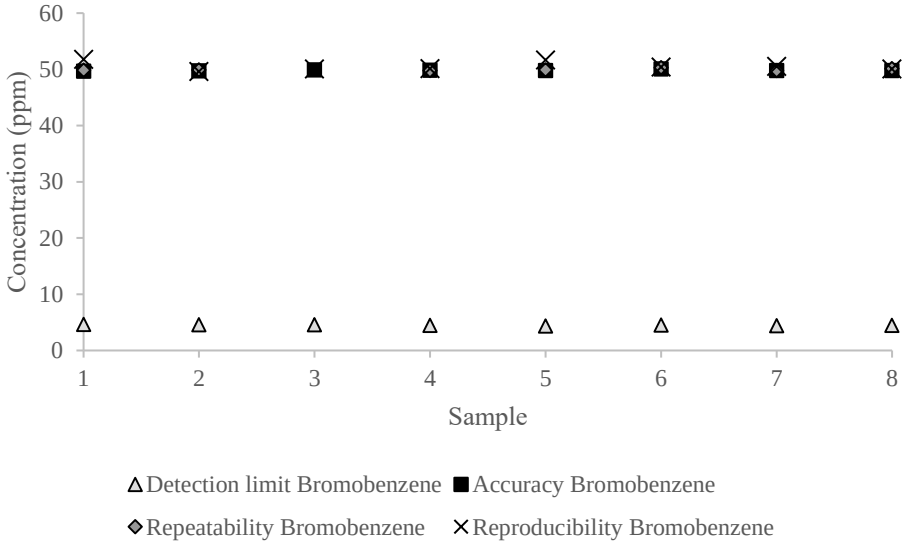

Figure 82: Validation curves of bromobenzene in reaction 1

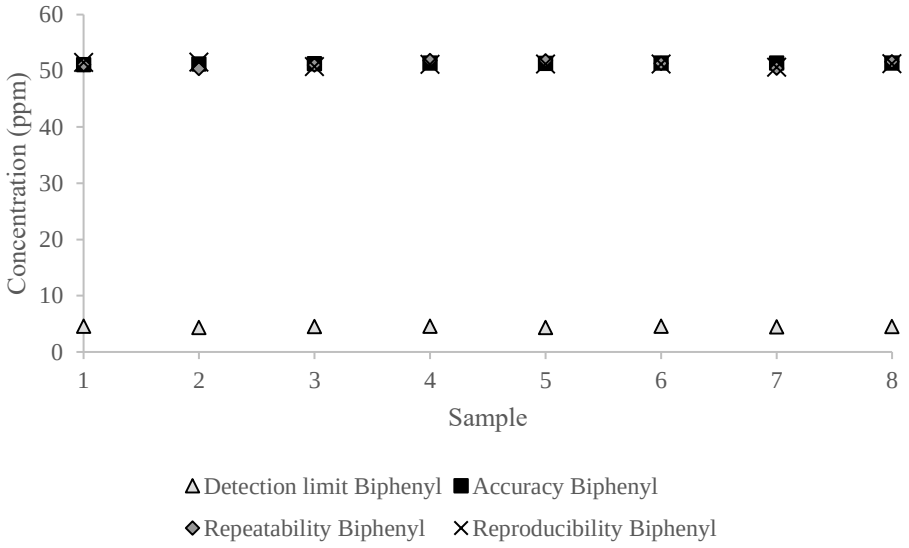

Figure 83: Validation curves of biphenyl in reaction 1

6.3.2 Reaction 2

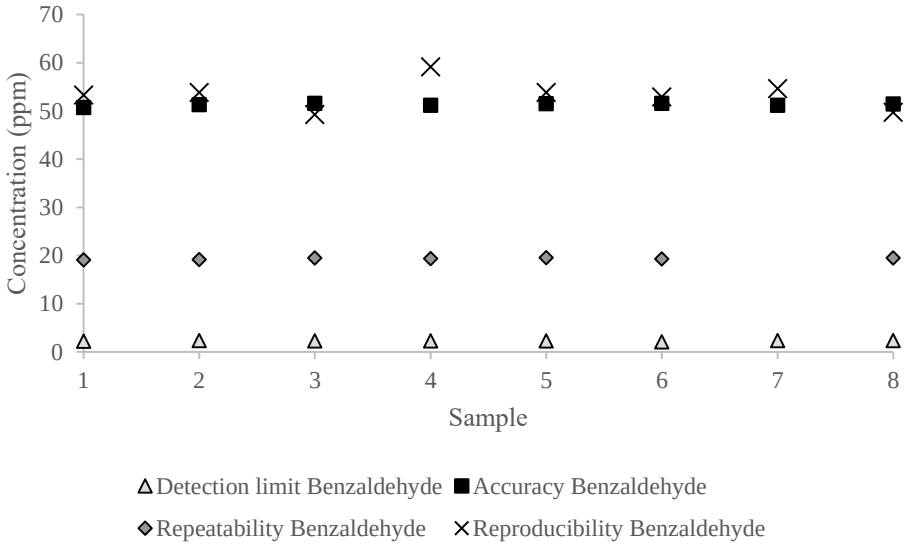

Figure 84: Validation curves of benzaldehyde in reaction 2

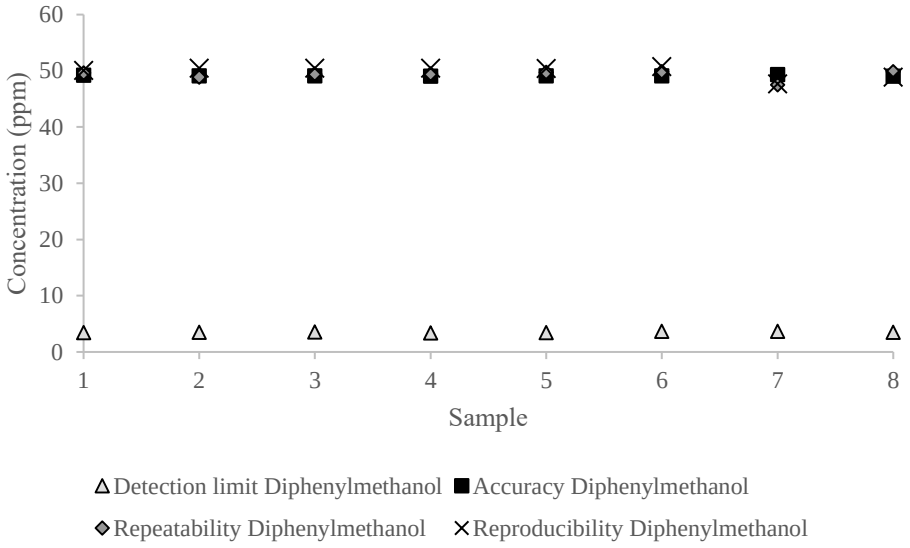

Figure 85: Validation curves of diphenylmethanol in reaction 2

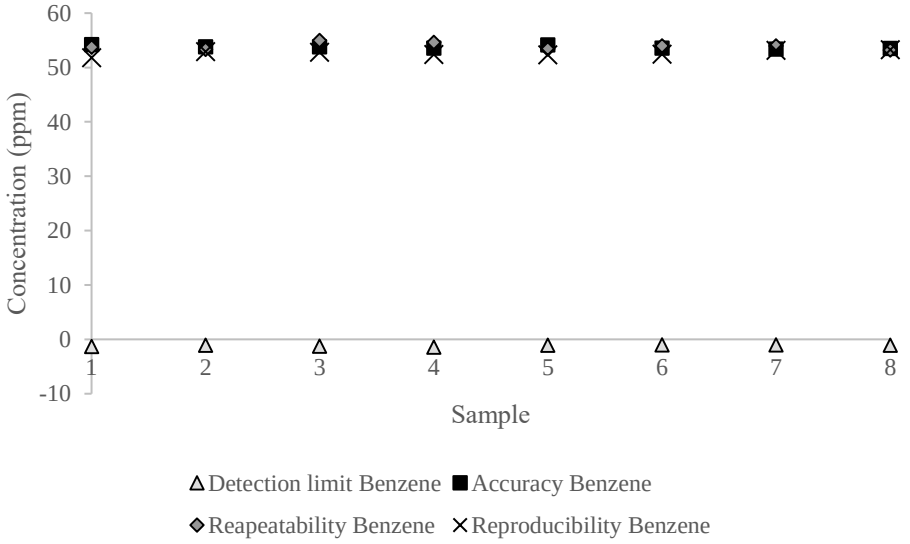

Figure 86: Validation curves of benzene in reaction 2

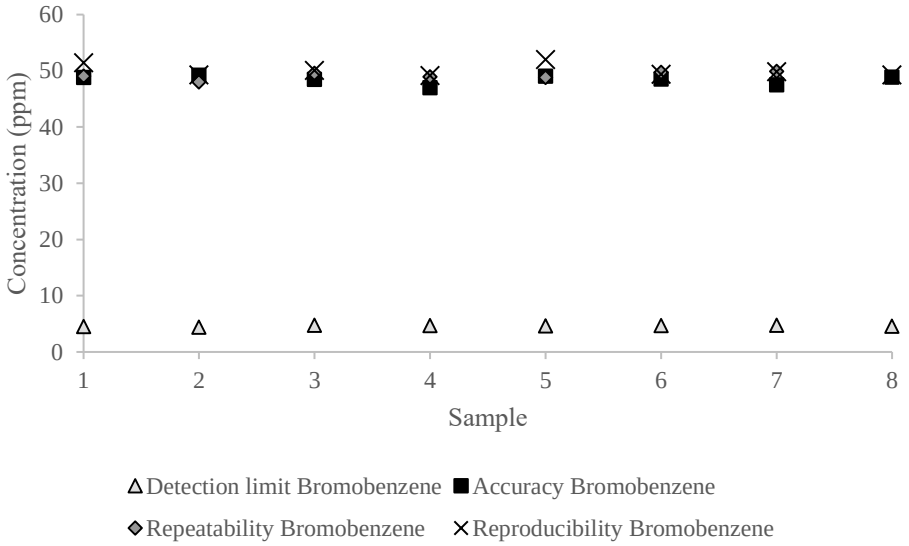

Figure 87: Validation curves of bromobenzene in reaction 2

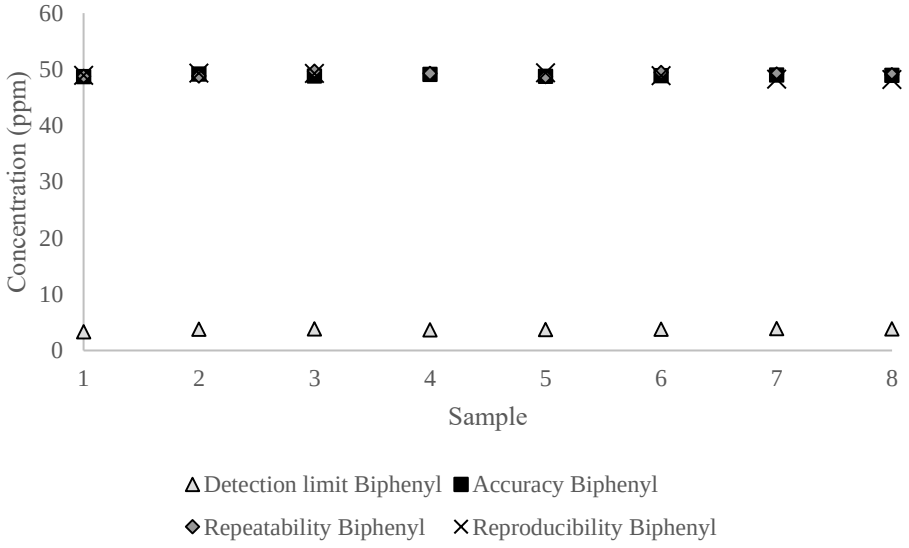

Figure 88: Validation curves of biphenyl in reaction 2

6.3.3 Recovery reaction 1 and 2

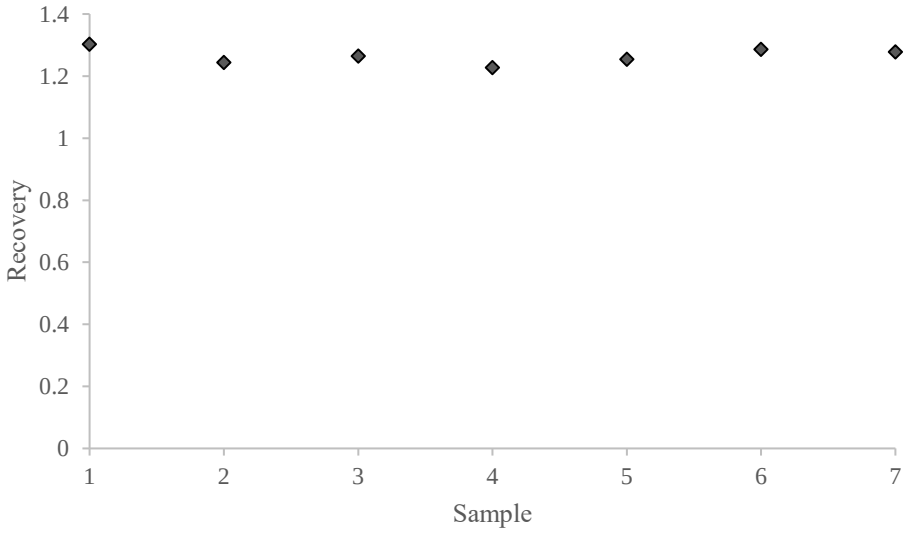

Figure 89: Recovery benzene

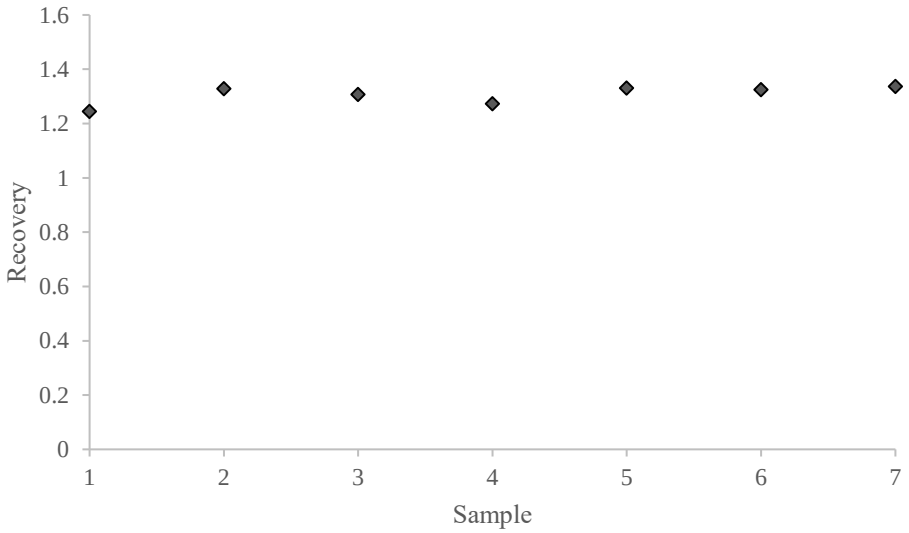

Figure 90: Recovery bromobenzene

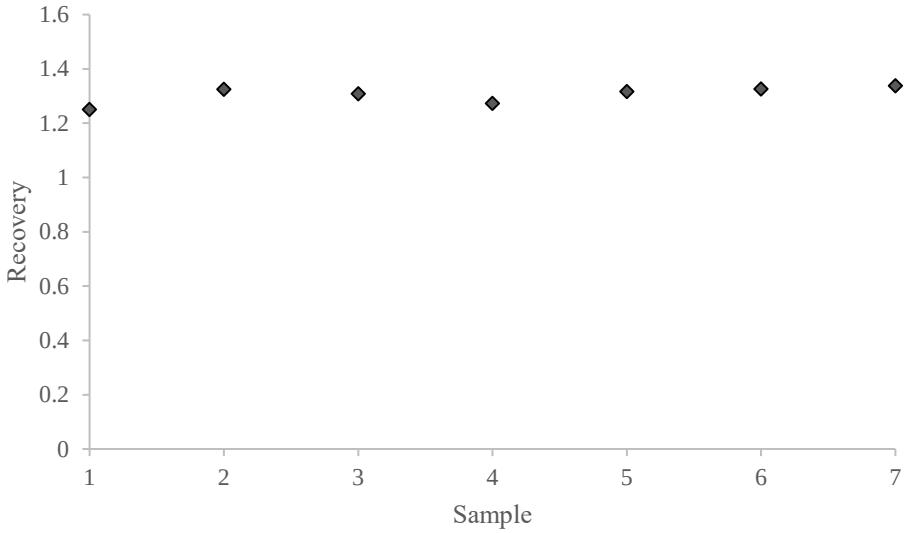

Figure 91: Recovery biphenyl

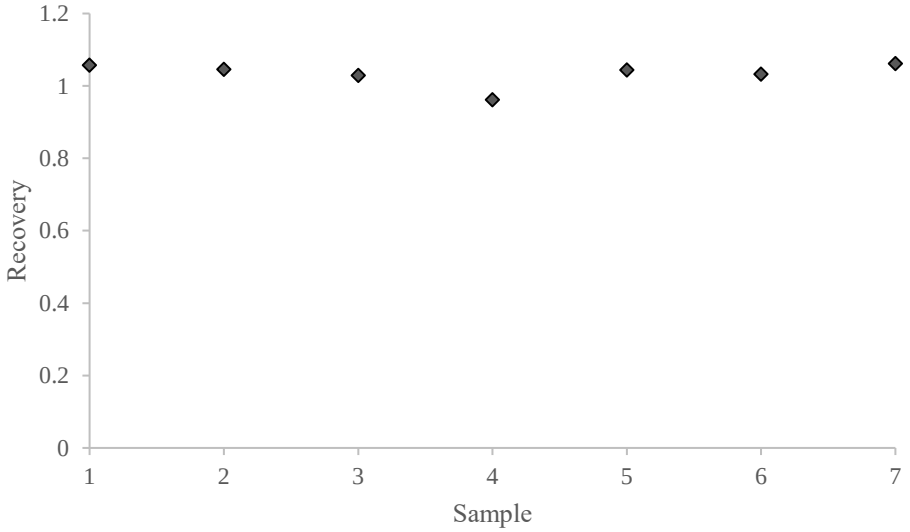

Figure 92: Recovery acetophenone

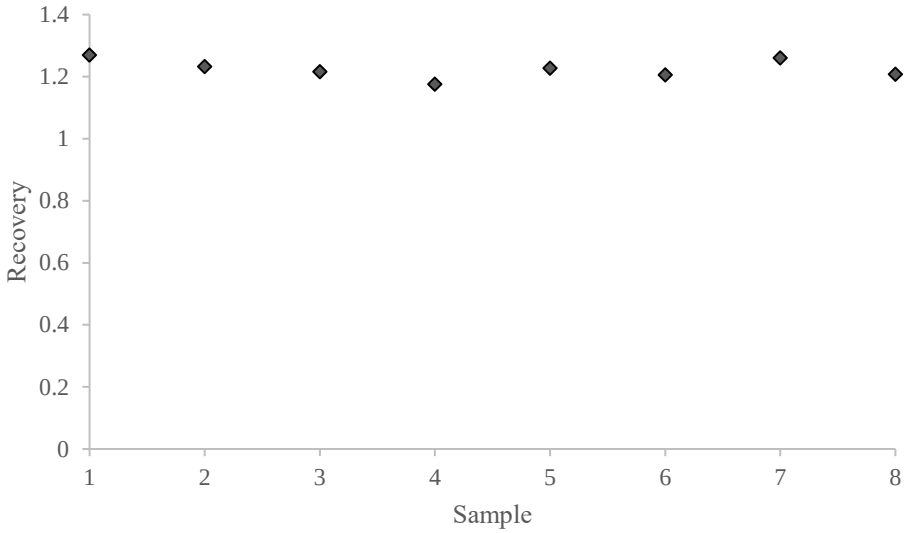

Figure 93: Recovery 1,1-diphenylethanol

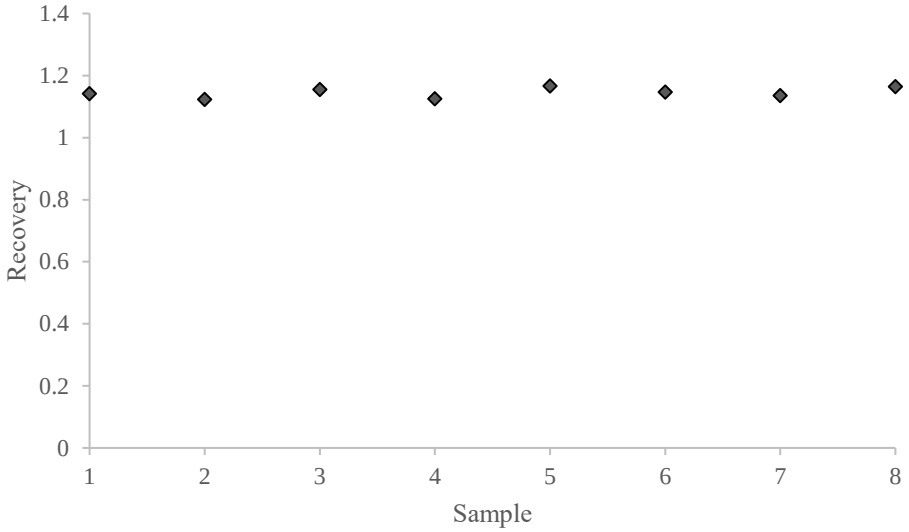

Figure 94: Recovery benzaldehyde

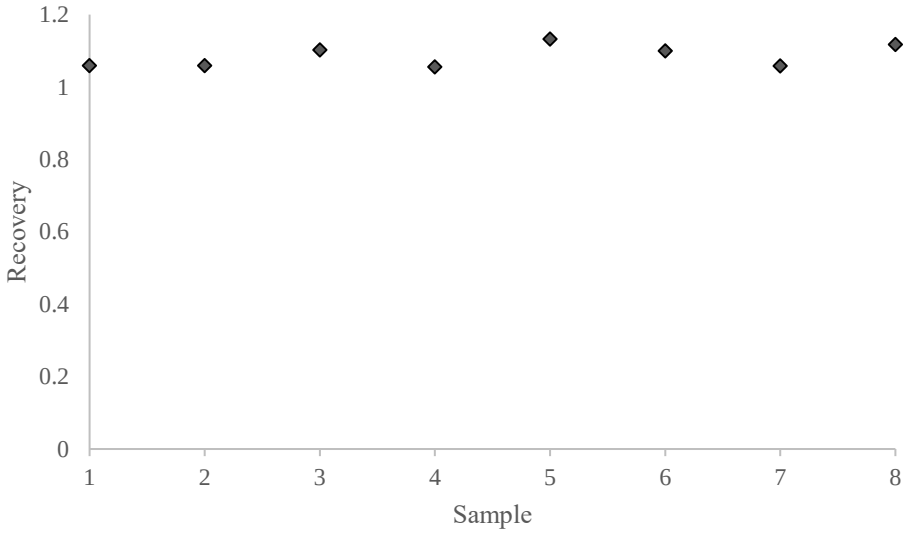

Figure 95: Recovery diphenylmethanol

6.3.4 Influence of matrix for reaction 1 and 2

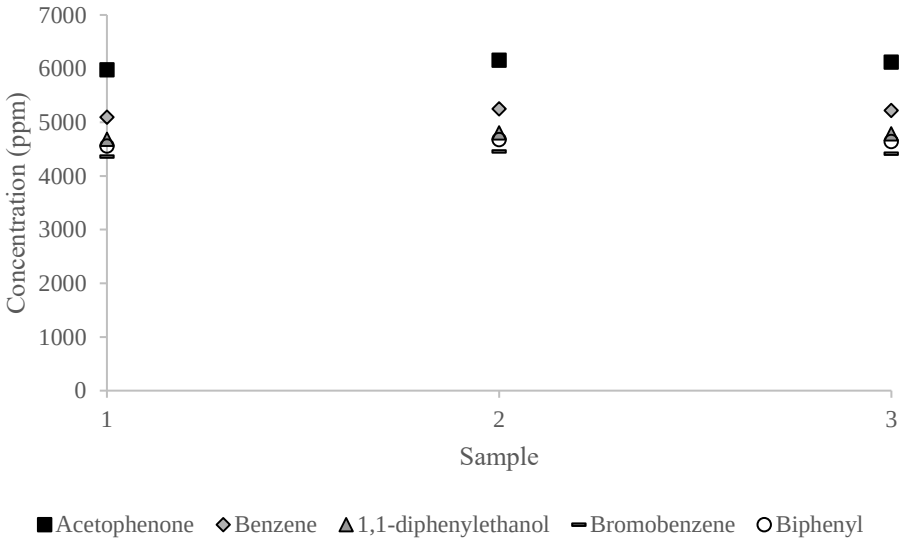

Figure 96: Influence of matrix for reaction 1

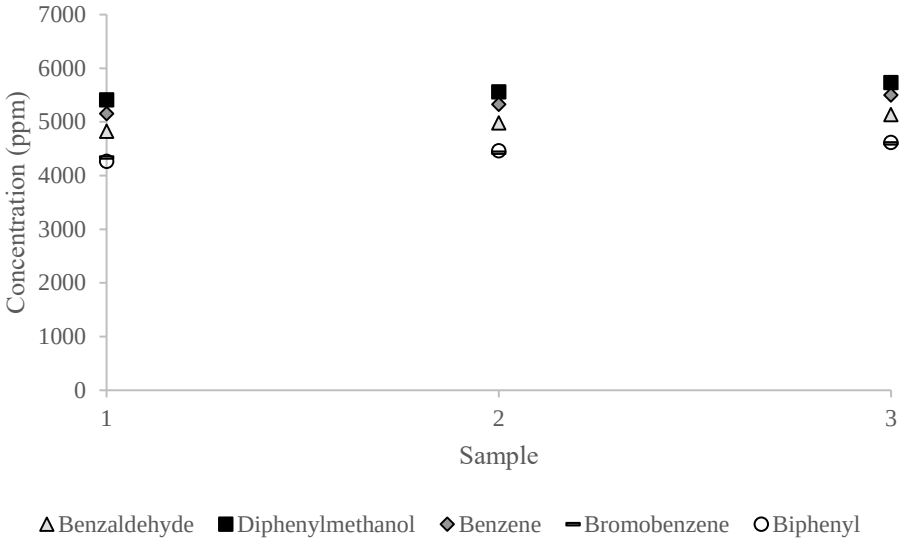

Figure 97: Influence of matrix for reaction 2

Auteursrechtelijke overeenkomst

Ik/wij verlenen het wereldwijde auteursrecht voor de ingediende eindverhandeling:
Design and characterization of a cascade of continuous stirred-tank reactors for a Grignard reaction

Richting: **master in de industriële wetenschappen: chemie**
Jaar: **2018**

in alle mogelijke mediaformaten, - bestaande en in de toekomst te ontwikkelen - , aan de Universiteit Hasselt.

Niet tegenstaand deze toekenning van het auteursrecht aan de Universiteit Hasselt behoud ik als auteur het recht om de eindverhandeling, - in zijn geheel of gedeeltelijk -, vrij te reproduceren, (her)publiceren of distribueren zonder de toelating te moeten verkrijgen van de Universiteit Hasselt.

Ik bevestig dat de eindverhandeling mijn origineel werk is, en dat ik het recht heb om de rechten te verlenen die in deze overeenkomst worden beschreven. Ik verklaar tevens dat de eindverhandeling, naar mijn weten, het auteursrecht van anderen niet overtreedt.

Ik verklaar tevens dat ik voor het materiaal in de eindverhandeling dat beschermd wordt door het auteursrecht, de nodige toelatingen heb verkregen zodat ik deze ook aan de Universiteit Hasselt kan overdragen en dat dit duidelijk in de tekst en inhoud van de eindverhandeling werd genotificeerd.

Universiteit Hasselt zal mij als auteur(s) van de eindverhandeling identificeren en zal geen wijzigingen aanbrengen aan de eindverhandeling, uitgezonderd deze toegelaten door deze overeenkomst.

Voor akkoord,

Cornelissen, Dries **Debrie, Robin**

Datum: **11/06/2018**